ACKNOWLEDGMENT

In the name of Allah, most gracious, most merciful.

"And say: Work (righteousness): Soon will Allah observe your work, and his messenger and the believers"

All praise and glory to Allah the almighty who alone made this small objective to be accomplished. I feel honored and privileged to glorify his name in the sincerest way through this small accomplishment and ask him to accept my efforts. Peace be upon the Prophet, his companions and all who followed him until the Day of Judgment.

My deep appreciation goes to my thesis advisor Dr. Yehia A. Khulief for his constant help, guidance and the countless hours of attention he devoted throughout the course of this work. His priceless suggestions made this work interesting and learning for me. I am especially thankful and grateful to my thesis committee member, Dr. Mohammed A. Mohiuddin, for his guidance in performing the dynamic analysis. Thanks are also due to my thesis committee member and department chairman, Dr. Faleh Al-Sulaiman for his useful comments on the research and review of the thesis. I would like also to place on record my great appreciation to all ME faculty members and my colleagues who helped throughout my study.

Acknowledgment is due to King Fahd University of Petroleum and Minerals and King Abdul Aziz City for Science and Technology (KACST) for extending facilities and support to this research work.

I wish to express my heartfelt gratitude to my parents for their encouragement, constant prayers and continuing support. I owe a lot of thanks to my dear wife and children for their extra patience and motivation. Thanks are due to my brothers and sisters who helped my in preparing the manuscript. Finally, My sincere appreciation is expressed to Mr. Mohammed Al-Sofi (Manager of ACEC) for his support and encouragement.

TABLE OF CONTENTS

LIST OF TABLES

LIST OF FIGURES

NOMENCLATURE

A	:	Cross-sectional area of the element
c	:	Damping coefficient
D_0	:	Outer diameter
D_i	:	Inner diameter
E	:	Modulus of elasticity
$\{e\}$	:	Nodal coordinate
f	:	Frequency
F_s	:	Static friction force
F_k	:	Kinetic friction force
g	:	Gravity acceleration
G	:	Shear modulus
$[G]$	:	Gyroscopic matrix
I_D	:	Diametral mass moment of inertia
I_P	:	Polar mass moment of inertia
I	:	Second moment of inertia
$[I]$	:	Identity matrix
k_t	:	Torsional stiffness of drillpipe
k	:	Stiffness coefficient
$[K]$	:	Global stiffness matrix
$[K_a]$	:	Axial stiffness matrix
$[K_{as}]$	:	Axial stiffening matrix
$[K_e]$	:	Elastic stiffness matrix

$[K_\phi]$	:	Torsional stiffness matrix
L	:	Lagrangian function
L_c	:	Drillcollar length
L_p	:	Drillpipe length
l	:	Length of the finite element
M	:	Mass of the BHA
m	:	Mass of the block
$[M]$	:	Global mass matrix
$[M_r]$	:	Rotary inertia mass matrix
$[M_t]$	:	Translational mass matrix
$[M_\phi]$	:	Torsional mass matrix
$[M_e]$	:	Coupled torsional-lateral mass matrix
N_t	:	Translational shape function
N_θ	:	Rotational shape function
N_ϕ	:	Torsional shape function
P	:	Normal force
KE	:	Kinetic energy of the drillstring element
t	:	Time
T	:	Torque on bit
u	:	Axial displacement
U	:	Total strain energy of the drillstring element
U_1	:	Strain energy due to bending deformation
U_2	:	Strain energy due to torsional deformation
U_3	:	Strain energy due to axial deformation

U_4	:	Strain energy due to axial stiffening
v	:	Lateral displacement in y-axis
v_0	:	Sliding velocity
w	:	Lateral displacement in z-axis
W_0	:	Mean weight on bit
ρ	:	Density
θ_y	:	Lateral rotation in y-direction
θ_z	:	Lateral rotation in z-direction
μ_s	:	Static friction coefficient
μ_k	:	Kinetic friction coefficient
μ	:	Mass density of the element
ω	:	Frequency of torsional vibrations
$\overline{\omega}$	:	Instantaneous angular velocity vector
α	:	Phase angle
ϕ	:	Angular displacement
Γ	:	Time period
Ω	:	Rotary table rotation

Abbreviations

BHA	:	Bottom Hole Assembly
MWD	:	Measurement While Drilling
PDC	:	Polycrystalline Diamond Compact
TOB	:	Torque on Bit
TSP	:	Thermally stable polycrystalline bit
WOB	:	Weight on Bit

ABSTARACT

Name of student	:	Salem Mohammed Bashmal
Title of study	:	Finite Element Analysis of Stick-Slip Vibrations in Drillstrings
Major field	:	Mechanical Engineering
Date of Degree	:	December 2004

Drillstring undergoes several modes of vibrations simultaneously. These vibrations can be classified into three main groups based on their directions: axial, transverse and torsional vibrations. Coupling between these vibrations is possible and it yields uncertainty in vibration analysis and monitoring. Stick-slip in drillstrings is a specific type of torsional vibrations. Stick-slip involves periodic fluctuations in bit rotational speed, ranging from almost zero velocity to a stage of high rotational speed, often more than twice the surface speed.

In this study, a dynamic model of the drillstring is formulated using consistent mass finite element approach. The developed model accounts for the coupling between axial and bending vibrations, the dynamic coupling between bending and torsional vibrations as well as the effect of rotary inertia, gyroscopic moment and gravitational axial stiffening. Stick-slip is modeled using proper downhole boundary conditions, which admit the excitation of stick-slip oscillations. The effects of stick-slip are investigated by studying the associated dynamic responses of the drillstring.

Master of Science Degree

King Fahd University of Petroleum and Minerals

Dhahran, Saudi Arabia

December 2004

ملخص الرسالة

الاسم : سالم محمد باشمال

عنوان الرسالة : التحليل الديناميكي لاهتزازات التوقف والانزلاق في محور الحفر باستخدام طريقة العناصر المحدودة

التخصص : هندسة ميكانيكية

تاريخ التخرج : ديسمبر 2004 م

يتعرض محور الحفر لصور متعددة من الاهتزازات في آن واحد. هذه الاهتزازات يمكن تقسيمها باعتبار اتجاه تأثيرها إلى ثلاثة أقسام: طولية و عرضية ولولبية. عادة ما يحدث تراكب بين هذه الأقسام مما يصعّب عملية مراقبة وتحليل الاهتزازات. ظاهرة التوقف والانزلاق تندرج تحت قسم الاهتزازات اللولبية لمحور الحفر. ظاهرة التوقف والانزلاق تؤثر على مثقاب الحفر مما يجعل سرعته تتردد بين التوقف التام و سرعة دوران عالية تصل في كثير من الأحيان إلى ضعف السرعة الثابتة لعجلة الدوران في السطح.

يتم في هذه الرسالة إعداد تحليل ديناميكي لحركة محور الحفر باستخدام طريقة العناصر المحدودة. هذا التحليل تم صياغته كي يستوعب التراكب بين الاهتزازات الطولية والعرضية بالإضافة إلى التراكب بين الاهتزازات العرضية واللولبية. التحليل يشمل كذلك التأثيرات الناشئة عن القصور الذاتي الدوراني ومقاومة الانحناء و التصلب الناتج عن وزن المحور. القوى المسببة لاهتزازات التوقف والانزلاق تم استنتاجها من خلال دراسة ظروف الحفر صيغت بطريقة تسمح بإنشاء اهتزازات التوقف والانزلاق بطريقة مطابقة لما يحدث في الواقع. تأثيرات هذه الاهتزازات تم رصدها من خلال تحليل حركة محور المصاحبة لها.

درجة الماجستير في العلوم

جامعة الملك فهد للبترول والمعادن

الظهران – المملكة العربية السعودية

ديسمبر 2004 م

1. INTRODUCTION

Oil industry is one of the most active industries in the world today. Oil is the heart of the new technology. It is the only efficient source of energy that can serve the various demands of the new industry. Extensive studies are carried out to investigate, develop and examine all fields of the oil industry. These studies included various aspects starting from exploration of oil fields to the final production and transportation of oil products, including drilling, refinement and storing.

Drilling is the only way to verify the existence and exploitation of oil reservoirs. Long drillstrings are used for exploration of oil reservoirs. Deep wells are drilled for exploration and production with a rock-cutting tool (bit) driven from the surface through a slender structure of pipes (drillstring).

Drilling is an extremely complicated operation. Different aspects influence the drilling operation and they vary a great deal throughout the world. These aspects include field geology, economics and technology. Nevertheless, some basic principles apply to all wells. Brief description is given, herein, to clarify the important concepts and terminology used in drilling technology.

1.1. Drilling System Components

The main goal of the driller is to make a usable hole at the least possible cost. In principle, maximizing the rotating speed and minimizing the tripping time can reduce the drilling cost. However, very fast drilling can create problems such as failure of the drillpipe and bit wear, in which extra cost is added. Drilling is a multi-

billion dollar industry. So, it is very important to deal with drilling problems in professional and efficient manners to minimize the drilling cost.

The speed at which the bit drills into the formation is called the rate of penetration (ROP). There are six basic factors that affect the rate of penetration [1]:

1. Bit type
2. Weight on bit
3. Rotary speed
4. Drilling fluid properties
5. Hydraulics
6. Formation properties.

Deep wells for the exploration and production of oil and gas are drilled using rotary drilling systems. The basic elements of the rotary drilling system are shown in Figure 1.1. The drilling assembly consists of a rock-cutting tool called a bit, connected to the surface drive system by means of a train of slender pipes. The bit is driven from the surface by a drive system, which consists of an electric motor, a gearbox and a rotary table. The driving power is generated by an electric motor and transmitted through a mechanical transmission gearbox. The lowest part of the drillstring is the Bottom Hole Assembly (BHA), which consists of thick-walled pipes, called the drillcollars. A fluid "mud" is pumped down through the hollow drillstring, through nozzles in the bit to compensate the pressure of contact with the rock, lubricate and remove the rock cuttings from the hole. The drilling process is normally steered by the hook load, the rotary speed at the surface and the mudflow rate. The function of the hook is to support the drillstring and apply axial reactive force at the top end of the drillstring [2, 3]. The drillstring is pulled at the hook by the hook load. This will prevent buckling by ensuring that the drillstring is kept under tension for most of its length [2].

The following subsections of this chapter are devoted to describe the main parts of the drilling rig and the parameters that influence drillstring dynamics during the drilling process. A glossary of the most common abbreviations used in drilling industry is listed in appendix A.

1.1.1. Drilling Bit

The cutting element used in drilling oil and gas wells is called the bit. A typical drilling bit consists of four main parts (as shown in Figure 1.2): shank, body, circulation element and cutters. The cutting tools are made of hard materials such as steel, tungsten carbide or diamond. The circulation element permits the passage of drilling fluid and utilizes the hydraulic force of the fluid stream to improve drilling rates. The bit's ability to drill depends on the size, material and shape of the cutters as well as the formation properties.

Unfortunately, no single bit can cut all types of formations. A great variety of bits are supplied by various manufacturers. During drilling operations, a bit selection is important to create optimum hole. Selecting the ideal bit depends on the formation and the type of rock to be drilled. Geologic prognosis aids in bit selection for a particular well. Incorrect bit selection can lead to a premature failure or low rate of penetration [4]. The key to develop more robust bits is to understand the fundamental mechanism that causes their failure. Simulating the new designs through bit vibration models can predict the vibration behavior with good degree of accuracy.

Drilling bits, in general, can be classified into two categories: roller cone bits, sometimes called rock bits, and fixed cutter bits, also referred to as fixed head or shear bits. The roller cone bits (see Figure 1.3) have either tungsten carbide or steel cutting tooth. Natural diamond and synthetic diamond are the two available types of

fixed cutter bits. The roller cone bits crush the rock by their hard material cutters while the synthetic diamond bits shear or slice the rock. Shearing the rock is an effective action that takes only one third of the energy and weight required for roller cone cutter. Figure 1.4 shows the drilling actions for roller cone cutter (with tungsten carbide insert bit) and fixed cutter bits.

The most popular type of roller cone cutter family is the tri-cone bit. It is a roller cone cutter in which three cone-shaped cutting devices are mounted in such a way that they intermesh and rotate together as the bit drills (Figure 1.3). The bit body is fitted with nozzles through which the drilling fluid is discharged.

One of the most common fixed diamond cutter bits is the Polycrystalline Diamond Compact (PDC) bits. The PDC bits have cutters made of synthetic diamond crystals bonded to a tungsten carbide insert brazed into pockets in the steel body or blades of the bit (see Figure 1.5). The PDCs are more expensive than tri-cone bits but when considering their fast penetration and fewer trips, the cost saving becomes significant for many drilling situations.

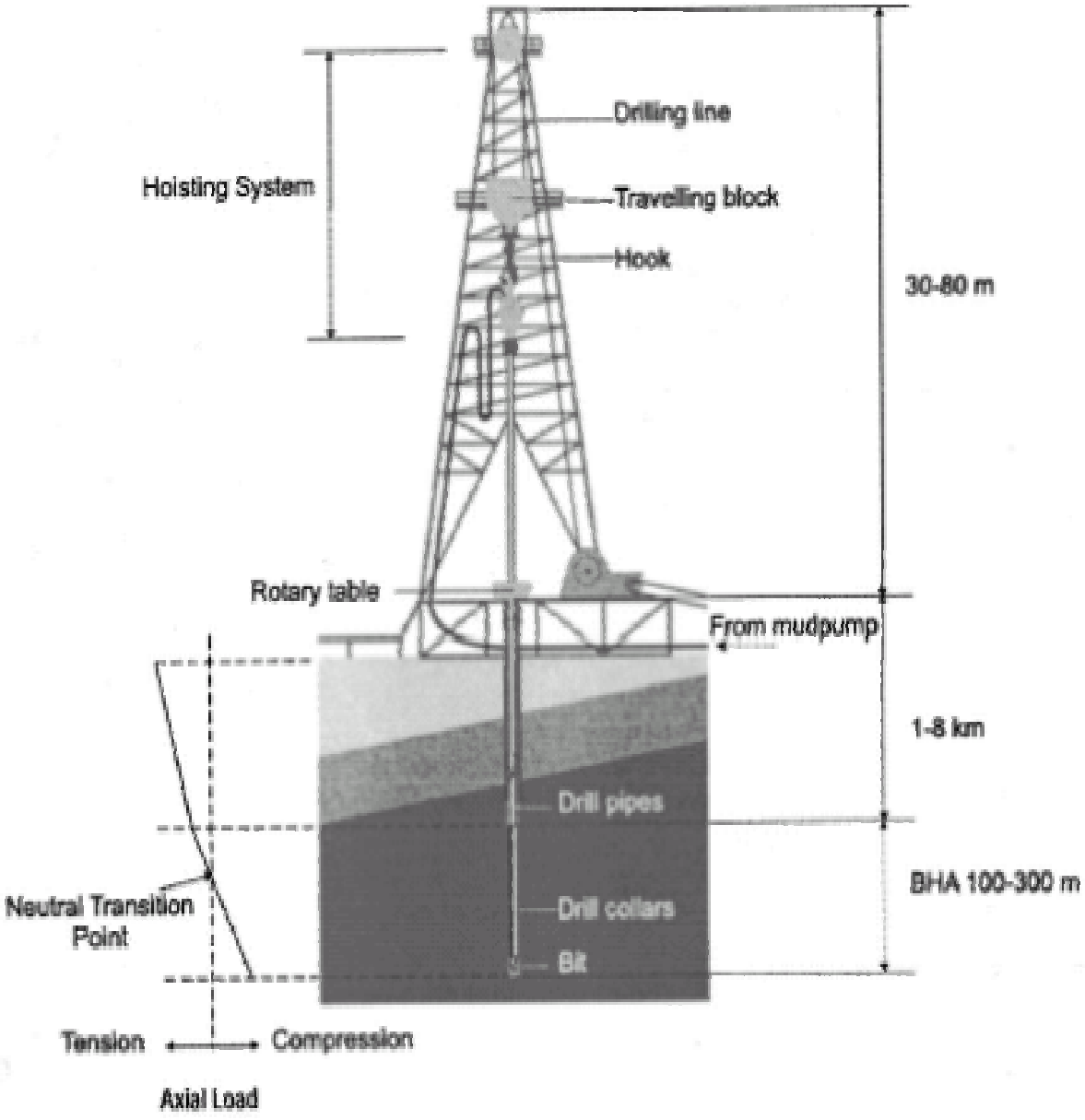

Figure 1.1: The drilling rig [1].

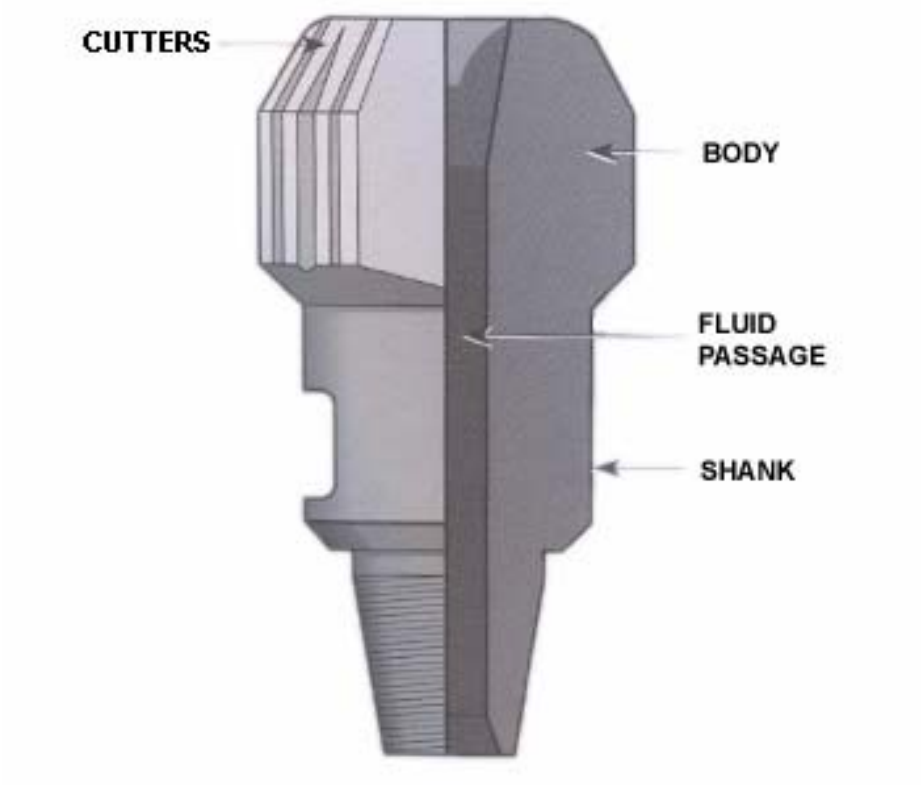

Figure 1.2: Main parts of the drilling bit [1].

Figure 1.3: the tri-cone bit is one type of the roller cutter family [1].

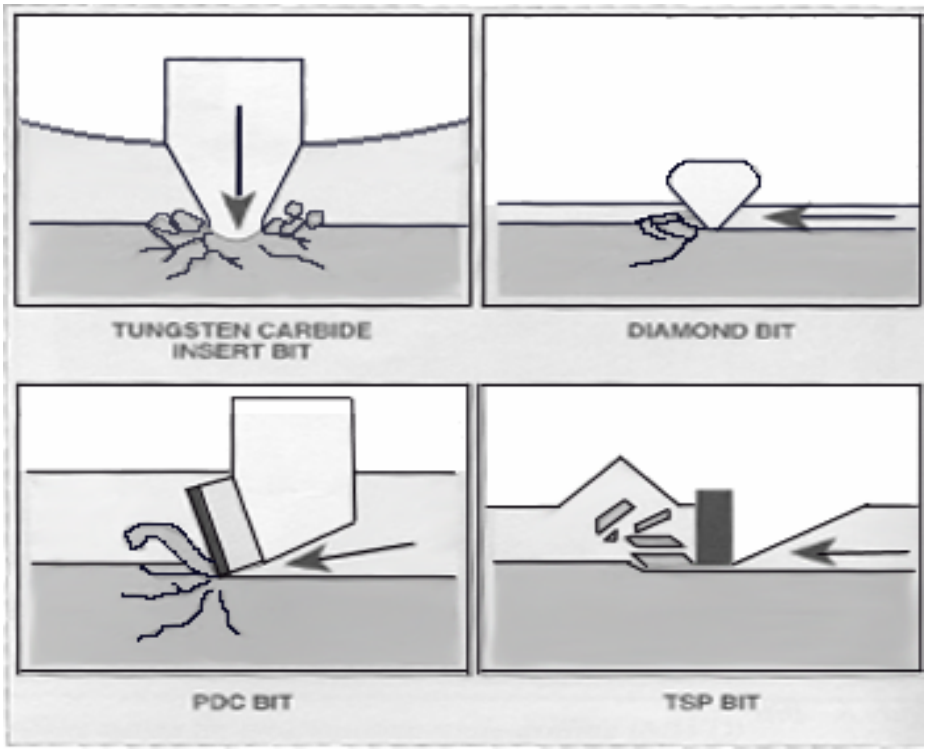

Figure 1.4: The drilling actions for various drilling bits [1].

Figure 1.5: Polycrystalline Diamond Compact bits (PDC)

1.1.2. Drilling Mud

Drilling mud is a special fluid that circulates down through the wellbore and then upwards through the annulus between the drillstring and borehole during the drilling operations. The functions of the drilling mud are (see Figure 1.6):

- Clean the bit teeth and the bottom of the hole;
- Transport formation cuttings to the surface;
- Prevent formation fluids from entering the wellbore causing a kick or blowout.
- Protect and support the walls of the wellbore;
- Cool and lubricate the bit and drillstring;
- Provide hydraulic power for downhole motors or turbines; and
- Help detect the presence of oil, gas and saltwater in formation.

Drilling mud is composed of three types of materials: one liquid and two solids. The liquid is usually water or oil or a mixture of both. Clays such as bentonite are added to thicken the mud. In addition, some cuttings, such as barite are added to control formation pressure and increase the density of the mud. The properties of the drilling mud must be controlled because it can significantly affect the rate of penetration or induce severe vibrations. The major mud properties that should be taken into consideration are density, viscosity, solid content and oil content.

1.1.3. Bottom Hole Assembly

The Bottom Hole Assembly (BHA) is the lowest part of the drillstring and consists of heavy–walled pipes called drillcollars [45]. Drillcollars have an inner diameter of about 64-76 mm and an outer diameter of 120-240 mm. The BHA's length ranges between 100 and 300 m.

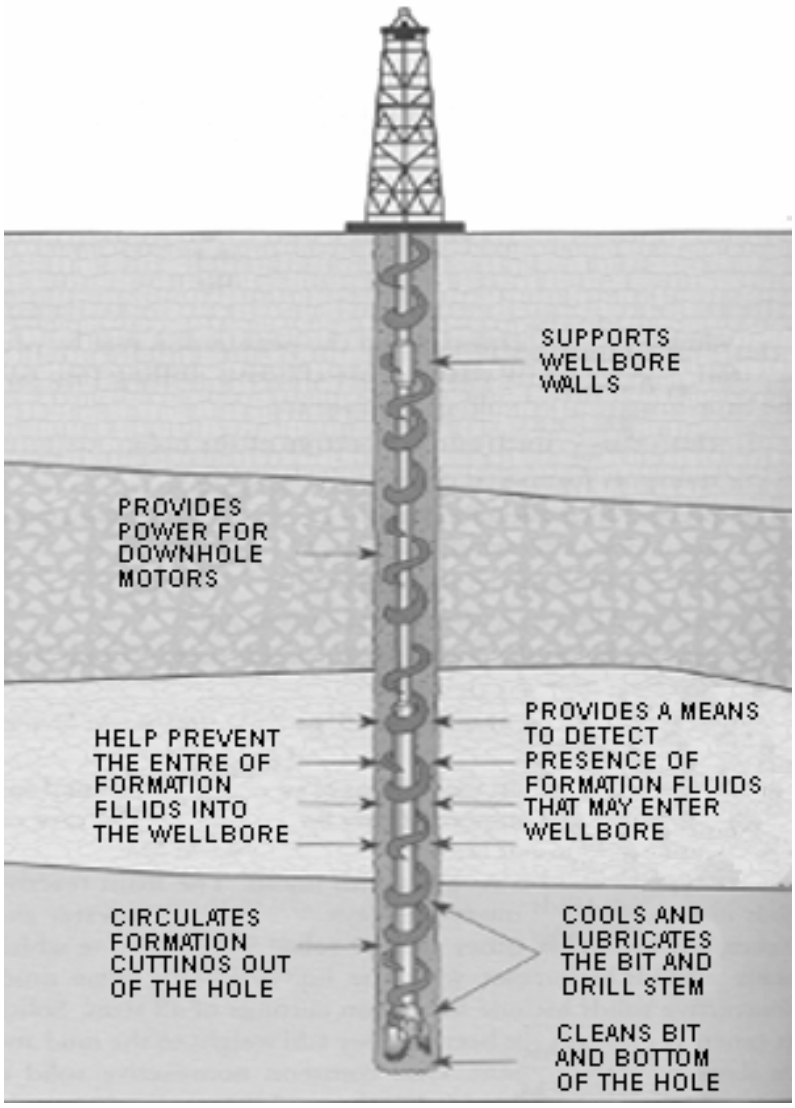

Figure 1.6: The functions of the drilling mud [1].

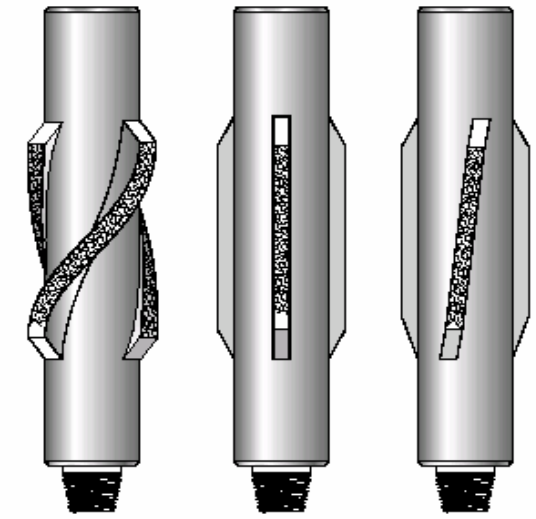

Figure 1.7: Various types of Stabilizers.

To prevent lateral vibration and buckling, stabilizers are used to keep the BHA in position. Stabilizers are coarsely grooved cylindrical elements of a larger diameter than the drillcollar that loosely fit in the borehole. Figure 1.7 shows some of the most common types of stabilizers. The typical stabilizer clearances with the borehole go up to 50 mm and the distance between stabilizers varies between 5 and 50 m. Stabilizers are designed to control hole deviation and reduce the risk of differential sticking.

An electric motor is used to derive the rotary table at the surface. This energy is transported to the BHA via the drillstring which consists of slender drillpipes (usually have 127 mm outer diameter and 9 mm thickness) [2]. The BHA provides the required force for cutting operation. The compressive force on the bit, which ranges between 10^4-10^5 N, is commonly referred to as the Weight on Bit (WOB) while the required torque to rotate the bit is called Torque on Bit (TOB). The rotational speed of the drillstring ranges between 50 and 200 revolutions per minute [5]. The length to diameter ratio of the drillstring is extremely large. Consequently, the drilling process can't be easily controlled because of the large flexibility of the drillstring [29].

1.2. Vibrations of the Drillstring

Drillstring and drilling bit vibrations are of major concern to the operators and engineers. The drillstring itself is composed of elements of different size, weight, and stiffness, which may deform in varying proportions. This, in combination with the reaction of the containing borehole, induces vibrations in the drillstring. These vibrations consume some of the energy supplied to the drillstring, thereby reducing the efficiency. Vibrations occur frequently during drilling operation and can cause catastrophic effects on the drilling process and equipment. Accordingly, Vibration control has become a key factor in the drilling process [4]. Understanding the dynamic behavior of the drillstring is important in the control of the vibrations. The

demand to real-time process feedback is required because of the response of BHA vibrations can change dramatically with just a small variation in drilling parameters. Furthermore, the successful detection and interpretation of the vibrations from surface measurements depends on one's understanding of the nature of the downhole phenomena. The lack of reliable high rate measurements increases the difficulties in obtaining the full understanding of the drilling process.

Drillstring undergoes several modes of vibrations simultaneously. This makes the drillstring vibrate in a complex and nonlinear manner. The non-linearity in the drillstring is caused by drilling fluid, stabilizer clearance, stabilizer friction and borehole wall contact [5]. The drillstring is highly flexible. The diameter to length ratio is in the order of $1{:}10^4$ to 10^5. Violent drillstring vibrations can cause serious problems such as twist-offs, bit bounce, premature bit failure, low rate of penetration and failure of other BHA's components. The vibrations must be reduced in order to increase the rate of penetration, maximize the rotating time and minimize the tripping time; thus reducing the drilling cost.

1.2.1. Introduction

As mentioned before, different modes of vibrations are acting on the drillstring and bit. Some of these vibrations are useful such as bit noise, which has been used as a signal for seismic while drilling. However, the frequency of these useful vibrations, which is 10 to 100 Hz, is different from the frequency of the deleterious vibrations, which is about 3 Hz for bit bounce [8].

Several principles are used to classify these vibrations. Dufeyte et al. [7] divided the torsional vibrations into transient and stationary. The transient vibrations are associated with the variation in the drilling conditions- like heterogeneity in the

rock. Stationary vibrations are caused by the natural resonance of the drillstring as in the case of self-excited oscillations [8].

According to their characteristics, vibrations can be divided into two major types; forced vibrations and self-excited vibrations. Forced vibration responses are produced by an externally time varying force which is independent from the motion it produces. For example, the longitudinal vibrations produced by roller cone rock bits are forced vibration responses because the three lobed patterns in the rock excite longitudinal modes in drillstrings independent of the vibration response. For self-excited vibrations, the exciting force is coupled with the vibration it produces [67]. Stick-slip vibration is a typical example of self-excited vibrations.

Usually, downhole drilling vibrations are classified based on their direction. There are three main groups: axial, transverse and torsional as shown in Figure 1.8. The drillstring is vibrating axially when the direction of vibrations is parallel to the length of the drillstring. With transverse vibration, the direction is perpendicular to the length of the drillstring. In torsional vibrations, the fluctuations are caused by twisting the drillstring around its longitudinal axes. Coupling between these vibrations is possible and it yields uncertainty in vibration analysis and monitoring. For example, high-speed torsional fluctuations can induce severe axial and lateral vibrations in the BHA [9, 10].

1.2.2. Axial Vibration

Axial vibrations have a deleterious effect on the bit and Bottom Hole Assembly. Bit bouncing and rough drilling are some forms of axial vibrations. Axial vibrations are most common in vertical holes through hard formation.

Axial vibration can be recognized at the surface. One of the extreme forms of axial vibrations is the bit bounce. When the bit loses the contact with the hole bottom,

it bounces up and down on the bottom of the hole as a result of resonance in the axial direction (see Figure 1.9). Accelerated bearing and tooth wear, inward thrust-induced seal failure, chipped and broken tooth cutters, damage to downhole tools and reduction in penetration rate can be attributed to the bit bounce [11].

In some situations, pulling off-bottom and changing the rotational speed or weight on bit can reduce axial vibration. If it is consistently encountered in a series of wells then the use of shock sub may be considered to absorb the axial movement and result in changing the resonant frequency of the BHA.

1.2.3. Torsional Vibration

Torsional vibrations cause irregular downhole rotations, which cause fatigue to the drillcollar connections, damage the bit and slow down the drilling operation. During rotation, the rigid BHA generates torsional oscillations, which are transmitted through the elastic drillstring. Field measurements revealed that torsional vibrations are common in hard formation [12]. Many factors can excite torsional vibrations but the most significant factor is static friction force between the drillstring and wellbore [14]. Torsional vibrations are normally initiated because of the low torsional stiffness of the drillstring and once initiated they may persist until adequate remedies are applied [12]. Low torsional stiffness implies that even low perturbation can generate large rotational displacement. In general, torsional vibrations can be detected at the surface by fluctuations in the power needed to maintain a constant rate of surface rotation.

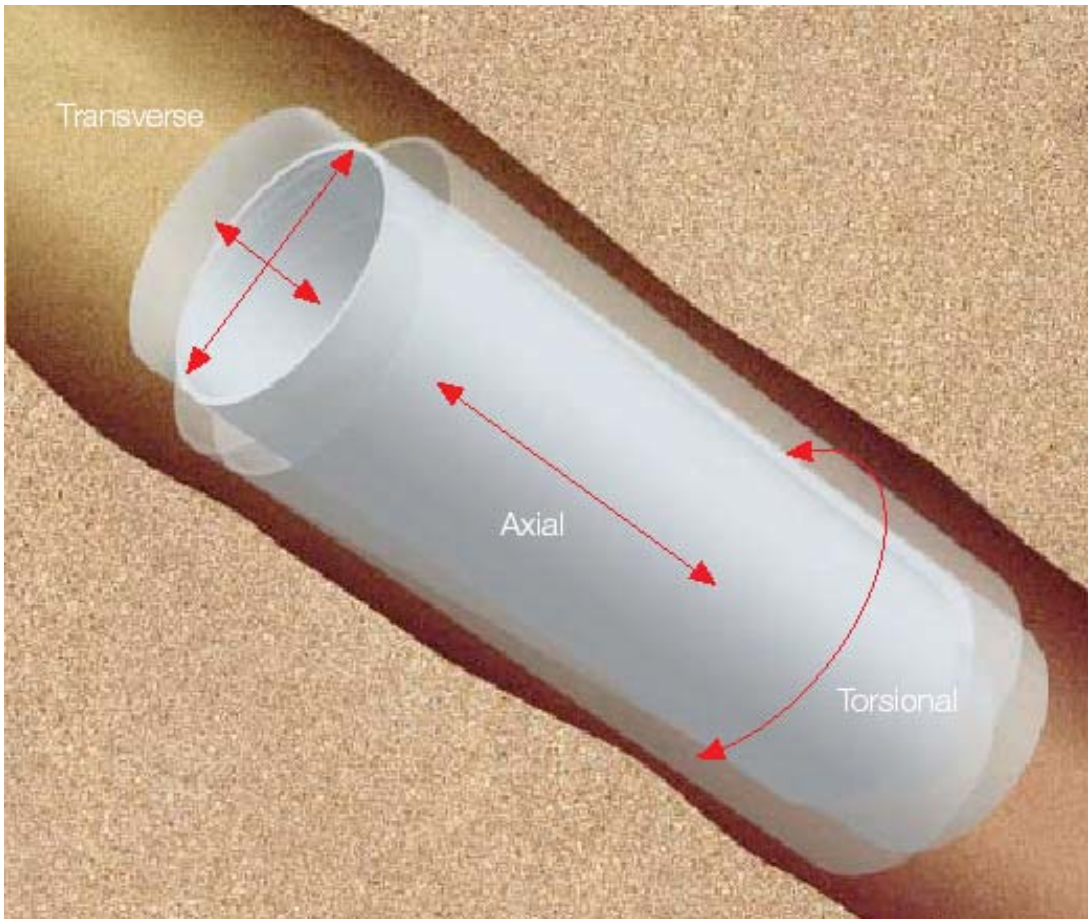

Figure 1.8: The three modes of drillstring vibration [8].

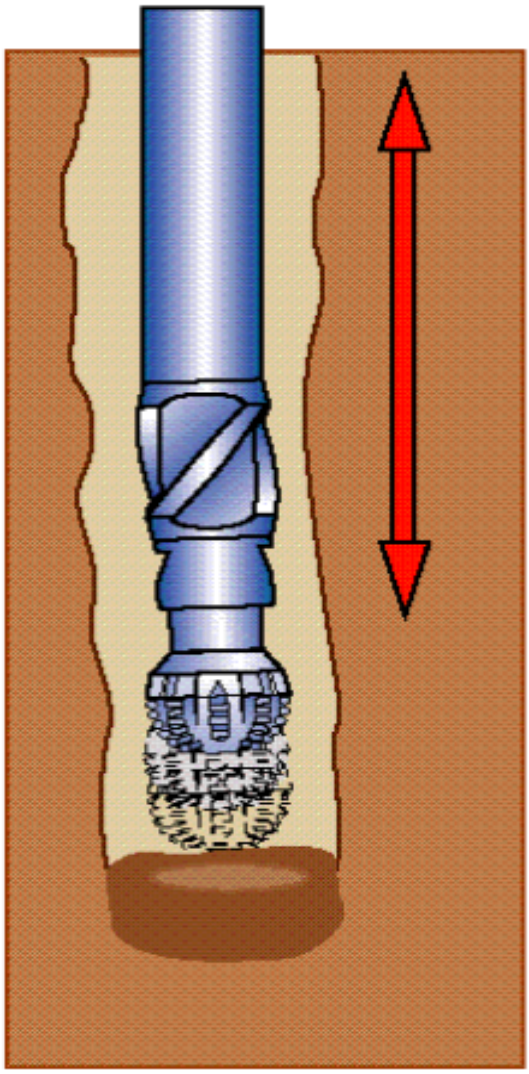

Figure 1.9: Bit bounce [12].

Stick-slip is a specific kind of torsional vibrations. Stick-slip involves periodic fluctuation in the bit rotational speed, ranging from almost zero velocity to a stage of high rotational speed, often more than twice the surface speed. Stick-slip is not the only type of torsional vibration that occurs in the drilling process [15]. However, stick-slip is the most detrimental one. The occurrence of stick-slip oscillation amounts to about 50% of on-bottom drilling time [16]. Further details of stick-slip vibrations are discussed in the next section.

1.2.4. Transverse Vibration

About 75% of the unexplained drillstring or BHA failure is estimated to be caused by the lateral vibrations. Transverse vibration can force the drillstring/bit to bend or whirl. It is often caused by pipe eccentricity and leads to centripetal forces while drilling. This type of vibration cannot be detected at the surface since the vibrations are not transmitted to the surface [11]. The probable effects of transverse vibration include failure of the drillstring, mainly at the diameter change points, connection fatigue and bit failure.

During field tests, very large bending moments were measured in the BHA [17]. Two types of whirling are frequently induced in the BHA; forward and backward whirling (see Figure 1.10).

Forward whirl is the rotation of a deflected drillcollar section around the borehole axis in the same direction as it rotates around its axis. The backward whirl is a rolling motion of the drillcollar or the stabilizer over the borehole wall in opposite direction as it rotates around the axis [2]. The main effect of forward whirling is the drillcollar wear, while connection failure is the main effect of the backward whirling. Whirling of the BHA is excited because of the contact with the wellbore, where the drillcollar hits the wellbore while rotating.

The bit is whirling when the bit geometric center moves around the hole centerline (either forward or backward). The bit whirl causes one of the most harmful vibrations to bit's life. While whirling, the bit is not rotating around its center. Instead, it follows a spiral motion (see Figure 1.11).

Mostly, whirling occurs in low strength formations when the applied weight is not enough and, as a result, an overguage hole is drilled. If the bit spins in hard rock, severe bit damage is the possible result if backward whirling exists. Several methods are introduced to minimize the bit whirl. Tools such as Anti-whirl and track-lock can reduce the bit whirl. Lowering the rotational speed or increasing the weight on bit can reduce bit whirl, as well.

Bit whirl is not the only form of lateral vibration the bit undergoes. A bit may vibrate laterally but not necessarily by whirling. In most cases, coupling occurs with other forms of vibrations. Therefore, the trajectory of the centerline is not a circle [15].

1.3. Stick-Slip Vibrations

In order to understand the complicated drillstring stick-slip phenomenon, it is essential to discuss the phenomenon in its elementary form. A stick-slip phenomenon is related to sliding-friction mechanics. Therefore, understanding the fundamentals of sliding friction is crucial to describe, predict and control stick-slip oscillations of a body. This section presents a general introduction to the fundamental aspects of sliding friction.

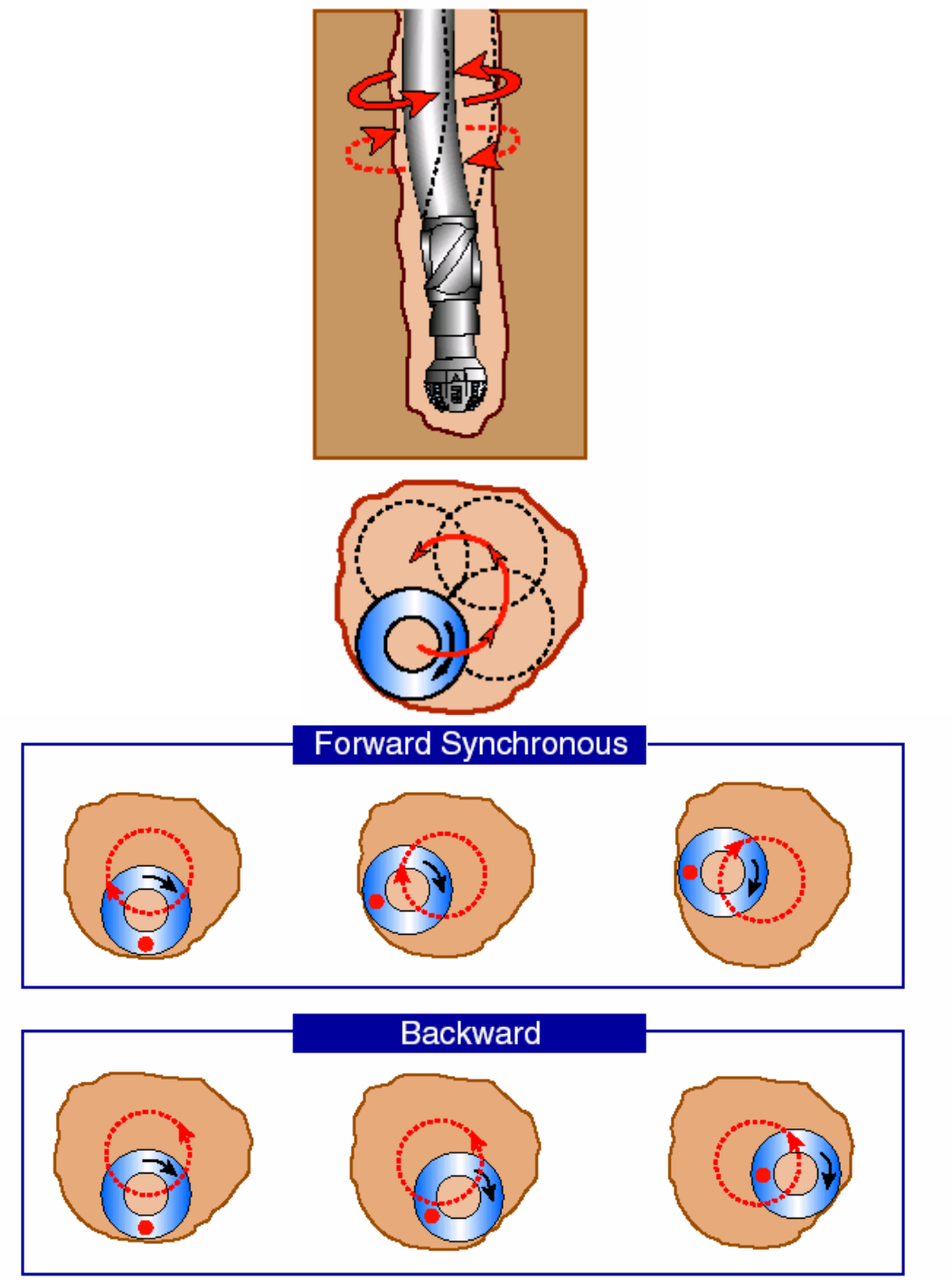

Figure 1.10: Drillstring whirling: Forward and Backward [12].

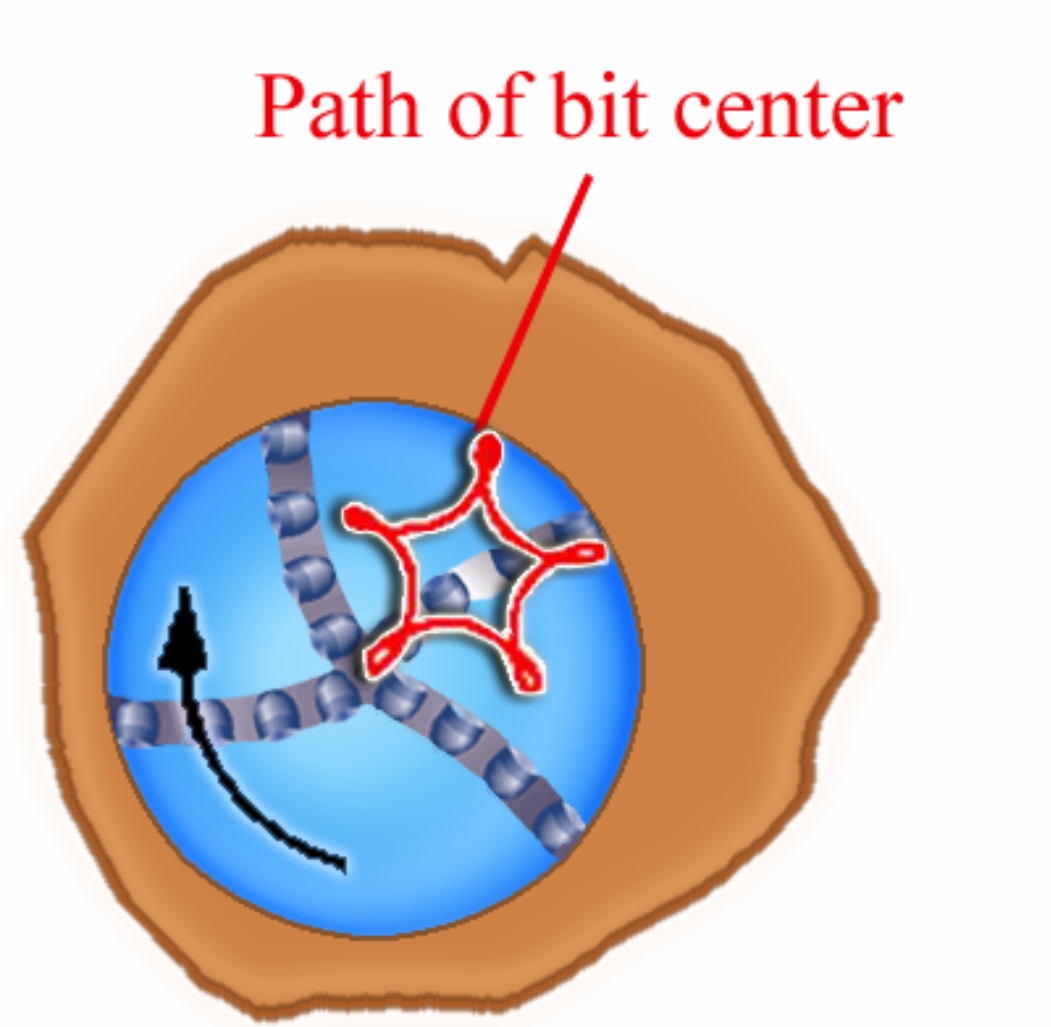

Figure 1.11: Bit whirl [8].

1.3.1. Characteristics of Dry Friction

The nature of dynamic friction forces developed between bodies in contact is extremely complex and is affected by several factors. Friction may be defined as a force of resistance acting on a body, which prevents or retards slipping of one body relative to another body or surface, with which it is in contact. This force always acts tangent to the surface at points of contact with other bodies and is directed so as to oppose the possible or existing motion of the body relative to these points [59].

In general, *dry friction* occurs between the contacting surfaces of bodies in the absence of lubricating fluid. This type of friction is often called *Coulomb friction*, since its characteristics were studied extensively by C. A. Coulomb in 1781. The theory of dry friction can best be explained by considering the example of pulling a block on a rough surface. Let us take a block with mass m which is sliding on a rough surface. The block is initially resting on the surface and a linear elastic spring, which has a stiffness k, is connected to its right end. The free end of the elastic spring is moving with a constant speed v_0 as shown in Figure 1.12.

The surface exerts a normal force acting upwards to balance the block weight and frictional force acting to the left to prevent the applied force from moving the block to the right. In equilibrium, the friction force is always equal to the applied force in magnitude but in a direction opposed to the direction of motion and the mass is acting as a fixed end of the spring. The spring force increases linearly with time while the block is stationary. Correspondingly, the friction force increases at the same rate to maintain equilibrium. When the friction force reaches a critical value, the block reaches unstable equilibrium since any further increase in the spring force will cause movement of the block. This critical value is called *static friction force* F_s . If the magnitude of the applied force is increased so that it becomes greater than F_s, the

block will start moving and the frictional force at the contacting surfaces drops slightly to a smaller value F_k, called *kinetic friction force*.

According to the theory of dry friction, both F_s and F_k are assumed to be directly proportional to the normal force P. This relation may be expressed mathematically as:

$$F_s = \mu_s P \tag{1.1}$$

$$F_k = \mu_k P \tag{1.2}$$

where μ_s and μ_k are coefficients of static and kinetic friction, respectively. For steady-state sliding, both coefficients are constants.

1.3.2. Sliding on Dry Surfaces and Stick-Slip Mechanics

The motion of a mass-spring system sliding on rough surface is described in the previous section for steady-state sliding. To understand the basic relation between friction and stick-slip oscillations, let us focus on the moment when the block is about to slide. At this instance, the block starts to move and the sliding dynamics of the block can be either steady, stick-slip or chaotic, as shown in Figure 1.13. For the steady-state sliding, the frictional force at the contacting surface drops slightly to a smaller value F_k, which is the *kinetic friction force* described in the previous section.

For stick-slip motion, stick-slip exists when the static friction coefficient is sufficiently higher than the dynamic friction coefficient. The block alternates between stick and slip modes in which the kinetic friction force can't be directly deduced, i.e. equation (1.2) is not valid anymore unless μ_k varies with time. Periodic stick-slip motion may result from various sources such as nonlinear properties of the system [60]. The amplitude of the stick-slip motion of the system shown in Figure 1.12 depends on the relative sliding velocity, stiffness of the spring and mass of the block.

The main difficulty in describing stick-slip motion is to define the kinetic friction forces which describe the encountered fluctuations. Several mathematical models have been proposed to tackle this problem. First, one needs to determine the parameters that influence the frictional force. Quite a few models are built based on the assumption that the frictional force depends on the instantaneous velocity. Some of these laws are depicted in Figure 1.14. Selecting the friction law that governs the sliding of a body on rough surfaces is an important step that must be taken into consideration while modeling the stick-slip oscillation.

In drillstrings, most of the studies follow the same principle mentioned above to describe stick-slip motion. However, the main dilemma is to adopt the most accurate law that will describe stick-slip easily but precisely. In the following section, the main concepts used to model stick-slip motion in drillstrings will be explained, and the discussion of details of the previous investigations and studies will be presented.

1.3.3. Stick-Slip Oscillations in Drillstrings

Stick-slip is the most detrimental kind of torsional vibration to the service life of oil well drillstring and downhole equipment. Successive stick-slip oscillations induce large cyclic stresses, which can lead to fatigue problems. Stick-slip oscillation as experienced in drilling process is an example of limit-cycle behavior. In mechanical systems, limit cycles often occur due to backlashes between contacting parts, nonlinear damping or geometrical imperfections.

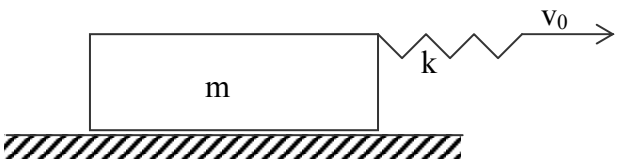

Figure 1.12: The mass spring model.

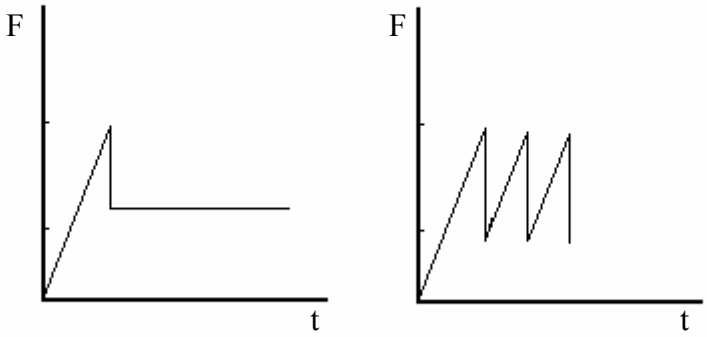

Figure 1.13: Sliding force response: (a) steady, and (b) periodic stick-slip.

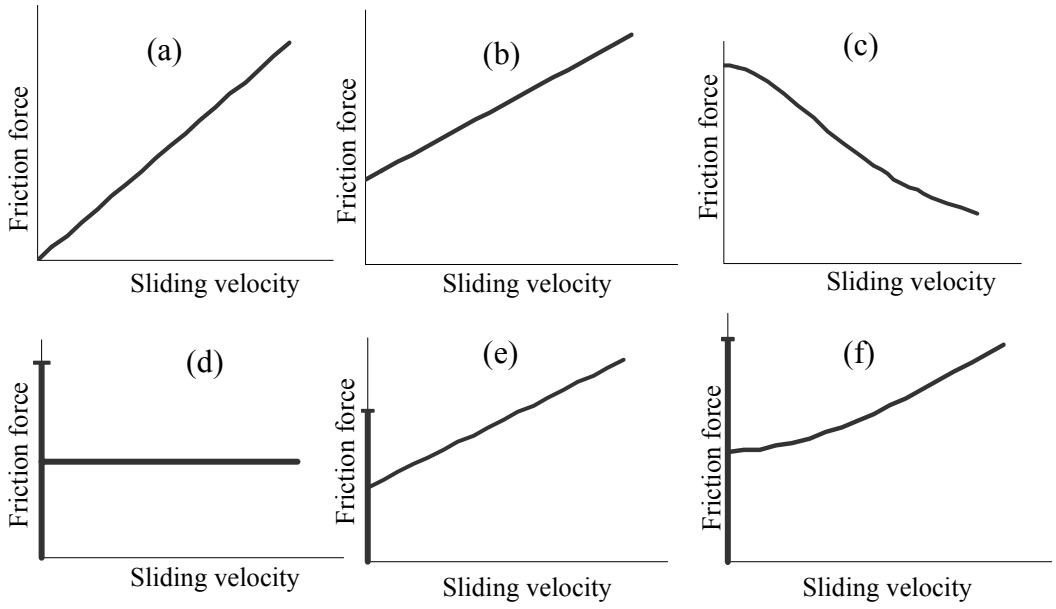

Figure 1.14: Some of proposed friction laws vs. sliding velocity.

Background

The terminology “stick-slip” comes from the nature of this phenomenon. It can be deduced from the term stick-slip that the phenomenon consists of two phases; the stick phase which represents the period when the rotational speed of the bit is almost zero and the slip phase, which is the interval when the angular velocity increases to reach two or three times the nominal surface velocity. The bit’s rotational speed is oscillating between these two phases due to the low torsional stiffness of the drillstring. Since the rotary table keeps on rotating with constant speed even when the bit is stuck, the string gets wound up, the torque is increased and the energy is stored in the string, which acts as a torsional spring. Field experience showed that the torque ramps up in a near-linear fashion until it reaches its maximum value [34]. When the bit can no longer withstand the increased torque, the energy is suddenly released and the bit starts spinning. The bit spins so fast that the drillstring unwinds and the torque drops. As a result, the bit slows down again until it finally comes to a complete halt, after which the whole process of winding and unwinding repeats itself [18].

In real field measurements [18], stick-slip vibrations appeared as low frequency torque fluctuations with periods of 2-10 seconds. During the stick phase, the torque builds up until it reaches an ultimate value, which can be determined by the static friction resistance of the BHA, i.e. the torque that can overcome the frictional forces of the rock. At this stage, more torque is required to overcome the friction in the stick phase than to keep the bit rotating. The developed energy is transformed as an increase in the velocity (slip phase). Figure 1.15 shows a comparison between downhole and surface speeds versus time. As shown in the figure, the rotary table speed is fluctuating between 45-65 RPM while the downhole speeds reach about 3-5 times the surface velocity. The average speed of the surface rotary table is 55 RPM,

which is constant over time, while the bit is oscillating between a complete standstill and a very high velocity during a period of 2-5 seconds. The amplitude depends upon the nature of the downhole frictional torque and the properties of the surface drive system.

The period of stick-slip vibrations depends on the length of the drillstring, the mechanical properties of the entire drilling system, the surface speed and the nature and location of friction [7]. On the contrary, the torsional resonance frequencies of the drillstring are nearly independent of the drilling parameters such as weight on bit and rotary table [9]. In general, torsional mode of the drillstring depends on the drillpipe length, size and mass of the BHA [12]. The natural frequency of the drillstring should be higher than the critical natural frequency to prevent the occurrence of stick-slip oscillations. It is known that, the critical natural frequency of the drillstring is proportional to the square root of the drillstring length [19], i.e. when the drillstring length is less than the critical length, the natural frequency will be higher than the critical natural frequency, and stick-slip will not occur. However, the drillstring is usually very long so that this condition is rarely satisfied. Beyond the critical length, stick-slip will be inevitable [20]. This can cause severe twist fluctuations in the drillstring of some 2-5 turns on top of the static twist.

It has been noticed that friction-induced vibrations are usually called self-excited vibrations to differentiate it from externally excited vibrations which are induced by external forces. Stick-slip is a self-excited vibration since it is induced by friction forces between the bit and wellbore [16, 22]. Stick-slip vibrations don't damp out because they perpetuate themselves. The drillstring rotates smoothly while off-bottom. The drillstring vibrations normally occur when the bit is on-bottom drilling.

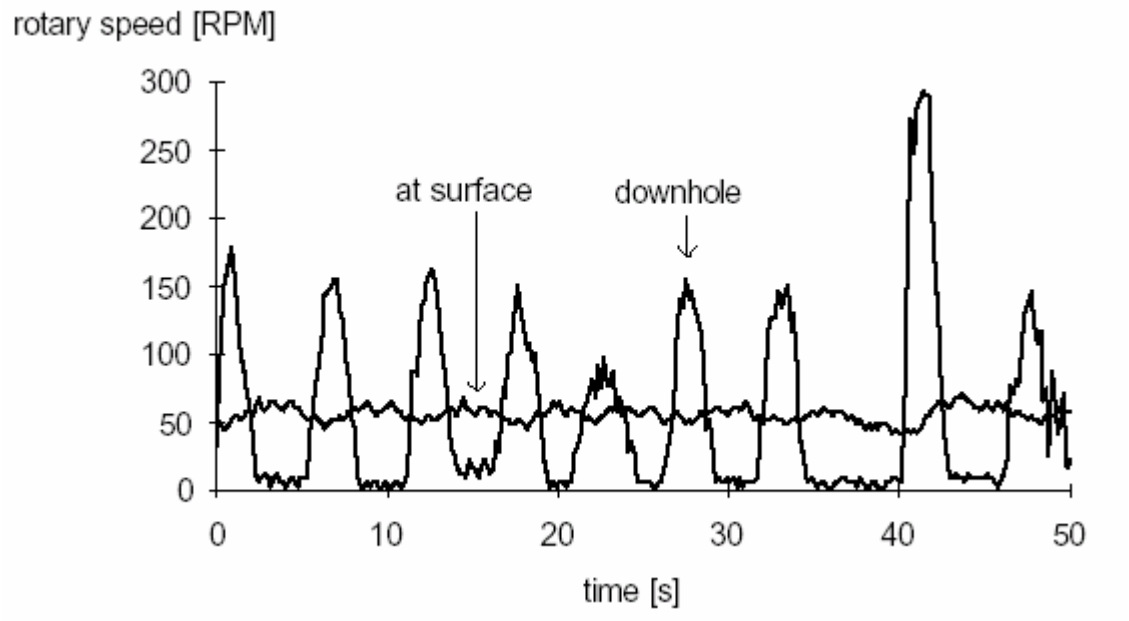

Figure 1.15: Comparison between surface and downhole rotary speeds during stick-slip oscillations [21].

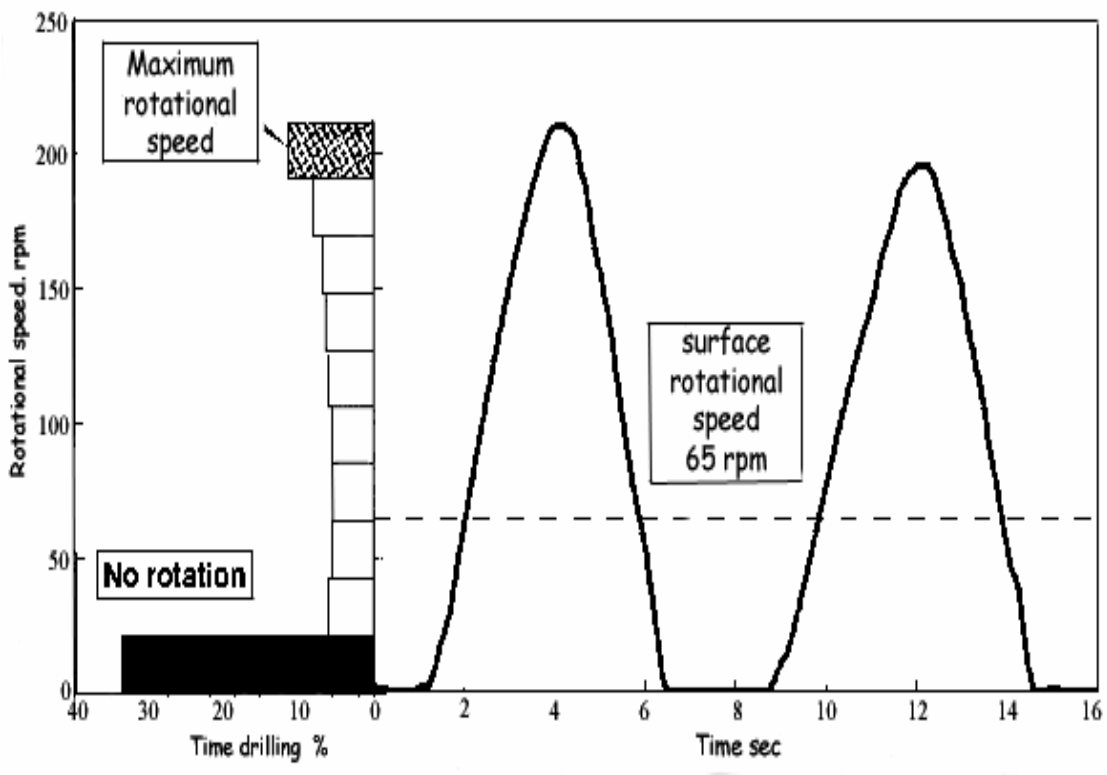

Figure 1.16: Bit speed fluctuations during stick-slip.

Effects of stick-slip Vibrations

Stick-slip vibrations have severe effects on the drilling bit and BHA. These vibrations occur in more than 50% of the total time of a classical drilling process. As illustrated in Figure 1.16, complete stop in stick phase may cover about 35% of the drilling time. Drillstring is occasionally subjected to high torque, which exceeds the maximum elastic limit of the drillpipe. However, the severity of these vibrations depends on the properties of the surface drive system, the rock/bit interaction and friction between drillstring and wellbore.

Stick slip vibrations can accelerate the bit and bearing wear, which result in premature failure of drillstring or breakage of the bit itself [45]. Furthermore, Stick-slip is a well-known cause of fatigue cracks, over-torqued drillpipe connections and twist-off of the drilling components. The damage of stick-slip is worse in hard rocks, at higher applied weight on bit, at lower rotary speed and with duller bits. Although stick-slip oscillations does not affect the rate of penetration, they can accelerate tooth breakage and reduce bearing/seal life [15]. Stick-slip is one of the major sources of the wellbore instability [18]. Stick phase can cause a stuck pipe problem. Axial and transverse vibrations can be excited by the high bit speed in the slip phase.

Monitoring Stick-slip Vibrations

Although the speed of the bit in the presence of stick-slip vibrations is fluctuating, the surface rotary speed is kept constant. Therefore, the downhole speed can’t be detected directly from the surface. However, torsional vibrations can be detected from the surface by monitoring the fluctuations of the surface torque. The frequency of surface torque oscillations will drop below the fundamental frequency; thus indicating the sticking time downhole. Moreover, peak surface torque will increase to a value higher than the one required to rotate the drillstring. Stick-slip

occurs when the difference between the maximum and minimum torque measured at the surface is more than 15% than the average torque [32]. Also because of the effect of inertia, the torque will decrease below the level required to rotate the drillstring as the bit and BHA break free downhole [34]. This can be measured directly by a torque sensor or indirectly by measuring the motor current of the surface drive system.

Most of torque gauges on the drilling rig cannot detect the small changes on torsional oscillations before stick-slip occurs. They can detect stick-slip when the torque fluctuations become large and deleterious stick-slip occurs [32]. Another indirect way is to monitor the fluctuations in the pressure drop over the hydraulic top drive [18]. Moreover, it is important to observe that the details of the downhole mechanism cannot be detected from the surface. The downhole measurements show that surface detection is not adequate in many practical applications. Comparisons between surface and downhole measurements show that the vibrations occurring on or close to the bit are up to one order of magnitude larger than the vibrations recorded at the surface [4]. Therefore, to increase the data reliability, the measuring instruments should be placed as close as possible to the drilling head [22].

Eliminating stick-slip Vibrations

It is always desired to cure or at least reduce the severity of vibrations in the drillstring. However, no single method exists that can solve this problem completely. In order to suppress all kinds of vibrations in the drilling process, it is important to define the parameters to be adjusted. Furthermore, measured parameters should describe the downhole situation completely and accurately. The genesis of stick-slip vibrations has to be really understood to improve the drilling process. Many remedies are proposed as solutions for this problem. In the field, stick-slip can be reduced by either decreasing the weight on the bit or increasing the rotary table speed [4, 45].

Some field investigations performed by Elf [32] indicated that every drilling operation has a unique critical speed above which stick-slip stops. This critical speed depends on the rig mast, the type of the drive used, the drillstring configuration and the conditions of the well. The amplitude of the stick-slip vibrations increased markedly as the rotary speed increased until the speed reached the critical threshold at which the vibrations vanish [20]. Stick-slip amplitude can be reduced by lowering the rotary speed but it will not die out until the rotary speed comes to zero [20]. Nevertheless, in some cases, there are some limitations on the range of speeds used to be compatible with other drilling objectives such as directional control. Therefore, the safe drilling speeds range needs to be investigated and optimized [31, 23]. Furthermore, increasing the rotary speed may cause lateral problems such as backward and forward whirling, impacts with the borehole wall and parametric instabilities. Hence, increasing the rotary speed or decreasing the weight on bit is not always a successful way to suppress stick-slip. Other solutions could be helpful such as lubricating the mud pills or adjusting mudflow rate and properties. Unfortunately, it is difficult and expensive to manipulate the mud properties to achieve the desired results. If downhole motor is used, it assists the decoupling of the drillstring from axial and torsional vibrations of the bit. One of the most promising methods is the torque feedback rotary table. The objective of this method is to damp the torsional vibration instead of reflecting it back to the BHA [10, 37].

2. LITERATURE REVIEW

Extensive research has been focused on the vibrations of drillstrings. This reflects the importance of this field in drilling technology. Various studies have concentrated on different aspects of drilling vibrations. Researchers attempted to clarify and understand the nature of vibrations of the drillstring, the bit and other components of the drilling rig. Since 1950s, numerous investigations have been reported on this topic. Some of these studies focused on theoretical and mathematical models to describe the dynamics of the drillstring while most of the studies concentrated on field investigations and measurements [9].

Drillstring vibration is a very complex phenomenon because many parameters are involved in generating multidimensional vibrations. The non-linearity of the problem and the ever-changing formation characteristics encountered in the drilling process complicate the drilling optimization process. Uncertainty still exists in the analysis of drillstring vibrations. The use of experimental measurements is normally utilized for solving drilling problems [25]. However, mathematical modeling is crucial to the understanding and validation of experimental and field measurements. In general, Field investigations, laboratory tests and mathematical models contribute to identify the types of vibrations encountered in the drilling process and the proper ways to cure them.

Before 1980s, torsional vibrations were not considered as one of the major sources of drilling process dysfunction. Therefore, torsional vibrations and their influence on the drilling performance have not been discussed extensively in the literature [26]. In 1986, Halsey et al. [9] postulated that torsional vibrations can lead to violent drilling problems when their amplitudes become very high. Since then,

torsional drillstring vibrations, in particular, stick-slip oscillations have attracted the interest of many investigators in the last two decades [9, 10, 22].

2.1. Review of Stick-Slip Phenomenon

Before reviewing the investigations reported in the area of drillstring vibrations, it is valuable to discuss briefly the investigations on the stick-slip phenomenon from the mechanics point of view. Several studies investigated the nature of friction between two sliding bodies. Most researchers used simple mass-spring system, similar to the system shown in Figure 1.12, in order to simplify the problem. The investigators, depending on the scope of the study, have followed different approaches. Some investigators addressed the stability of the system while others search for the most suitable function that describes this nonlinear contact phenomenon.

Galvanetto and Bishop [53] studied the effects of friction and damping on the dynamics of a single degree of freedom oscillator (see Figure 2.1) wherein the belt is moving at a constant velocity (v_0). The block will move at velocity equal to belt's velocity until the reaction forces (stiffness and damping forces) become equal, in magnitude, to the static friction force. Hence, the stick phase can be represented by the following inequality:

$$-F_s < F < F_s$$

where F represents the combined damping and stiffness forces. The force F_s is the static friction force given by $\mu_s mg$. For the slip phase, the block starts slipping when $|F| > F_s$. At this instant, relative velocity is still zero. The governing equation is

$$m\ddot{x} + c\dot{x} + kx = \mu_d F_s \tag{2.1}$$

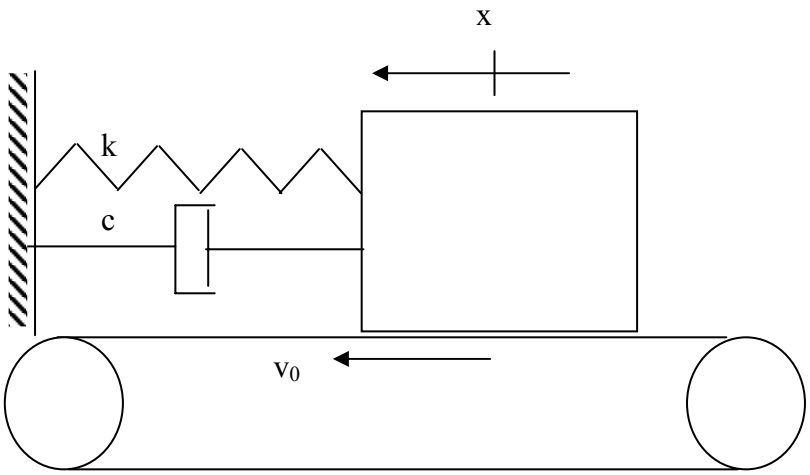

Figure 2.1: single degree of freedom oscillator.

where μ_d is the ratio between the dynamic friction coefficient and the static friction coefficient, which is a function of the relative velocity $(\dot{x} - v_0)$ between the block and the belt.

Equation (2.1) is the basic equation in most of the studies concerning stick slip oscillations. The main difference between the proposed models is in the assumptions made to define the force term in equation (2.1). Several approaches have been followed in order to make the numerical results comply with real systems. Some studies suggested the utilization of variable friction coefficient as a function of relative velocity [53, 56]. Other studies used constant friction coefficient but assumed the force as a function of sliding velocity [20, 23, 25, 29].

Oden et al. [54, 55] studied the effect of normal oscillations on sliding friction using a simple two-degree of freedom system of mass *m* restrained by a horizontal spring *k*. The body is sliding on a surface at constant velocity. The system is similar to the one depicted in Figure 1.12. Two main approaches are proposed in their analysis. The first approach employs a mechanical law which takes into account the normal contact constitutive relations. This law includes the normal-to-surface force (weight of the body) as a major contributor in the initiation of stick-slip oscillation. The second approach is a friction law, wherein no distinction between the coefficients of static and kinetic friction is made.

Unfortunately, most of the investigations made in stick-slip phenomenon cannot be applied directly to the drillstring motion although it gives an insight into the phenomenon itself. These investigations furnish the basis for the assumptions made in order to understand the drillstring nonlinear behavior.

2.2. Causes of Stick-Slip Motion in Drillstring

Brett [23] attributed the torsional vibrations genesis to the bit characteristics. He relied on theoretical models, experimental investigations and field data to prove that inherent PDC bit characteristics can initiate torsional vibrations even though the drillstring may rotate smoothly when the bit is off-bottom. He explained the torsional vibrations in different cases for PDC bits under different conditions. Furthermore, he explained why torsional vibrations are more common in PDC bits than tri-cone bits. Based on laboratory studies, he showed that PDC damage could occur after only a short period of time if a PDC bit spins backward in relatively hard rocks [27]. These laboratory measurements confirmed the reduction in bit torque as rotary speed decreases. It was also shown that a nonlinear negative damping exists between the torque at the bit and the rotary speed.

Most of the investigations in the literature attributed the stick-slip to static friction effects [9, 26]. The rock/bit interaction is one of the major sources of stick-slip oscillations [16, 22]. Challamel et al. [22] proved that the rock cutting process is responsible for the self-excited phenomenon and they explained the fundamental mechanism of stick-slip vibrations using rock mechanics considerations. Their description was verified by theoretical and experimental investigations.

Wang and Lin [20] performed a numerical simulation to study the effect of dry friction on the drillstring torsional vibrations. They discussed the effects of viscous damping, rotary speed and natural frequency of the drillstring on the amplitude, frequency and mean distortion of the stick-slip vibrations. Their results were in good agreement with field data for the case of drilling bit off-bottom. However, severe stick-slip vibrations occurred only when the drill is on-bottom and these vibrations were not encountered while the bit was off-bottom [23].

Baumgart [29] considered the pressure and the rate of flow of the mud as major parameters that affect the drillstring vibrations. His proposed model explained the influence of the flow of compressible, viscous mud on the motion of the drillstring as well as other parameters. He observed that there was a strong relationship between the pressure of the mud and buckling of the drillstring. Mud properties may assist the initiation of stick-slip and bit bounce.

Richard and Detournay [4] argued that the stick-slip vibrations are induced due to rock/bit interaction. They considered the coupling between vertical and torsional vibrations as alternative cause of stick-slip vibrations. Based on laboratory data, they observed that such a coupling is sufficient to generate stick-slip oscillations without the need to assume a decreasing friction coefficient.

Yigit and Christoforou [30, 31] considered the coupling between torsional and bending vibrations in their lumped parameter model [30]. The axial effect was included later [31]. They noticed that axial vibrations had positive effect in reducing stick-slip vibrations, while stick-slip can enhance axial and lateral vibrations.

2.3. Mathematical Modeling of Drillstring with Stick-Slip

In order to understand the stick-slip phenomenon, some mathematical models have been proposed to simulate the drillstring dynamics under various conditions. Both analytical and numerical approaches are employed to describe the BHA movement. There are common difficulties associated with the existing models which lead to inconsistency with field data. One of the major problems is the inaccurate description of some of the involved parameters and/or downhole boundary conditions, which affect the model. Neglecting some of the factors and reducing the number of key parameters decreases the overall accuracy of the model. Seeking universality of the model and detailed description of drilling processes are often compromised by

practical limitations of the model's complexity [39]. Moreover, the analysis of stick-slip phenomenon is difficult because the modeling of the static and kinetic friction mechanism lead to discontinuous differential equations [40].

The lack of a coherent model in the literature that is free from unwarranted assumptions makes it difficult to assess the nature of many approximate treatments and thereby to get a clear overview of the significance of model predictions [41]. Most existing mathematical models of such phenomenon ignored the effects of essential non-linearities inherent in the stress-strain constitutive relations; for instance the nature of frictional forces between string, bit and borehole, large amplitude excitations, in addition to the effects produced by combined axial, flexural and torsional wave propagation along the drillstring. The importance of dynamic non-linear interactions is recognized by drilling engineers but little detailed theoretical understanding of their origins exists [38].

For the last several years, various mathematical models are based on a single degree of freedom torsional pendulum [4, 9, 16, 19, 20, 23, 26, 30, 33, 42]. They have used a rigid body with constant mass and moment of inertia to model the BHA and a linear spring to model the drillstring. Most often, the friction is taken as a non-linear function and is fitted using field data [4, 23]. These simple models can provide, to some degree, a qualitative insight into a specific complex phenomenon occurring in reality. The aim of these models is to explain the observed phenomenon and identify possible causes. However, such models cannot address the other effects due to the continuum nature of the drillstring and hence the torsional wave propagation was neglected. These models were limited to the lowest torsional mode of the drillstring. The twisting of BHA was neglected in such models as well as the inertia of the drillpipe.

The general equation used to model the drillstring as single degree of freedom torsional pendulum is given by:

$$I_p\ddot{\phi} = -k_t(\phi + \dot{\Omega}t) - T \tag{2.2}$$

where I_p is the mass moment of inertial of the drillcollar (some authors included the drillpipes inertia partially), T is the torque on bit and ϕ is bit angle of rotation, k_t is the torsional stiffness of the drillpipe and $\dot{\Omega}$ is the rotary table speed.

Halsey et al. [9] presented a mathematical analysis to compute the torsional resonance frequency of the drillstring and verified the results with experimental data. The resonance frequencies were found to be very sensitive to geometric parameters and downhole conditions, while they were nearly independent of rotational rate, WOB and damping ratio [26]. Halsey et al. [26] discussed several parameters that induced or sustained stick-slip oscillation. They presented a non-linear mathematical model to describe stick-slip phenomenon assuming that drillstring behaves like a simple torsional pendulum. In their model, they adopted the assumption that stick-slip was already generated and developed a steady-state motion. Furthermore, the twisting of the BHA was neglected and the rotary speed was kept constant. The last two assumptions were also adopted by Dawson et al. [42] and Brett [23].

In general, the simple torsional model can describe the nonlinear behavior of only the lowest torsional mode in a drillstring. In reference [26], they calculated the period of the oscillation, the time while the bit was stuck and the maximum induced torque. It was found that two factors may be considered in order to cure stick-slip problem. These are reducing downhole static friction and/or controlling rotary table speed. However, in their study, no backward rotations were included. They divided the stick-slip oscillation into two regimes identified by stick and slip modes. In each regime, the torque term is represented by a distinct expression. The torque was

assumed to be constant during slip phase while it varied by a constant amount during stick phase, as expressed by the following equation:

$$\begin{aligned} &\text{slip} \quad \text{phase}: \quad T = T_c \qquad\qquad \text{for} \quad \frac{d\phi}{dt} > 0 \\ &\text{stick} \quad \text{phase}: \quad |T| \le T_c + \Delta T \quad \text{for} \quad \frac{d\phi}{dt} = 0 \end{aligned} \tag{2.3}$$

where T_c is the constant Coulomb friction torque and ΔT is the extra torque needed to start or to break the BHA loose. This torque is also depicted in Figure 2.2 where Γ is the time period and t_0 is the duration of slip phase.

If one plots torque vs. velocity, the graph becomes identical to that of case (d) in Figure 1.14 regarding the constant coulomb friction torque. In Figure 2.2, the bit is assumed to start slipping at t=0. At this instant, the torque must be equal to the maximum friction torque in equation (2.3), i.e. $T=T_c+\Delta T$. This is the initial condition used to solve the equation during slip phase. The initial conditions for equation (2.2) are:

$$\begin{aligned} &\phi = \frac{-(T_c + \Delta T)}{k_t} \\ &\left.\frac{d\phi}{dt}\right|_{t=o} = 0 \end{aligned} \tag{2.4}$$

The displacement was assumed to be harmonic as follows:

$$\phi = A\cos(\omega\, t - \alpha) + B \tag{2.5}$$

where A and B are constants and α is phase angle.

Dawson [42] used the following piecewise linear function to model the torque term in equation (2.2):

(2.6)

$$f(\dot{\phi}) = \begin{cases} F_1 - \dfrac{F_1 - F_2}{\dot{\Omega}}\dot{\phi} & 0 \le \dot{\phi} < \dot{\Omega} \\ F_2 & \dot{\phi} \ge \dot{\Omega} \end{cases}$$

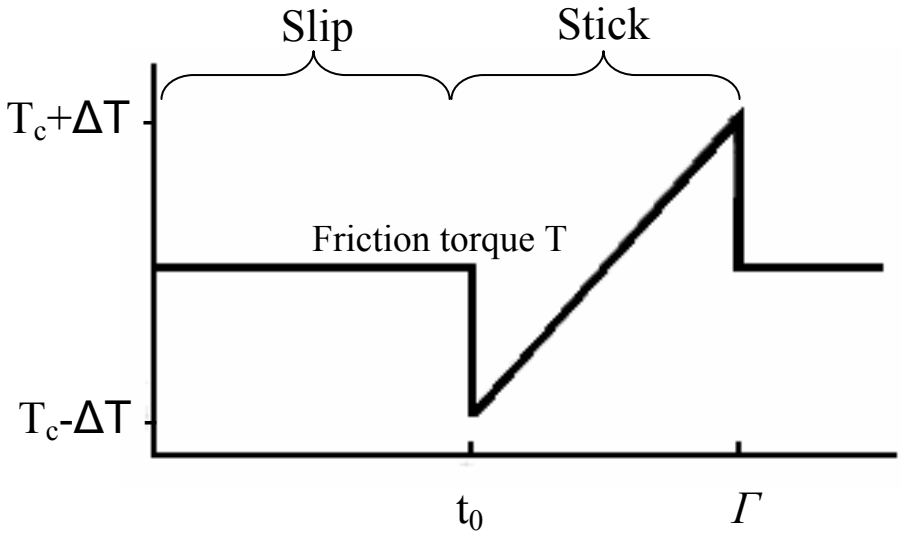

Figure 2.2: Friction torque (T) vs. time during slip and stick phases.

where F_1, F_2 are the maximum and minimum values of friction, respectively, and $\dot{\Omega}$ is the rotary table speed.

A similar approach was followed by Wang and Lin [20]. They stated that the piecewise linear model used by Dawson in equation (2.6) does not seem accurate enough. However, they presented an exponential expression to model dry friction while off-bottom:

$$f(\dot{\phi}) = F_2 + (F_1 + F_2)\exp(-\gamma\dot{\phi})^{\delta} \tag{2.7}$$

where ϕ is angular displacement, F_1, F_2 are the maximum and minimum values of friction, respectively, and γ, δ are constants.

Brett [23] used similar model to the one proposed by Halsey et al. [26]. No damping term was introduced in his model, but he introduced a negative damping at the bit. To model the torque term, two terms were introduced: drillpipe frictional torque and bit torque. When rotating off-bottom, the friction torque was taken as constant because numerous observations show that the off-bottom torque has only weak dependency on rotary speed. Figure 2.3 shows an example of such a relationship of bit torque vs. rotary speed, as observed in the field and followed in the model. It was shown that dependence of torque on speed may have caused stick-slip vibrations.

Richard et al. [16, 45] adopted some assumptions to simplify the torsional model. This model assumed that PDC bits were used in the drilling operation. They assumed the borehole and the drillstring are both vertical and straight, and lateral vibrations did not influence them. A constant upward force and a constant angular velocity at the rotary table were considered as the applied boundary conditions. The friction was taken at the bit only. Their attempt was directed to study the effect of axial force on torsional vibration. In this model, the WOB and TOB were divided into two terms: cutting and friction forces. The cutting components correspond to the

forces transmitted by the cutting face of each cutter and the friction components by the other contact between the bit and the rock. The cutting force is assumed to be proportional to the cross-section area of the cut. Friction torque depends on the WOB. The WOB is assumed to oscillate harmonically around its mean value ($W_0 = Mg$) at frequency equal to the first axial natural frequency.

Jansen [19] attempted to simplify the torsional spring model by representing the static and sliding torques as linear functions to set up a linear set of equations that can be analyzed using linear system theory. The torque is taken as a simple step function; see case (d) in Figure 1.14. It is assumed that the bit will not rotate backward but it can come to a complete momentarily standstill while the drillpipe never come to a complete stop. They produced two systems of equations (one for stick phase and another for slip phase). No coupling with lateral and axial excitations was introduced.

Leine et al. [2] combined the torsional pendulum model and drillcollar lateral motion to describe the stick-slip whirl interaction. The BHA was modeled as a rigid disk at the end of massless flexible drillpipe. They attempted to identify the possible causes of the transition from stick-slip to whirl or vise versa. This transition was attributed to the interaction between bending and torsional motion [2]. From the four possible sources of the interaction (eccentricity, gyroscopic effects, anisotropic bending stiffness and mud fluid force), they considered fluid force as the possible cause of such interaction. The study, however, could not assure that the existing phenomenon is due to fluid force.

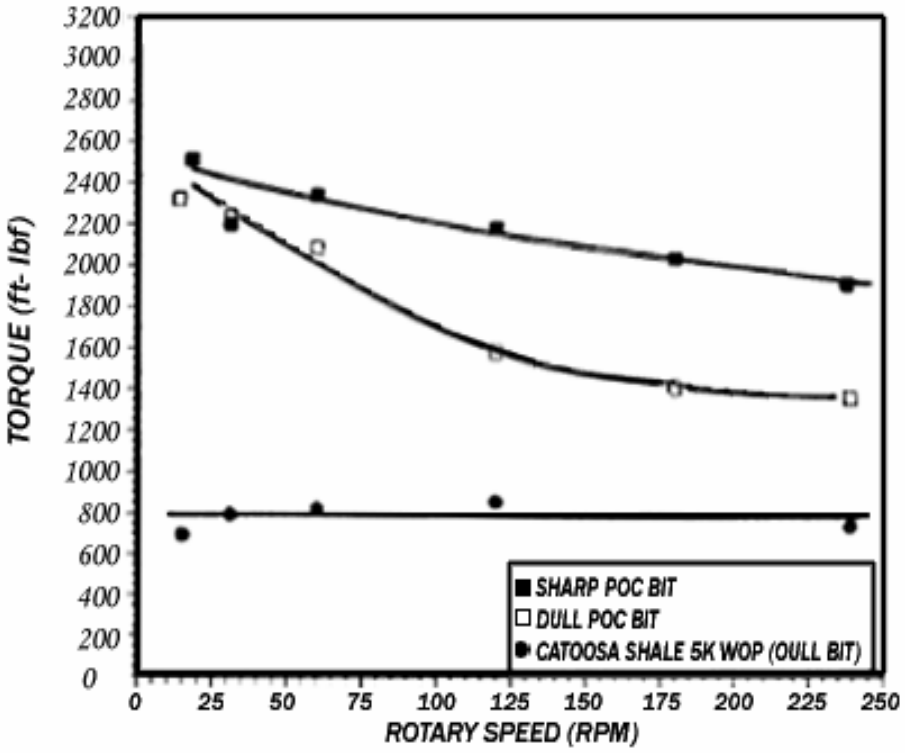

Figure 2.3: Torque on bit vs. rotary speed [23].

Yigit and Christoforou [25, 30] used the assumed mode method to model the drillstring. The drillpipe inertia was included partially in the equation. Fluid forces, damping and bending-torsional coupling were included. Stabilizers were modeled as simply supported boundaries. The BHA was rigid and the drillstring was fixed to the rotary table. The governing equations were derived for bending and torsional vibrations. Later, they extended their model to include axial motion [31]. Both WOB and TOB were redefined to be a function of ROP as well as angular displacement [31].

Recently, Tucker and Wang [33, 38, 41] developed a numerical approach using a six continuous independent degrees of freedom model to describe the motion of the drillstring; defined as Cosserat rod model; three to describe the motion of the line of centroids of drillstring cross-section while the remaining three defines the elastic deformation of the drillstring about that line. The drillpipe is connected to lumped elements with inertia at each end to represent the BHA and the rotary table. Empirical accommodations of the interaction between the borehole and BHA were added to formulate a mathematical model that describes the drilling assembly. The model includes the coupling between axial, lateral and torsional motion as well as the boundary and initial conditions of the drillstring and BHA. The torsional wave propagation in the drillstring was investigated to address the control of vibration by torque feedback at the rotary table. The solution was obtained by ignoring lateral and axial vibrations and assuming a torsional pendulum. Torques are assumed to be at the rotary table (motor torque) and on the bit (friction torque).

The low dimensional models have some limitations due to their simplicity. Parameters such as axial stiffening or elastic coupling can't be modeled precisely. Such models were based on simple lumped mass-spring-damper systems. The major shortcoming of the simplified models is ignoring the dynamics of the drillpipe by

assuming it to act as a massless spring. It is crucial to develop a general model that produces a reasonably accurate numerical solution. The finite element analysis is considered as one of the most practical method for the analysis of drillstring systems. Some studies were carried out to capture the complexity of drillstring motion using the finite element method.

Baumgart et al. [24, 29, 56] developed a finite element model to simulate BHA whirl and stick-slip phenomenon. Each nodal point represented a stabilizer, a collar connection or a wear knot moving viscously damped inside an open hole or a casing. The friction force was treated as being dependent on the contact velocity. Axial degree of freedom was not included in the analysis. Moreover, full coupling between structural vibrations was not introduced in the study. They derived the governing equation by applying the virtual work principle to the finite field elements and nodes. Gravitational effects were taken as distributed external forces. The tangential force followed coulomb friction law, equation (1.2), but the coefficient of friction μ was taken as a function of lateral and torsional velocities and defined by a characteristics curve as shown in Figure 2.4.

Although the problem of stick-slip was not studied extensively using finite element models, many investigations tackled different aspects of the drillstring using FEM. The bottom hole assembly behavior was studied using a general purpose finite element program by Millheim et al. [65]. Commercial finite element software was employed to model the BHA only. A beam element with six degrees of freedom was used to idealize the drillcollar. A gapping element was used to model the annulus between the borehole centerline and the borehole walls. Drillpipe was not taken into consideration in this study. This model analyzed the BHA under various static conditions. A nonlinear stress-strain relationship was included to represent the contact

between the drillcollar and borehole walls. The dynamic coupling as well as rotational effects were not considered.

The lateral vibration generated by axially-induced bit excitations was studied by Dunayevsky et al. [66]. They discussed the stability of drillstring under fluctuating WOB. The principal assumption underlying their model was that the drillstring remains in permanent contact with the wellbore wall along its entire length. This implied that there will be no possibility of impact between the drillstring and the borehole. Torsional and gyroscopic forces have been ignored. The axial and lateral motions were coupled only through the parametric resonance mechanism, which is valid for small curvature boreholes. The finite element model was used to analyze the lateral vibrations of the drillstring. This model did not simulate the actual time evolution of drillstring vibrations. It only indicated possible failure mode.

The forced harmonic response of BHA was performed by Mitchell and Allea [68] using a general purpose finite element program. Their model was limited to predict lateral vibrations and the critical rotation speeds that caused BHA failure. The predicted speeds were compared to the operating conditions encountered in practice at the time of failure.

Although many investigations tackled the modeling and analysis of drillstring dynamics, a comprehensive understanding of all vibration phenomena involved is still lacking. Most of the cited investigations were restricted to the dynamics of the BHA. Accordingly, the effects of the gyroscopic motion as well as other coupling mechanisms of the drillstring vibrations have not been fully considered. Moreover, the gravitational field stiffening effect was not taken into account in most previous studies.

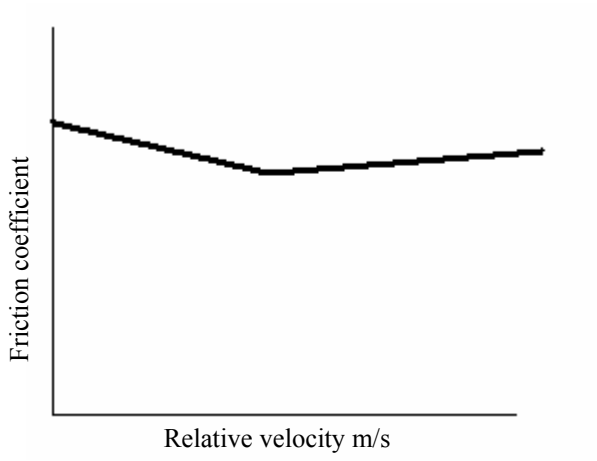

Figure 2.4: Definition of characteristics curve for bit formation cutting.

Apparently, there is a need to formulate a finite element model that includes the dynamics of the drillstring and BHA. A fairly general model must account for the axial-bending coupling and the dynamic coupling between bending and torsional deformations, in addition to rotary inertia, gyroscopic effects and gravitational stiffening as well as the variation in drillstring geometry. Such a model will provide a reliable platform to investigate the stick-slip phenomenon and to gain more insight into the dynamic behavior of drillstrings.

2.4. Objectives and Approach

The objective of this study is to establish an accurate mathematical model to dynamically analyze stick-slip behavior in drillstrings using a consistent mass finite element formulation. The model is developed to accommodate various boundary conditions and external excitations that may exist in real field applications. The adopted finite element has two nodes at its ends. Each node has six degree of freedom: two transverse displacements, two bending rotations, one axial displacement and one torsional rotation. The developed finite shaft element permits different geometries of the drillstring components, whereas elements of different lengths and cross sectional properties are permitted. This model accounts for all the dynamic effects and structural coupling mechanisms pertinent to drillstring elastic motion. The following are the objectives of this study:

1. To develop a model that accounts for the coupling in the drillstring. Two types of coupling are introduced in this model: axial-bending and torsional-bending coupling. These couplings are dependent on the nodal coordinate of the system. Axial-bending coupling is introduced in the stiffness matrix while torsional-

bending coupling is in the inertia matrix. The explicit forms of coupling matrices are derived and tabulated.

2. To develop a finite element program that assembles the dynamic model of the whole drillstring in terms of the consistent finite element matrices. In addition to the axial-bending and torsional-bending coupling effects, the coefficient matrices account for the effect of rotary inertia, gyroscopic moments and axial stiffening at the element level. This program is capable of performing modal and time response analyses for both full-order and reduced-order models. In the reduced-order model, a modal transformation is invoked to represent the dynamic system in terms of a reduced set of modal degrees of freedom. In this case, only the significant modes are retained. A subroutine is developed to recover the nodal coordinate at every time-step to update the forcing vector and the elemental coupling matrices at each time-step. The system matrices and the global force vector are then computed using the updated elemental matrices and force vectors.
3. To perform a numerical study of the natural frequencies and mode shapes of the drillstring by solving for the generalized eigenvalues, which are associated with the free vibrational problem. The effect of different drillpipe/drillcollar ratios on the drillstring natural frequencies is then investigated.
4. To establish a stick-slip model by identifying the key parameters pertinent to this phenomenon. A mathematical model will be formulated to simulate stick-slip under various conditions. A profile is chosen to accommodate the expected variation of the friction torque as a function of bit angular velocity.
5. To integrate the governing equations of motion forward in time to obtain the dynamic response of the drillstring due to stick-slip excitations, for a wide range of parameter variations; e.g. rotary table speed, WOB, TOB, etc.

3. DYNAMIC MODEL OF THE DRILLSTRING

This chapter is devoted to derive the dynamic model of the drillstring in the form of a set of differential equations that govern the general motion of the drillstring. The basic drillstring consists of drillpipes, drillcollars and stabilizers. The kinetic and potential energy expressions are obtained and utilized to derive the governing equations using Lagrangian approach. The dynamic model of the drillstring adopts the following assumptions: a) The material of the drillstring is elastic, isotropic and homogeneous. b) The drillstring is assumed to be vertical and straight. c) The deflection of the drillstring is represented by displacement of points of its centerline. d) The internal damping and flow-induced forces are neglected. e) The drillstring boundary conditions are as shown in Figure 3.1, wherein the top of the drillstring is assumed to be fixed to the rotary table, while the bit is modeled as a laterally constrained end. Stabilizers are accounted for by locking the lateral displacement at their locations [57]. The following formulation of the developed finite element is an extension of the work performed in reference [57].

Referring to Figure 3.2, two reference frames are employed to describe the motion of the drillstring. The $X\ Y\ Z$ Cartesian coordinate system represents fixed reference frame and the other is a rotating reference $x\ y\ z$. The *X*- and *x*-axis are collinear and coincident with the undeformed drillstring centerline. The angular displacement between the two reference frames is $\Omega(t)$.

The finite element method is used to model the drillstring. Let $X^i\ Y^i\ Z^i$ be a Cartesian coordinate system with its origin fixed to the undeformed element. The coordinate $x\ y\ z$ is a Cartesian coordinate system after the deformation of the element. Consider an arbitrary point p^i on the undeformed element. With respect to

$X^i\ Y^i\ Z^i$ coordinate system, point p^i is defined by the vector $\bar{r}_0$. Point p^i is then transformed into point p in the deformed state of the element. The location of p with respect to $X^i\ Y^i\ Z^i$ coordinate system is given by the vector $\bar{r}$. The global position of point p is defined by the vector $\bar{r}_p$ as.

$$\bar{r}_p = \bar{R} + \bar{r} \tag{3.1}$$

where $\bar{R}$ defines the location of the origin of the $X^i\ Y^i\ Z^i$ coordinate system with respect to global coordinate system $X\ Y\ Z$. The vector $\bar{r}$ can be represented as

$$\bar{r} = \bar{r}_0 + \bar{u} \tag{3.2}$$

Therefore, the position vector $\bar{r}_p$ of point p can be written as

$$\bar{r}_p = \bar{R} + \bar{r}_0 + \bar{u} \tag{3.3}$$

where $\bar{u}$ represents the deformation vector of point p^i.

The element undergoes axial deformation u in the X direction and two bending deformations v and w in the Y and Z direction, respectively. Referring to Figure 3.3, the $x\ \ y\ \ z$ coordinate system is related to the $X^i\ Y^i\ Z^i$ coordinate system through a set of angles ϕ, θ_y and θ_z. To achieve the orientation of any cross-section of the element, first, the element is rotated by an angle $(\Omega + \phi)$ about the X^i axis, then, by an angle θ_y about the new y-axis, and by an angle θ_z about the final z-axis. The instantaneous angular velocity vector $\bar{\omega}$ of the $x\ \ y\ \ z$ frame can be expressed as

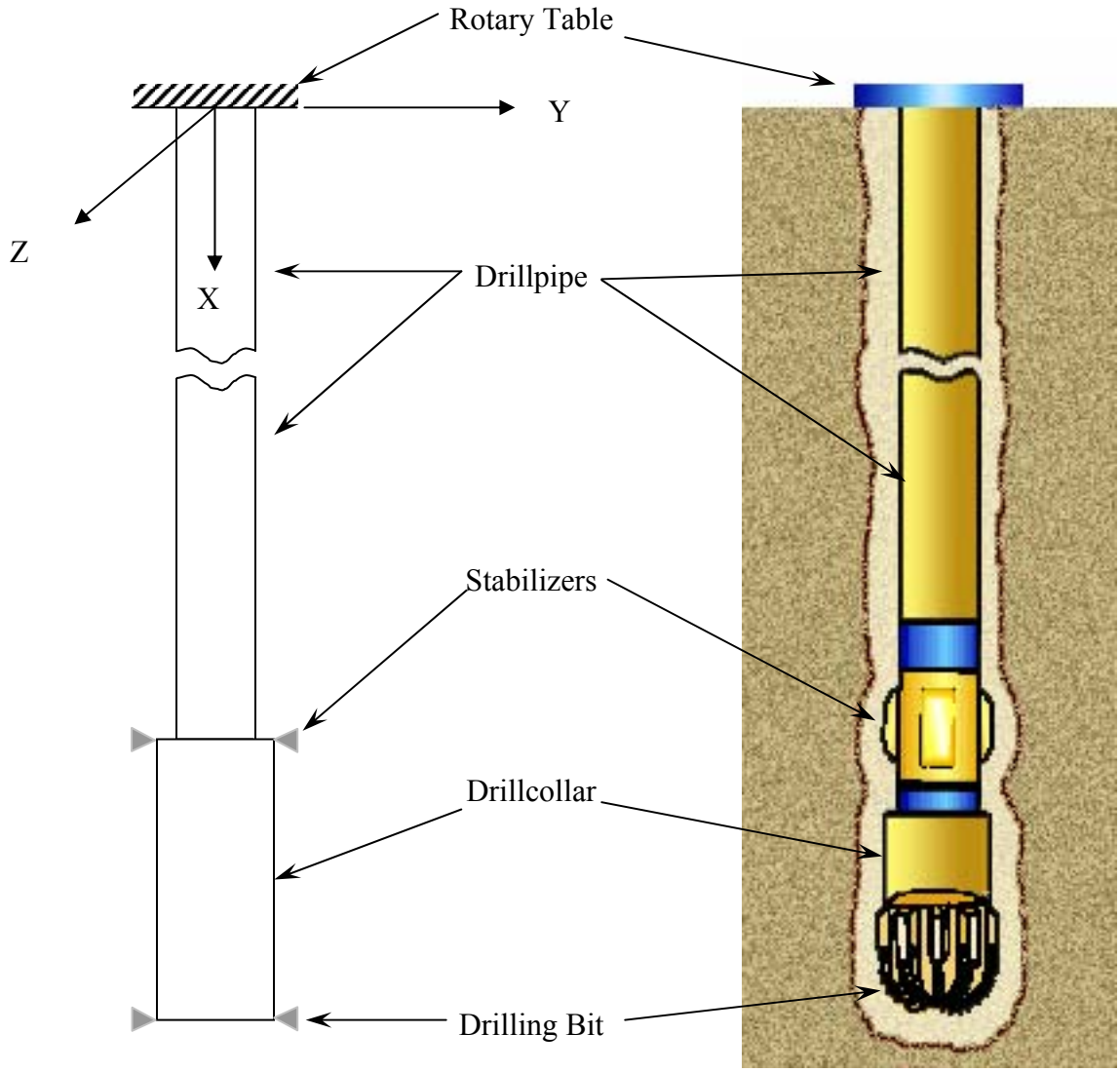

Figure 3.1: Drillstring configuration.

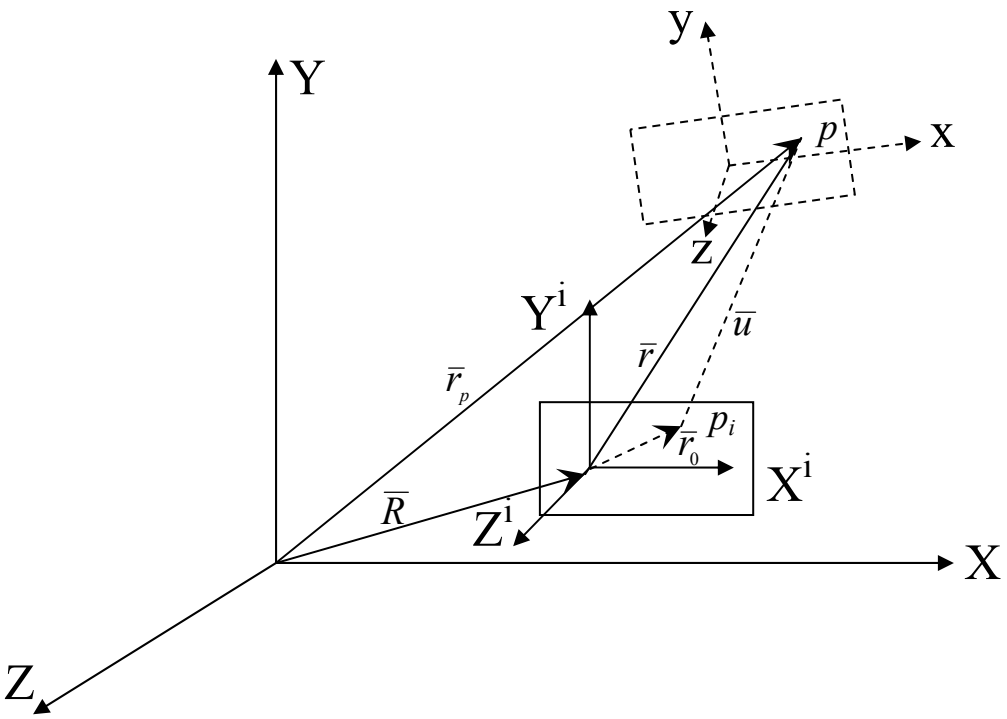

Figure 3.2: Generalized Coordinate of the ith element.

$$\overline{\omega} = (\dot{\Omega} + \dot{\phi})\hat{I} + (\dot{\theta}_y)\hat{j}_1 + (\dot{\theta}_z)\hat{k}_2 \tag{3.4}$$

where $\hat{I}, \hat{j}_1$ and $\hat{k}_2$ are unit vectors along the *X*, y_1 and z_2 axes, respectively. The term $\dot{\Omega}$ represents the constant angular speed of the rotary table. Transforming equation (3.4) into $X\ Y\ Z$ coordinate leads to the following expression:

$$\begin{aligned}\overline{\omega} = {} & (\dot{\Omega} + \dot{\phi})\hat{I} + \dot{\theta}_y[\cos(\Omega + \phi)\hat{J} + \sin(\Omega + \phi)\hat{K}] \\ & + \dot{\theta}_z\left[-\sin(\theta_y)\hat{I} - \sin(\Omega + \phi)\cos(\theta_y)\hat{J} + \cos(\theta_y)\cos(\Omega + \phi)\hat{K}\right]\end{aligned} \tag{3.5}$$

Assuming θ_y and θ_z are so small deformations and utilizing the linear theory of elasticity, the following substitutions can be introduced:

$$(\cos(\theta_y) = \cos(\theta_z) = 1)\ , \quad (\sin(\theta_y) = \theta_y) \quad and \quad (\sin(\theta_z) = \theta_z)$$

Now, equation (3.5) can be rewritten as:

$$\begin{aligned}\overline{\omega} = {} & (\dot{\Omega} + \dot{\phi})\hat{I} + \dot{\theta}_y[\cos(\Omega + \phi)\hat{J} + \sin(\Omega + \phi)\hat{K}] \\ & + \dot{\theta}_z[-\theta_y\hat{I} - \sin(\Omega + \phi)\hat{J} + \cos(\Omega + \phi)\hat{K}] \\ & = (\dot{\Omega} + \dot{\phi} - \dot{\theta}_z\theta_y)\hat{I} + [\dot{\theta}_y\cos(\Omega + \phi) - \dot{\theta}_z\sin(\Omega + \phi)]\hat{J} \\ & + [\dot{\theta}_y\sin(\Omega + \phi) + \dot{\theta}_z\cos(\Omega + \phi)]\hat{K}\end{aligned} \tag{3.6}$$

Or, as

$$\overline{\omega} = \begin{Bmatrix}\omega_x \\ \omega_y \\ \omega_z\end{Bmatrix}\begin{Bmatrix}\dot{\Omega} + \dot{\phi} - \dot{\theta}_z\theta_y \\ \dot{\theta}_y\cos(\Omega + \phi) - \dot{\theta}_z\sin(\Omega + \phi) \\ \dot{\theta}_y\sin(\Omega + \phi) + \dot{\theta}_z\cos(\Omega + \phi)\end{Bmatrix} \tag{3.7}$$

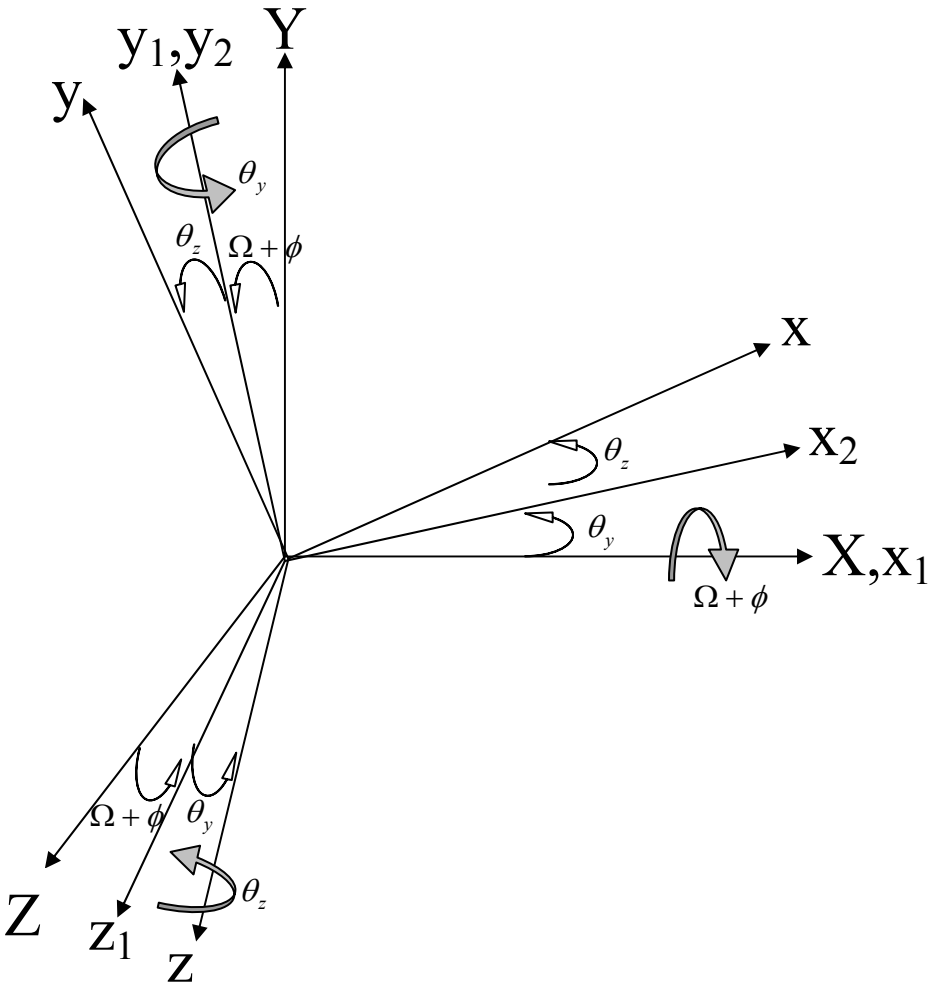

Figure 3.3: Cross-section Rotational Angles.

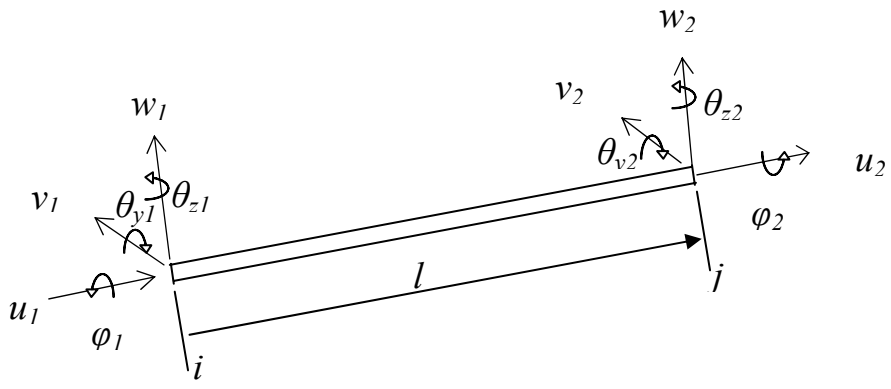

Figure 3.4: Degrees of freedom for drillstring element.

The drillstring configuration can be defined by a properly generated mesh of finite shaft elements. In this formulation, the drillstring element has circular cross-section and consists of two nodes. Each node has six degrees of freedom, one axial displacement, two transverse displacements, two bending rotations and one torsional rotation. The typical finite element used in this formulation is sketched in Figure 3.4.

The elemental nodal deformation vector is defined as

$$\{e(t)\} = \{u_1 \quad v_1 \quad w_1 \quad \theta_{y1} \quad \theta_{z1} \quad \phi_1 \quad u_2 \quad v_2 \quad w_2 \quad \theta_{y2} \quad \theta_{z2} \quad \phi_2\} \tag{3.8}$$

Utilizing the assumed admissible displacement field, the translational and axial deformations of an element is represented in terms of a set of shape functions as

$$\begin{Bmatrix} u(x,t) \\ v(x,t) \\ w(x,t) \end{Bmatrix} = \begin{bmatrix} N_{u1} & 0 & 0 & 0 & 0 & 0 & N_{u2} & 0 & 0 & 0 & 0 & 0 \\ 0 & N_{v1} & 0 & 0 & N_{v2} & 0 & 0 & N_{v3} & 0 & 0 & N_{v4} & 0 \\ 0 & 0 & N_{v1} & N_{v1} & 0 & 0 & 0 & 0 & N_{v3} & -N_{v4} & 0 & 0 \end{bmatrix} \{e(t)\}$$

$$= [N_t(x)]\{e(t)\} = \begin{bmatrix} N_u \\ N_v \\ N_w \end{bmatrix} \{e(t)\} \tag{3.9}$$

The rotation of a typical cross section of the element is then approximated by

$$\begin{Bmatrix} \theta_y \\ \theta_z \end{Bmatrix} = \begin{bmatrix} 0 & N_{\theta 1} & 0 & 0 & N_{\theta 2} & 0 & 0 & N_{\theta 3} & 0 & 0 & N_{\theta 4} & 0 \\ 0 & 0 & -N_{\theta 1} & N_{\theta 2} & 0 & 0 & 0 & 0 & -N_{\theta 3} & N_{\theta 4} & 0 & 0 \end{bmatrix} \{e(t)\}$$

$$= [N_{\theta yz}(x)]\{e(t)\} = \begin{bmatrix} N_{\theta y} \\ N_{\theta z} \end{bmatrix} \{e(t)\} \tag{3.10}$$

Similar relationship can be written for the torsional displacement of a typical cross section as

$$\phi(x,t) = [0 \quad 0 \quad 0 \quad 0 \quad 0 \quad N_{\phi 1} \quad 0 \quad 0 \quad 0 \quad 0 \quad 0 \quad N_{\phi 2}]\{e(t)\}$$

$$= [N_\phi]\{e(t)\} \tag{3.11}$$

where N_u, N_v, and N_w represent the shape functions associated with axial and lateral translations. The static rotation shape functions associated with bending rotations are $N_{\theta y}$ and $N_{\theta z}$ while N_φ represents torsional shape functions associated with torsional rotation. The explicit expressions of the aforementioned shape functions are given in Table B-1 in appendix B.

The displacement variables used to define the nodal deformation vector can be expressed in terms of the shape functions as follows

$$\begin{aligned}
u &= [N_u]\{e\}, \qquad \frac{du}{dx} = [B_u]\{e\} \\
v &= [N_v]\{e\}, \qquad \frac{dv}{dx} = [B_v]\{e\} \\
w &= [N_w]\{e\}, \qquad \frac{dw}{dx} = [B_w]\{e\} \\
\phi &= [N_\phi]\{e\}, \qquad \dot{\phi} = [N_\phi]\{\dot{e}\} \\
\theta_y &= [N_{\theta_y}]\{e\}, \qquad \dot{\theta}_y = [N_{\theta_y}]\{\dot{e}\} \\
\theta_z &= [N_{\theta_z}]\{e\}, \qquad \dot{\theta}_z = [N_{\theta_z}]\{\dot{e}\}
\end{aligned} \tag{3.12}$$

where $[B_i] = \dfrac{d}{dx}[N_i]$ and i is a notation used to refer to the type of deformation.

3.1. Kinetic Energy

To evaluate kinetic energy of element i, it is first necessary to derive an expression for the velocity vector of an infinitesimal volume at point p. Differentiating $\bar{r}_p$ in equation (3.3) with respect to time yields the velocity of point p as

$$\begin{aligned}\frac{d\bar{r}_p}{dt} &= \dot{\bar{r}}_p + \bar{\omega} \times \bar{r}_p \\ &= \{\dot{\bar{r}}_p\} + [\tilde{\omega}]\{r_p\}\end{aligned} \tag{3.13}$$

where $(\dot{\cdot})$ denotes differentiation with respect to time and the skew symmetric matrix $[\tilde{\omega}]$ is given by

$$[\tilde{\omega}] = \begin{bmatrix} 0 & -\omega_z & \omega_y \\ \omega_z & 0 & -\omega_x \\ -\omega_y & \omega_x & 0 \end{bmatrix} \tag{3.14}$$

Using the finite element notation, the vector $\bar{u}$ can be written as

$$\bar{u} = \{u\} = [N_t]\{e\} \tag{3.15}$$

where $\{e\}$ is the vector containing the nodal coordinates and $[N_t]$ is the translation shape function.

There is no change in the magnitude of $\bar{R}$ and $\bar{r}_0$ when the element deforms. Therefore the rate of change of magnitude of the position vector $\bar{r}_p$ is given by:

$$\{\dot{r}_p\} = \{\dot{\bar{u}}\} = [N_t]\{\dot{e}\} \tag{3.16}$$

Substituting equation (3.16) in equation (3.13), we get

$$\begin{aligned}\frac{d\bar{r}_p}{dt} &= [N_t]\{\dot{e}\} + [\tilde{\omega}]\{r_p\} \\ &= \begin{bmatrix} N_t & \tilde{\omega} \end{bmatrix} \begin{Bmatrix} \dot{e} \\ r_p \end{Bmatrix}\end{aligned} \tag{3.17}$$

The kinetic energy of the element is obtained by integrating the kinetic energy of the infinitesimal volume at point *p* over the volume *V*

$$KE = \frac{1}{2}\int_V \mu \left\{\frac{dr_p}{dt}\right\}^T \left\{\frac{dr_p}{dt}\right\} = \frac{1}{2}\int_V \mu \begin{bmatrix}\dot{e}^T & r_p{}^T\end{bmatrix} \begin{Bmatrix} N_v{}^T \\ \tilde{\omega}^T \end{Bmatrix} \begin{bmatrix} N_v & \tilde{\omega} \end{bmatrix} \begin{Bmatrix} \dot{e} \\ r_p \end{Bmatrix} dV \tag{3.18}$$

$$= \frac{1}{2}\int_V \mu \Big[\{\dot{e}\}^T [N_t]^T [N_t]\{\dot{e}\} + \{\dot{e}\}^T [N_t]^T [\tilde{\omega}]\{r_p\} + \{r_p\}^T [\tilde{\omega}]^T [N_t]\{\dot{e}\} + \{r_p\}^T [\tilde{\omega}]^T [\tilde{\omega}]\{r_p\}\Big] dV \tag{3.19}$$

where μ is the mass density of the element.

The first term in equation (3.19) gives the kinetic energy due to translation; the second and third terms are identically zero if moments of inertia are calculated with respect to center of mass of the element. The last term gives kinetic energy due to rotation that includes gyroscopic moments. To evaluate the last term, one can utilize the following expression:

$$[\tilde{\omega}]^T [\tilde{\omega}] = \begin{bmatrix} \omega_z^2 + \omega_y^2 & -\omega_x\omega_y & -\omega_z\omega_x \\ -\omega_x\omega_y & \omega_z^2 + \omega_x^2 & -\omega_y\omega_z \\ -\omega_x\omega_z & -\omega_y\omega_z & \omega_y^2 + \omega_x^2 \end{bmatrix} \tag{3.20}$$

Therefore,

$$= \frac{1}{2}\int_V \mu \{r_p\}^T [\tilde{\omega}]^T [\tilde{\omega}]\{r_p\} dV = \frac{1}{2}\int_0^l \mu \left(I_x\omega_x^2 + I_y\omega_y^2 + I_z\omega_z^2\right) dx \tag{3.21}$$

Substituting equation (3.7) in equation (3.21), we get

$$\int_V \mu \{r_p\}^T [\tilde{\omega}]^T [\tilde{\omega}]\{r_p\} dV = \int_0^l \mu \Big\{I_x(\dot{\Omega} + \dot{\phi} - \dot{\theta}_z\theta_y)^2 + I_y(\dot{\theta}_y \cos(\Omega + \phi) - \dot{\theta}_z \sin(\Omega + \phi))^2 + I_z(\dot{\theta}_y \sin(\Omega + \phi) + \dot{\theta}_z \cos(\Omega + \phi))^2\Big\} dx \tag{3.22}$$

which can be written as

$$\frac{1}{2}\int_V \mu\{r_p\}^T[\tilde{\omega}]^T[\tilde{\omega}]\{r_p\}dV = \frac{1}{2}\int_0^l I_p\left(\dot{\Omega}^2+\dot{\phi}^2\right)dx + \int_0^l I_p\left(\dot{\Omega}\dot{\phi}\right)dx - \int_0^l I_p\left(\dot{\Omega}+\dot{\phi}\right)\dot{\theta}_z\theta_y dx + \int_0^l I_D\left(\dot{\theta}_y^2+\dot{\theta}_z^2\right)dx \tag{3.23}$$

Or simply as

$$= \frac{1}{2}\int_0^l I_p\dot{\Omega}^2 dx + \int_0^l I_p\dot{\phi}^T\dot{\phi}\,dx + \int_0^l I_p\dot{\Omega}\dot{\phi}\,dx - \int_0^l I_p\left(\dot{\Omega}+\dot{\phi}\right)\dot{\theta}_z^T\theta_y dx + \int_0^l I_D\begin{Bmatrix}\dot{\theta}_y\\ \dot{\theta}_z\end{Bmatrix}^T\begin{Bmatrix}\dot{\theta}_y\\ \dot{\theta}_z\end{Bmatrix}dx \tag{3.24}$$

Where

$$\mu I_y = \mu I_y = I_D \text{ and } \mu I_x = I_p \tag{3.25}$$

Therefore, equation (3.24) becomes

$$\frac{1}{2}\int_V \mu\{r_p\}^T[\tilde{\omega}]^T[\tilde{\omega}]\{r_p\}dV = \frac{1}{2}\int_0^l I_p\dot{\Omega}^2 dx + \int_0^l \{\dot{e}\}^T[N_\phi]^T I_p[N_\phi]\{\dot{e}\}\,dx + \int_0^l I_p\dot{\Omega}\dot{\phi}\,dx - \int_0^l \{\dot{e}\}^T[N_{\theta_z}]^T I_p\dot{\Omega}[N_{\theta_y}]\{\dot{e}\}\,dx - \int_0^l \{\dot{e}\}^T[N_{\theta_z}]^T I_p[N_{\theta_y}]\{e\}[N_\phi]\{\dot{e}\}\,dx + \int_0^l \{\dot{e}\}^T\begin{Bmatrix}[N_{\theta_y}]\\ [N_{\theta_z}]\end{Bmatrix}^T I_D\begin{Bmatrix}[N_{\theta_y}]\\ [N_{\theta_z}]\end{Bmatrix}\{\dot{e}\}\,dx \tag{3.26}$$

The term $\int_0^l I_p\dot{\Omega}\dot{\phi}\,dx$ gives the inertial coupling between rigid body coordinates and elastic coordinates. For constant $\dot{\Omega}$ this term has no contribution to the equation of motion of the drillstring. Neglecting this term and introducing the following expressions:

$$\frac{1}{2}\int_0^l I_p dx = C_1$$

$$\int_0^l [N_\phi]^T I_p [N_\phi]\, dx = [M_\phi]$$

$$\int_0^l [N_{\theta_z}]^T I_p [N_{\theta_y}]\, dx = [G_1] \tag{3.27}$$

$$\int_0^l I_p [N_{\theta_z}]^T [N_{\theta_y}]\{e\}[N_\phi]\, dx = [M_e]$$

$$\int_0^l \begin{Bmatrix}[N_{\theta_y}]\\ [N_{\theta_z}]\end{Bmatrix}^T I_D \begin{Bmatrix}[N_{\theta_y}]\\ [N_{\theta_z}]\end{Bmatrix} dx = [M_r]$$

Equation (3.26) reduces to

$$\begin{aligned}\frac{1}{2}\int_V \mu \{r_p\}^T [\tilde{\omega}]^T [\tilde{\omega}]\{r_p\} dV = {} & \frac{1}{2} C_1 \dot{\Omega}^2 + \frac{1}{2}\{\dot{e}\}^T [M_\phi]\{\dot{e}\} - \dot{\Omega}\{\dot{e}\}^T [G_1]\{e\} \\ & - \{\dot{e}\}^T [M_e]\{\dot{e}\} + \frac{1}{2}\{\dot{e}\}^T [M_r]\{\dot{e}\}\end{aligned} \tag{3.28}$$

Where $[M_e]$ is the inertia coupling between torsional and transverse vibration which is time dependent. It is proved that this coupling can be written in the following alternative form [58]:

$$[M_e] = \int_0^l I_p [N_\phi]^T [N_{\theta_z}]\{e\}[N_{\theta_y}] - [N_\phi]^T [N_{\theta_y}]\{e\}[N_{\theta_z}]\, dx \tag{3.29}$$

Hence, the kinetic energy of the element given by equation (3.18) can be written as

$$\begin{aligned} KE = {} & \frac{1}{2}\{\dot{e}\}^T [M_t]\{\dot{e}\} + \frac{1}{2} C_1 \dot{\Omega}^2 + \frac{1}{2}\{\dot{e}\}^T [M_\phi]\{\dot{e}\} - \dot{\Omega}\{\dot{e}\}^T [G_1]\{e\} \\ & - \{\dot{e}\}^T [M_e]\{\dot{e}\} + \frac{1}{2}\{\dot{e}\}^T [M_r]\{\dot{e}\} \\ = {} & \frac{1}{2}\{\dot{e}\}^T [M]\{\dot{e}\} + \frac{1}{2} C_1 \dot{\Omega}^2 - \dot{\Omega}\{\dot{e}\}^T [G_1]\{e\}\end{aligned} \tag{3.30}$$

where

$$[M] = [M_t] + [M_r] + [M_\phi] - 2[M_e] \tag{3.31}$$

is the composite mass matrix and $\dot{\Omega}$ denotes the rigid body rotation. The coefficient sub-matrices are given by

$$[M_t] = \int_0^l [N_v]^T \mu A [N_v]\, dx \tag{3.32}$$

$$[M_r] = \int_0^l [N_\theta]^T I_D [N_\theta]\, dx \tag{3.33}$$

$$[M_\varphi] = \int_0^l [N_\varphi]^T I_p [N_\varphi]\, dx \tag{3.34}$$

$$[M_e] = \int_0^l I_p \left([N_\varphi]^T [N_{\theta z}] \{e\} [N_{\theta y}] - [N_\varphi]^T [N_{\theta y}] \{e\} [N_{\theta z}] \right) dx \tag{3.35}$$

where $[M_t]$ is the translational mass matrix, $[M_r]$ is the rotary inertia mass matrix, $[M_\varphi]$ is the torsional mass matrix, and $[M_e]$ is the coupled torsional-transverse mass matrix. The gyroscopic matrix $[G]$ and can be expressed by the following expression

$$[G] = [G_1] - [G_1]^T \tag{3.36}$$

Now, for constant rotating speed, one can write

$$[G_1] = \int_0^l [N_{\theta z}]^T I_p [N_{\theta y}]\, dx \tag{3.37}$$

and for constant I_p

$$[G_1] = I_p \int_0^l [N_{\theta z}]^T [N_{\theta y}]\, dx \tag{3.38}$$

Integrating equations (3.32), (3.33), (3.34), (3.35) and (3.38), the matrices are obtained and their non-zero entries are presented Table B-8 through Table B-12 in

appendix B. It has to be noticed that all mass and gyroscopic matrices are state independent except for the coupled torsional-transverse mass matrix [M_e] which is nonlinear and function of the elastic nodal coordinates. This matrix does not affect the modal characteristics of the system. Moreover, state independent mass matrices are symmetric while gyroscopic matrix is skew-symmetric. The coupled torsional-transverse mass matrix [M_e] is a general matrix.

3.2. Strain Energy

The deformation of a typical cross-section of the drillstring may be expressed by three translations and three rotations. Two of the translations (v,w) are due to bending in the Y and Z directions and the third one (u) is due to axial translation. The three rotations are (θ_y, θ_z) due to bending and (ϕ) due to torsion. The bending rotations are related to bending deformations (v,w) by the following expressions:

$$\theta_y(x,t) = \frac{\partial v(x,t)}{\partial t}$$
$$\theta_z(x,t) = -\frac{\partial w(x,t)}{\partial t} \tag{3.39}$$

3.2.1. Strain Energy due to Bending

The deformations in lateral directions (Y and Z) cause axial strain in the axial direction only, since strains in lateral direction are insignificant. Hence, the strain energy expression due to bending U_1 is

$$U_1 = \frac{1}{2}\int_V \varepsilon\ \sigma\ dV \tag{3.40}$$

Recalling the stress-strain relationship $(\sigma = E\varepsilon)$, the strain energy can be expressed as

$$U_1 = \frac{1}{2}\int_V E\varepsilon^2 dV \tag{3.41}$$

where ε is the strain due to bending, which is given by

$$\varepsilon = -y\frac{\partial^2 v}{\partial x^2} - z\frac{\partial^2 w}{\partial x^2} \tag{3.42}$$

Substituting this relation in strain energy expression of equation (3.41) yields

$$\begin{aligned} U_1 &= \frac{E}{2}\int_0^l\iint_A \left(-y\frac{\partial^2 v}{\partial x^2} - z\frac{\partial^2 w}{\partial x^2}\right)^2 dAdx \\ &= \frac{E}{2}\int_0^l\iint_A \left[y^2\left(\frac{\partial^2 v}{\partial x^2}\right)^2 + 2yz\frac{\partial^2 v}{\partial x^2}\frac{\partial^2 w}{\partial x^2} + z^2\left(\frac{\partial^2 w}{\partial x^2}\right)^2\right] dAdx \end{aligned} \tag{3.43}$$

Because of symmetry, the integral corresponding to the second term is zero. Now, let us define the following:

$$I_z = \int_A y^2 dA \quad \text{and} \quad I_y = \int_A z^2 dA \tag{3.44}$$

Therefore, the strain energy due to bending becomes

$$U_1 = \frac{E}{2}\int_0^l \left[I_z\left(\frac{\partial^2 v}{\partial x^2}\right)^2 + I_y\left(\frac{\partial^2 w}{\partial x^2}\right)^2\right] dAdx \tag{3.45}$$

Because of symmetry, we can set

$$I_y = I_z = I(x) \tag{3.46}$$

Substituting the relations of equation (3.39), the strain energy due to bending can be written as

$$U_1 = \frac{E}{2}\int_0^l \left\{ I(x)\left[\left(\frac{\partial \theta_y}{\partial x} \right)^2 + \left(\frac{\partial \theta_z}{\partial x} \right)^2 \right] \right\} dx \tag{3.47}$$

This equation can be written in the finite element notations as

$$\begin{aligned} U_1 &= \frac{E}{2}\int_0^l \left\{ I(x)\left[\{e\}^T [B_{\theta_y}]^T [B_{\theta_y}]\{e\} + \{e\}^T [B_{\theta_z}]^T [B_{\theta_z}]\{e\} \right] \right\} dx \\ &= \frac{1}{2}\{e\}^T \left\{ \int_0^l \left[[B_\theta]^T EI [B_\theta] dx \right] \right\} \{e\} \end{aligned} \tag{3.48}$$

3.2.2. Strain Energy due to Torsion

The strain energy due to torsion is given by

$$U_2 = \frac{1}{2}\int_0^l GI_p \left(\frac{\partial \phi}{\partial x} \right)^2 dx \tag{3.49}$$

where G is the shear modulus and I_p is the polar moment of inertia. The strain energy due to torsion is written in matrix form as

$$U_2 = \frac{1}{2}\{e\}^T \left(\int_0^l [B_\phi]^T GI_p [B_\phi] dx \right) \{e\} \tag{3.50}$$

3.2.3. Strain Energy due to Axial Deformation with Geometric Nonlinearity

A comprehensive analysis of drillstring dynamics should account for the coupled vibrations and other sources of nonlinearities in the drillstring dynamics. In general, two types of nonlinearities occur in structural problems. The first type is referred to as material nonlinearity and is due to the nonlinearly elastic, plastic or visco-elastic behavior of the structural material. The second type is referred to as geometric nonlinearity, and it occurs when the deflections are large enough to cause

significant changes in the geometry of the structure, so that the equations of equilibrium must be formulated for the deformed configuration [71]. In rotary machines, several investigations have been performed to study the coupling in rotor systems [58, 69, 70, 72]. However, some of modeling approaches are rendered inadequate to study the dynamic behavior of drillstrings due to neglecting the bending-axial coupling. Laboratory experiments and field investigations verified that severe vibrations could be induced due to the coupled motion in drillstring.

A complete account of bending-axial coupling is introduced in our model to account for large deformation in the drillstring. The nonlinear axial strain is considered in this analysis to account for the effect of large flexural deflection on the axial deformation. Hence, the axial component of the strain tensor can be expressed in terms of Eulerian strain tensor, as [63]

$$\varepsilon = \frac{du}{dx} - \frac{1}{2}\left[\left(\frac{du}{dx}\right)^2 + \left(\frac{dv}{dx}\right)^2 + \left(\frac{dw}{dx}\right)^2\right] \tag{3.51}$$

The first term in equation (3.51) is the linear term of axial strain and it will generate the linear terms in the stiffness matrix. The remaining terms are second order terms which are usually neglected in linear structural analysis. The strain energy is obtained by the following relationship:

$$U_3 = \frac{1}{2}\int_V \varepsilon\sigma \;\; dV = \frac{1}{2}EA\int_0^L \varepsilon^2 dx \tag{3.52}$$

Substituting equation (3.51) into strain energy equation leads to

$$U_3 = \frac{1}{2}EA\int_0^L \left\{\frac{du}{dx} - \frac{1}{2}\left[\left(\frac{du}{dx}\right)^2 + \left(\frac{dv}{dx}\right)^2 + \left(\frac{dw}{dx}\right)^2\right]\right\}^2 dx \tag{3.53}$$

$$= \frac{1}{2} EA \int_0^L \left\{ \left(\frac{du}{dx}\right)^2 - \left(\frac{du}{dx}\right)^3 - \frac{du}{dx}\left(\frac{dv}{dx}\right)^2 - \frac{du}{dx}\left(\frac{dw}{dx}\right)^2 \right.$$
$$+ \frac{1}{4}\left(\frac{du}{dx}\right)^4 + \frac{1}{2}\left(\frac{du}{dx}\right)^2\left(\frac{dv}{dx}\right)^2 + \frac{1}{2}\left(\frac{du}{dx}\right)^2\left(\frac{dw}{dx}\right)^2$$
$$\left. + \frac{1}{4}\left(\frac{dv}{dx}\right)^4 + \frac{1}{4}\left(\frac{dw}{dx}\right)^4 + \frac{1}{2}\left(\frac{dv}{dx}\right)^2\left(\frac{dw}{dx}\right)^2 \right\} dx$$

Neglecting higher order terms results in

$$U_3 = \frac{1}{2} EA \int_0^L \left\{ \left(\frac{du}{dx}\right)^2 - \left(\frac{du}{dx}\right)^3 - \frac{du}{dx}\left(\frac{dv}{dx}\right)^2 - \frac{du}{dx}\left(\frac{dw}{dx}\right)^2 \right\} dx \tag{3.54}$$

This can be written in matrix form using the definitions of deformation coordinates mentioned previously, as follows:

$$U_3 = \frac{1}{2} EA \int_0^L \left\{ \{e\}^T [B_u]^T [B_u] \{e\} - \{e\}^T [B_u]^T [B_u] \{e\} [B_u] \{e\} \right.$$
$$\left. - \{e\}^T [B_u]^T [N_{\theta_y}] \{e\} [N_{\theta_y}] \{e\} - \{e\}^T [B_u]^T [N_{\theta_z}] \{e\} [N_{\theta_z}] \{e\} \right\} dx \tag{3.55}$$

In general, the coupling expressions are nonlinear and state-dependent. Consequently, this may lead to higher computational time and cause some numerical problems. Coupling may also destroy the symmetry of stiffness or mass matrices in the governing equation. These issues will be discussed in section 4.4 when addressing the numerical solution procedure of solving the differential equations.

3.2.4. Strain Energy due to Gravitational Axial Stiffening

The strain energy associated with the axial stiffening due to gravity can be expressed as

$$U_4 = \frac{1}{2}\int_0^l EA\frac{\partial u}{\partial x}\left[\left(\frac{\partial w}{\partial x}\right)^2 + \left(\frac{\partial v}{\partial x}\right)^2\right]dx \tag{3.56}$$

In this case, the term $EA\dfrac{\partial u}{\partial x}$ represents the gravitation force F, and therefore one can rewrite strain energy due to axial stiffening as

$$U_4 = \frac{1}{2}\int_0^l F\left[\left(\frac{\partial w}{\partial x}\right)^2 + \left(\frac{\partial v}{\partial x}\right)^2\right]dx \tag{3.57}$$

Or, in matrix form as

$$U_4 = \frac{1}{2}\{e\}^T\left(\int_0^l F\left[[B_v]^T[B_v] + [B_w]^T[B_w]\right]dx\right)\{e\} \tag{3.58}$$

The drillpipe segment is the longest portion of the drillstring, which has low resistance to any applied bending moments and tend to fail by buckling when subjected to a vertical compression load. Therefore, drillpipe is generally under tension load, while drillcollar is normally under compressive load. The point separating the tension field from the compression filed within the drillstring is called "Neutral Point". The neutral point is the point having zero axial force. Details of the derivation of an expression for the axial force F at different locations are presented in reference [57]. The explicit expressions of the non-zero entries of this matrix are given in Table B-6 for drillpipes and Table B-7 for drillcollar in appendix B.

Now the total strain energy is obtained by adding strain energies due to various deformations, and can be written in compact form as

$$U = U_1 + U_2 + U_3 + U_4 \tag{3.59}$$

Now, the total strain energy is given by

$$U = \frac{E}{2}\int_0^l \left\{ I(x)\left[\left(\frac{\partial \theta_y}{\partial x}\right)^2 + \left(\frac{\partial \theta_z}{\partial x}\right)^2 \right] \right\} dx + \frac{1}{2}\int_0^l GI_p \left(\frac{\partial \phi}{\partial x}\right)^2 dx$$
$$+ \frac{1}{2} EA \int_0^L \left\{ \left(\frac{du}{dx}\right)^2 - \left(\frac{du}{dx}\right)^3 - \frac{du}{dx}\left(\frac{dv}{dx}\right)^2 - \frac{du}{dx}\left(\frac{dw}{dx}\right)^2 \right\} dx \qquad (3.60)$$
$$+ \frac{1}{2}\int_0^l EA \frac{\partial u}{\partial x}\left[\left(\frac{\partial w}{\partial x}\right)^2 + \left(\frac{\partial v}{\partial x}\right)^2 \right] dx$$

The strain energy expression of the rotating string element of length l is written in matrix form as

$$U = \frac{1}{2}\{e\}^T [K]\{e\} \qquad (3.61)$$

where the matrix $[K]$ is the augmented stiffness matrix given by

$$[K] = [k_e] + [k_a] + [k_\phi] + [k_{as}] \qquad (3.62)$$

where

$[k_e] = \int_0^l [B_\theta]^T EI [B_\theta] dx \quad \equiv$ Elastic stiffness matrix

$[k_\phi] = \int_0^l [B_\phi]^T GI_p [B_\phi] dx \quad \equiv$ Torsional stiffness matrix

$[k_{as}] = \int_0^l F\left[[B_v]^T [B_v] + [B_w]^T [B_w] \right] dx \quad \equiv$ Gravitational axial stiffening matrix

$[k_a] = [k_1] - [k_2] - [k_3] - [k_4] \quad \equiv$ Axial stiffness matrices

where

$$[k_1] = \int_0^L [B_u]^T EA[B_u] dx \tag{3.63}$$

$$[k_2] = \int_0^L \frac{3}{2} EA[B_u]^T [B_u]\{e\}[B_u] dx \tag{3.64}$$

$$[k_3] = \int_0^L EA\left(\frac{1}{2}[B_u]^T [N_{\theta_y}]\{e\}[N_{\theta_y}] + [N_{\theta_y}]^T [B_u]\{e\}[N_{\theta_y}]\right) dx \tag{3.65}$$

$$[k_4] = \int_0^L EA\left(\frac{1}{2}[B_u]^T [N_{\theta_z}]\{e\}[N_{\theta_z}] + [N_{\theta_z}]^T [B_u]\{e\}[N_{\theta_z}]\right) dx \tag{3.66}$$

All stiffness matrices are state independent and symmetric except $[k_2]$, $[k_3]$ and $[k_4]$ which are state-dependent and nonsymmetrical. The nonlinearity in these matrices is due to bending-axial coupling. The nonzero entries of these stiffness matrices are given in Table B-2 through Table B-5 in appendix B.

4. EQUATIONS OF MOTION OF THE DRILLSTRING

4.1. Elemental Equation of Motion

The equation of motion of the element can be derived using Lagrangean approach by substituting the Lagrangean function (L=T-U) into the following equation:

$$\frac{d}{dt}\left(\frac{\partial L}{\partial \dot{q}}\right)-\frac{\partial L}{\partial q}=Q \tag{4.1}$$

where

$q=\{\Omega \quad e^T\}^T$: generalized coordinates

Q : vector of generalized forces

T : total kinetic energy

U : total strain energy

Carrying out the differentions in equation (4.1), one obtains the following elemental equations of motion:

$$C_1\dot{\Omega}=\{Q\} \tag{4.2}$$

$$[M]\{\ddot{e}\}+\dot{\Omega}[G]\{\dot{e}\}+[K]\{e\}=\{Q\} \tag{4.3}$$

where

C_1 = $\frac{1}{2}\int_0^l I_p dx$

$[M]$: Augmented mass matrix

$[G]$: Gyroscopic matrix

$[K]$: Augmented stiffness matrix

Since the rotary table of the drillstring is rotating with constant angular velocity $\dot{\Omega}$, equation (4.2) will vanish. Equation (4.3) represents the dynamic equation of motion at the element level. The equation of motion of the whole drillstring is then derived by assembling the discretized element equations.

4.2. The Assembled Equations of Motion

The equation of motion for an element is rewritten again with an index for an element *i* as

$$[M_i]\{\ddot{e}_i\} + \dot{\Omega}[G_i]\{\dot{e}_i\} + [K_i]\{e_i\} = \{Q_i\} \tag{4.4}$$

Using the standard finite element assembly procedure, the equation of motion of the whole drillstring can be written as:

$$[M]\{\ddot{e}\} + \dot{\Omega}[G]\{\dot{e}\} + [K]\{e\} = \{Q\} \tag{4.5}$$

The solution of the general equation of motion is obtained by representing it in the following state space form:

$$\begin{bmatrix} [0] & -[M] \\ [M] & [G] \end{bmatrix} \begin{Bmatrix} \{\ddot{e}\} \\ \{\dot{e}\} \end{Bmatrix} + \begin{bmatrix} [M] & [0] \\ [0] & [K] \end{bmatrix} \begin{Bmatrix} \{\dot{e}\} \\ \{e\} \end{Bmatrix} = \begin{Bmatrix} \{0\} \\ \{Q\} \end{Bmatrix} \tag{4.6}$$

Or in more compact form:

$$[A]\{\dot{y}\} + [B]\{y\} = \{\overline{Q}\} \tag{4.7}$$

where

$$[A] = \begin{bmatrix} [0] & -[M] \\ [M] & [G] \end{bmatrix}$$

$$[B] = \begin{bmatrix} [M] & [0] \\ [0] & [K] \end{bmatrix}$$

$$\{y\} = \begin{Bmatrix} \{\dot{e}\} \\ \{e\} \end{Bmatrix}$$

$$\{\overline{Q}\} = \begin{Bmatrix} \{0\} \\ \{Q\} \end{Bmatrix}$$

The vector $\{\overline{Q}\}$ is the generalized force vector. Because of the nonlinearity introduced in the mass and stiffness matrices due to bending-torsional and bending-axial coupling, $[A]$ and $[B]$ are non symmetric state space matrices.

4.3. Stick-Slip Forces on the Drillstring

In this section, a forcing term is introduced to represent the effect of dry friction on the drillstring oscillations. This friction force is responsible for the self-excited nonlinear phenomenon of stick-slip in the drillstring. The nonlinear behavior and the long list of parameters that affect this force complicate the task of accurate modeling. Parameters such as angular displacement, WOB and angular velocity may have a great influence on the characteristics of TOB and, consequently the friction force. To establish a reasonably accurate model, it is essential to take all these factors into consideration.

Several models have been proposed in the literature to describe stick-slip oscillations. We will start the derivation by defining the WOB and then proceed to define the TOB, which takes into account all the above mentioned parameters.

The WOB is assumed to oscillate harmonically around its mean value i.e. it can be expressed as follows:

$$W = W_0 \sin(2\pi f t) \tag{4.8}$$

where W_0 is the amplitude and f is the frequency of fluctuations. It is assumed that WOB oscillates around the mean value W_0. This mean value is normally known because it can be measured while drilling from the top of the drillstring.

Let us explain the characteristics of a cutting process in order to end up with a relationship between axial and angular motion of the drilling bit. Initially, the bit is resting on the formation and WOB is equal to the constant value needed to maintain the location of the neutral point at constant position. The desired location of the neutral point is about the connection between drillpipe and drillcollar to ensure that the drillpipe is kept in tension to avoid buckling.

If we focus on the bit/rock interaction, the bit is applying a constant compressive force on the rock. In order to balance this force, a reaction force is applied by the formation to the bit. This force can be approximated if we know the stiffness of the formation (k_f), and can be expressed by the following formula:

$$W_f = k_f x_0 \tag{4.9}$$

where x_0 is the initial depth of cut.

During cutting process, it is assumed that the time taken for the bit to rotate one revolution with an angular velocity $\dot{\phi}_0$ is equal to the time taken by the bit traveling by a velocity $\dot{x}$ to drill a volume of depth x_0. Using this assumption, we can relate the ROP to the angular velocity by the following relation:

$$(\text{time})_{\text{rotation}} = (\text{time})_{\text{axial}} \quad \text{i.e.} \quad \frac{2\pi}{\dot{\phi}_0} = \frac{\mathrm{x}_0}{\dot{\mathrm{x}}} \tag{4.10}$$

According to the above assumptions, the bit is resting on the formation with at a depth of x_0. In other words, the bit will remove $\pi R^2 x_0$ volume from the rock per revolution where R is the radius of the hole. At this instant, the depth of cut vanishes

and the reaction force in equation (4.9) becomes zero. To maintain a constant WOB and to start another cutting revolution, the bit is pushed against the formation until the depth of cut returns to its optimum value x_0.

If one focuses on WOB fluctuations, the initial value of WOB can be expressed as $W_0 + k_f x_0$. After one revolution, the term $k_f x_0$ will vanish, and WOB is reduced to its constant value W_0. The bit is pushed towards the formation to make x_0 depth and the WOB will retrieve its maximum value. Therefore, WOB can be expressed as:

$$W = W_0 + k_f x_0 (1 - \sin(2\pi f t)) \tag{4.11}$$

The amplitude of the fluctuating part depends on the depth of cut, while the frequency f can be calculated from equation (4.10). In this analysis, it is assumed that the bit never loses contact with the formation.

In order to include the effect of axial motion on the torsional oscillations, the coupling between the axial degree of freedom and angular velocity is introduced in defining the torque term. As a result, TOB is assumed to be dependent on WOB; i.e.

$$TOB = \mu_k W[f(\dot{\phi})] \tag{4.12}$$

where W is WOB as expressed by equation (4.11).

The function $f(\dot{\phi})$ relates TOB to the angular velocity of the bit. Such a profile accommodates the expected variation of the friction torque as a function of angular velocity. However, experimental and field data investigations proved that the applied friction torque is proportional to the high fluctuations in bit angular velocity. This relation is depicted in Figure 2.3. Unfortunately, there is no field data available to describe this relation at low velocity, and engineers usually perform extrapolation to plot the curve at low velocities. To describe stick-slip, a relationship should be

established between TOB and the angular velocity. Several functions have been suggested to model this relation.

Some investigators used the basic law of friction to set up the relationship between TOB and $\dot{\phi}$ [26, 19]. Others modified this law at low velocity region to obtain more accurate models [42, 20, 2], wherein they focused on the low velocity region because the transition between static and kinetic force must be modeled carefully. Some authors used characteristics curves to model this relation [23, 56]. At high velocity, all functions tend to converge to a constant value of force. Expressions reported in the literature for the nature of the function $f(\dot{\phi})$ are listed in Table 4-1. In general, one can divide these functions into two groups: continuous and discontinuous functions. The discontinuity in some proposed expressions at zero velocity is a major source of computational difficulties in friction problem. It is apparent that the expression given by equation (5) in Table 4-1 can be regarded as the most appropriate. This expression is given by

$$f(\dot{\phi}) = \tanh(\dot{\phi}) + \frac{\alpha_1 \dot{\phi}}{1 + \alpha_2 \dot{\phi}^2} \tag{4.13}$$

The main features of this expression are that it is continuous and easily adjustable to match field data measurement. The advantage of using a continuous model is further discussed in the next section.

Table 4-1: Proposed expressions to simulate the relation between friction torque and angular velocity

Equation	Expression	Reference	Comments
1	slip phase: $T = T_c$ for $\frac{d\phi}{dt} > 0$ stick phase: $\lvert T \rvert \le T_c + \Delta T$ for $\frac{d\phi}{dt} = 0$	(Halsey et al. [26])	Discontinuous function
2	$f(\dot{\phi}) = \begin{cases} F_1 - \frac{F_1 - F_2}{\dot{\Omega}}\dot{\phi} & 0 \le \dot{\phi} < \dot{\Omega} \\ F_2 & \dot{\phi} \ge \dot{\Omega} \end{cases}$	Dawson [42]	Discontinuous function
3	$f(\dot{\phi}) = F_2 + (F_1 + F_2)\exp(-\gamma\dot{\phi})^{\delta}$	Wang and Lin [20]	Discontinuous function
4	$T = -\operatorname{sgn}\dot{\phi}\frac{T_c}{1 + \delta\lvert\dot{\phi}\rvert}$	Leine et al. [2]	Discontinuous function
5	$f(\dot{\phi}) = \tanh(\dot{\phi}) + \frac{\alpha_1\dot{\phi}}{1 + \alpha_2\dot{\phi}^2}$	Tucker and Wang [38]	Continuous function
6	$f(\dot{\phi}) = AB\dot{\phi}\left(ab^2 + b^2 + B^2\dot{\phi}^2\right)/\left(b^2 + B^2\dot{\phi}^2\right)\sqrt{1 + B^2\dot{\phi}^2}$	Tucker and Wang [41]	Continuous function

4.4. Programming Scheme

The governing equations derived previously will be solved numerically to obtain the modal characteristics and dynamic response of the drillstring under different excitations. The drillstring assemblies treated by this program can be of any complexity in terms of number of elements, element length and drillpipes/drillcollar length ratio. The developed computer program is written in MATLAB® code. The computer program is developed to carry out the following tasks:

- Numerical evaluation of the elemental mass and stiffness matrices and assembling the global matrices.
- Solving for the modal characteristics.
- Introduce dynamic and kinematics coupling into system matrices to be evaluated for the dynamic response calculations.
- Applying state and time dependent forces and updating system matrices at every time step.
- Integrate the equations of motion numerically to evaluate the time response.

A flow chart of the developed computer scheme is represented by a control flow chart as given in Figure 4.1. The important tasks carried out by the program are further explained in the following paragraph.

I. Input data

This is the first module invoked by the main program. The drillstring is discretized into finite number of element specified in this subroutine. It also contains the material properties, problem geometry, boundary conditions, element connectivity data and element properties. The geometric properties include length, outer radius, inner radius and flag to indicate weather the element is drillpipe or drillcollar. The material properties (mass

density, modulus of elasticity and shear modulus) are specified for every element. The constant speed of the rotary table is predefined in the input data.

II. System Matrices

This module establishes the elemental mass, stiffness and gyroscopic matrices based on the data and boundary conditions given. Then, the global matrices are then assembled for the whole drillstring system.

III. Modal characteristics module

In this module the modal characteristics of the drillstring system are obtained by solving the eigenvalue problem. Two reduction schemes, namely planar and complex, are implemented. The details of these reduction schemes and their programming aspects can be found in [74, 75]. The function of this module is to select a smaller set of eigenvectors, which represents the significant frequencies of the system, and construct the modal transformation matrices.

IV. Dynamic analysis module

The equations of motion are integrated forward in time to predict the time response. The module solves for the drillstring transient response based on initial displacement conditions, initial velocity and/or any forcing function chosen by the user. Dynamic coupling due to bending-torsional coupling in the inertia matrix and due to axial-bending coupling in the stiffness matrix are incorporated. The forcing function is chosen to induce stick-slip oscillation. This function is time and state-dependent and it has to be updated at every time step by recovering the nodal coordinate.

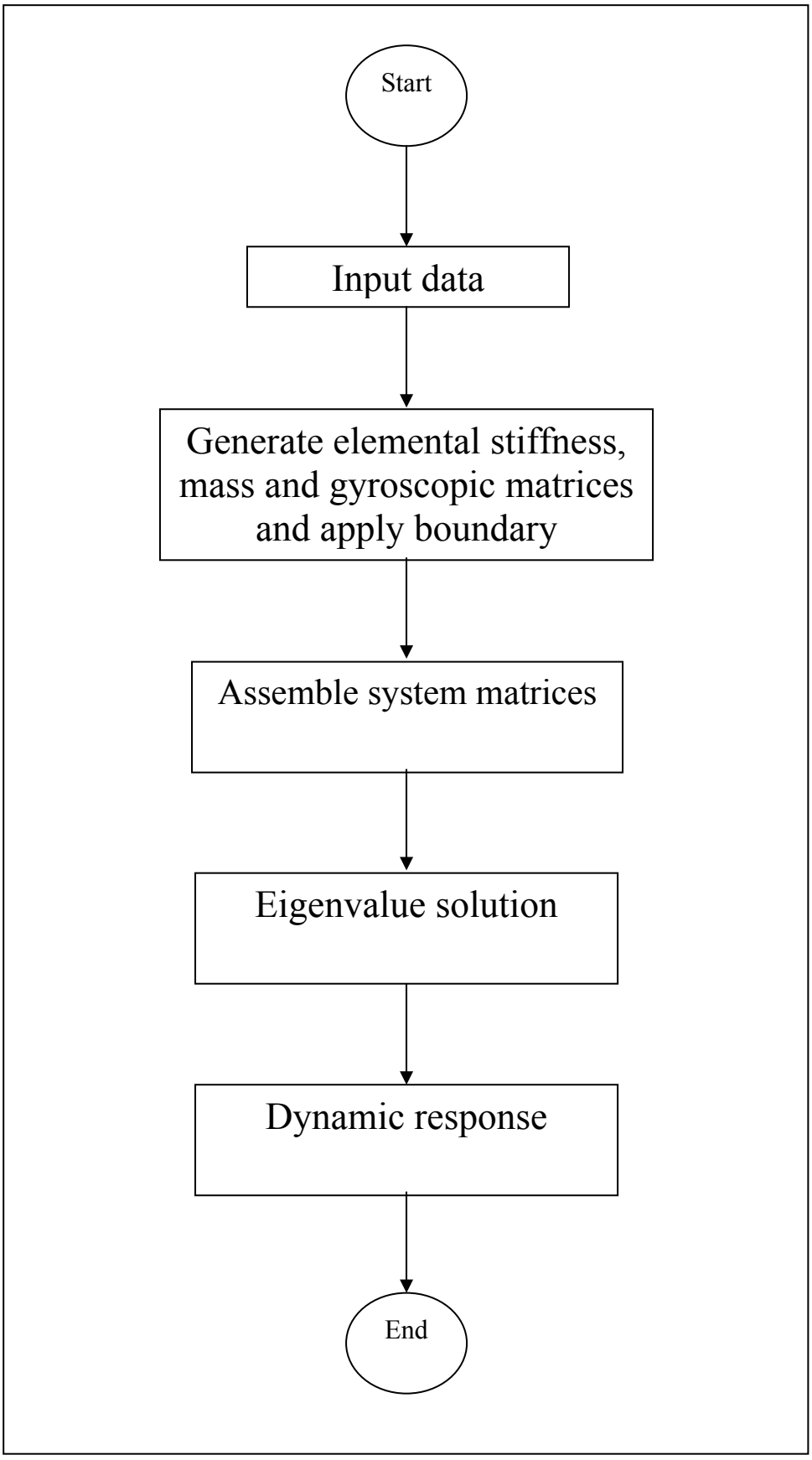

Figure 4.1: Control flow diagram of the developed computational scheme.

The equations of motion are arranged such that the coupled terms are kept in the right hand side along with the forcing term. For full-order model, the unconstrained elemental nodal coordinate is recovered at every integration step to update the forcing vector and elemental coupling matrices. For reduced-order model, the modal coordinate is recovered and transformed to the nodal coordinate. Then, the forcing and elemental coupling matrices are updated for the new nodal coordinate. The system matrices and global force vector are established using the updated elemental matrices and force vectors. This procedure has to be implemented at the end of every numerical integration step which makes the numerical integration time consuming. Therefore, it is recommended if the coupling is insignificant to eliminate its effect in order to enhance the program efficiency. The control flow diagram for the evaluation of the forcing vector is shown in **Error! Reference source not found.**.

As discussed in the previous section, it is obvious that stick-slip involves high nonlinearity and discontinuity which are potential sources of numerical problems during integration process. Many studies modeled stick-slip force as piecewise discontinuous function. However, integration process can't be performed at the discontinuity point. The integration starts from an initial state with a set of differential equations. Two sets of equations have to be derived to represent the two distinct modes (stick and slip). Depending on the initial conditions, the appropriate set of equation is selected to represent the behavior of drillstring during this time period. Standard integration methods integrate a set of differential equations over a specified time interval. The numerical integration is started until the first transition point is reached. The integration process is halted and the state of this point is defined as the initial state of next time period. Impulse momentum is evaluated at the transition point. Then, a new integration process is started with a new set of differential equations and initial conditions identical to the state defined at the transition

point. When a new transition point is reached, the process is halted again and a new set of initial conditions are defined to start a new integration process over the third time period with the set of equations implemented in the first period. Evaluation of impulse momentum at every point of discontinuity is very difficult. Moreover, the needs to halt the integration process, determine the time of the transition point and restart the integration again is undesirable from a numerical point of view and increase the start-up cost in the standard ODE-solvers.

Several schemes have been proposed to circumvent the need of piecewise analysis. One of the most effective methods is the smoothing method. The idea behind this method is to replace the region of discontinuity by an approximated continuous function. Using this method, there is no need to halt the integration process or specify transition between stick and slip modes since this transition will be smooth but very close to the original discontinuous transition. Therefore, a continuous function is used to simulate the relationship between TOB and angular velocity of the drilling bit. Generally, the proposed functions are furnished with a set of constant to improve the accuracy of the approximation. Referring to Table 4-1, the two continuous functions have constants that are used to control the shape of the approximated curve. One disadvantage of smoothing method is that it may yield to numerically stiff differential equations which consequently lead to large computational time. Very accurate functions may increase the probability of stiff differential equations. As long as the difference between the maximum static friction and the typical kinetic friction is not excessive, such continuous approximations are found to yield acceptable alternatives. Fortunately, in stick-slip cases the problem of stiffness is easily avoided by selecting appropriate constants for the selected function without affecting the accuracy of the result. It will be shown in the next chapter that this method is very accurate and can replace the discontinuous traditional models used to simulate stick-slip problems.

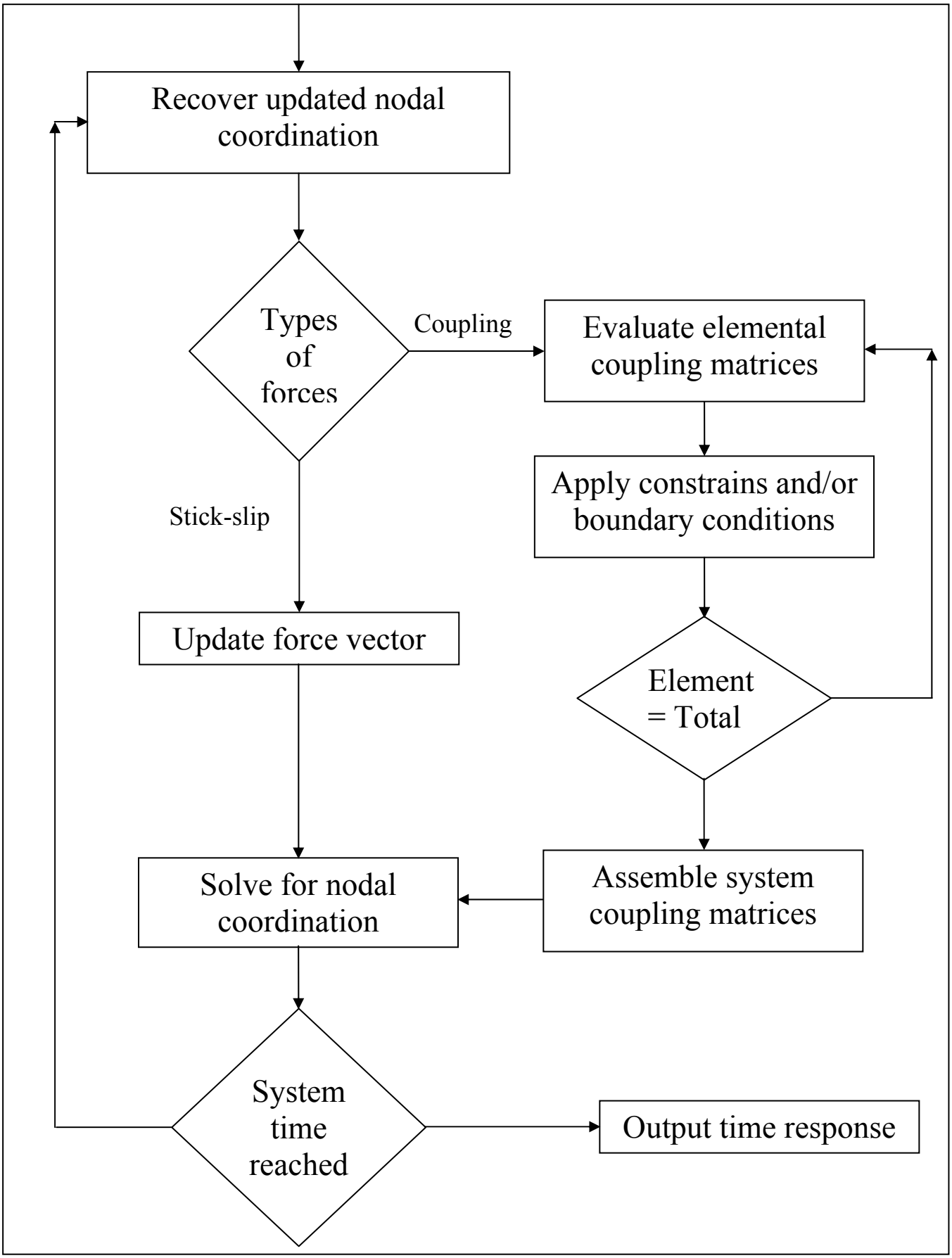

Figure 4.2: Control flow diagram to compute time and state-dependent forces.

5. RESULTS AND DISCUSSIONS

In this chapter, the dynamics of a typical configuration of a drillstring is simulated using the finite element dynamic model developed in this study. The capability of the developed dynamic model in predicting the actual dynamic behavior of the drillstring is demonstrated.

5.1. Modeling Accuracy

The number of elements used to represent the drillstring system plays an important role in establishing the accuracy and required computational time of the developed model. In order to test the accuracy of the finite element discretization, a study of stick-slip response is conducted with different number of elements in order to establish an assessment of accuracy for the required number of finite elements to be used in the system model. The parameters used in the following simulations are shown in Table 5-1. Figure 5.1, and Figure 5.2 show improved convergence of stick-slip response for the model discretized into 3, 12 and 24 elements. Similar observation can be noticed in torque profiles as shown in Figure 5.3 and Figure 5.4. It can be noticed that there is no significant difference between stick-slip response for 3, 12 and 24 elements. This implies that if an investigation is dedicated to study the torsional oscillations of the drillstring system isolated from other contributions i.e. (ignoring coupling), a system with lower degrees of freedom is adequate.

However, one of the important features of the developed model is generality, which is manifested by the versatility of the FEM in handling large scale complex systems. The developed scheme should be capable of studying the vibrations of the system associated with any selected set of degrees of freedom. Moreover, the coupling between different types of vibrations can be taken into account. Hence, the selected number of elements should meet the accuracy requirement in all directions. In a previous study [57], the

optimum number of elements for accurate lateral results for the same drillstring configuration has been selected as 24 elements [57]. The same drillstring system is used in this study and has been discretized into 24 elements to ensure that the FEM model gives accurate results for any particular condition with regard to the different types of vibrational motions.

Now, the drillstring is discretized into 24 finite elements. Proportionally, more elements are used to discretize the drillpipe section than drillcollar because larger deflections and rotations are expected in the drillpipe portion. The ratio of the number of drillpipe elements to drillcollar elements is 5:1. Including the constrained nodes, the total number of nodes is 25 nodes. Each node has six degrees of freedom, two transverse displacements, two bending rotations, one torsional rotation, and one axial displacement. After applying the boundary conditions for the system, a total of 140 unconstrained degrees of freedom are attained.

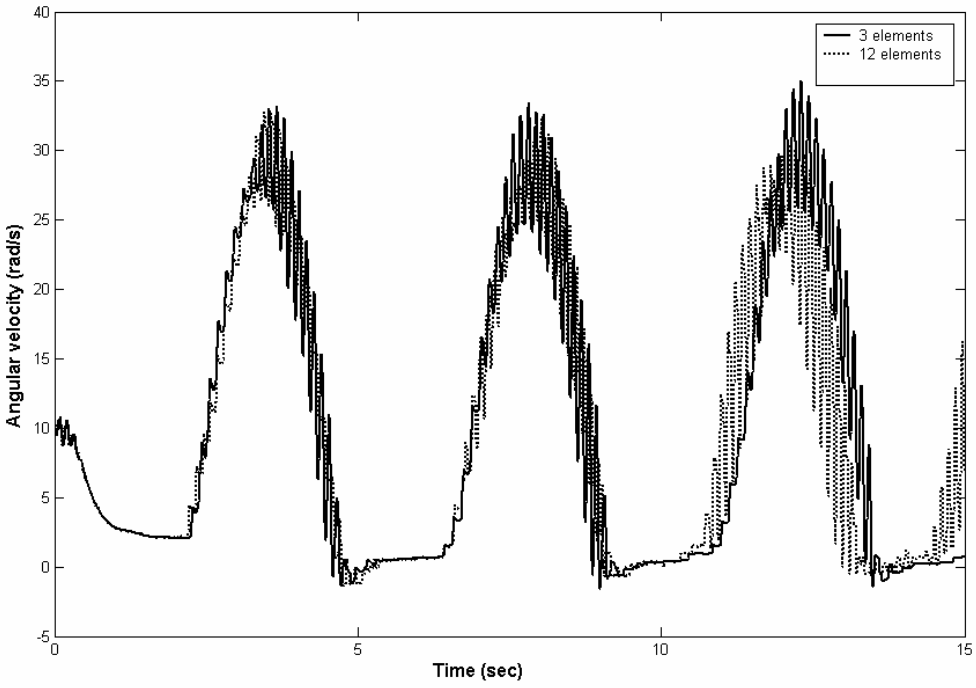

Figure 5.1 : Comparison of stick-slip response for 3 and 12 elements

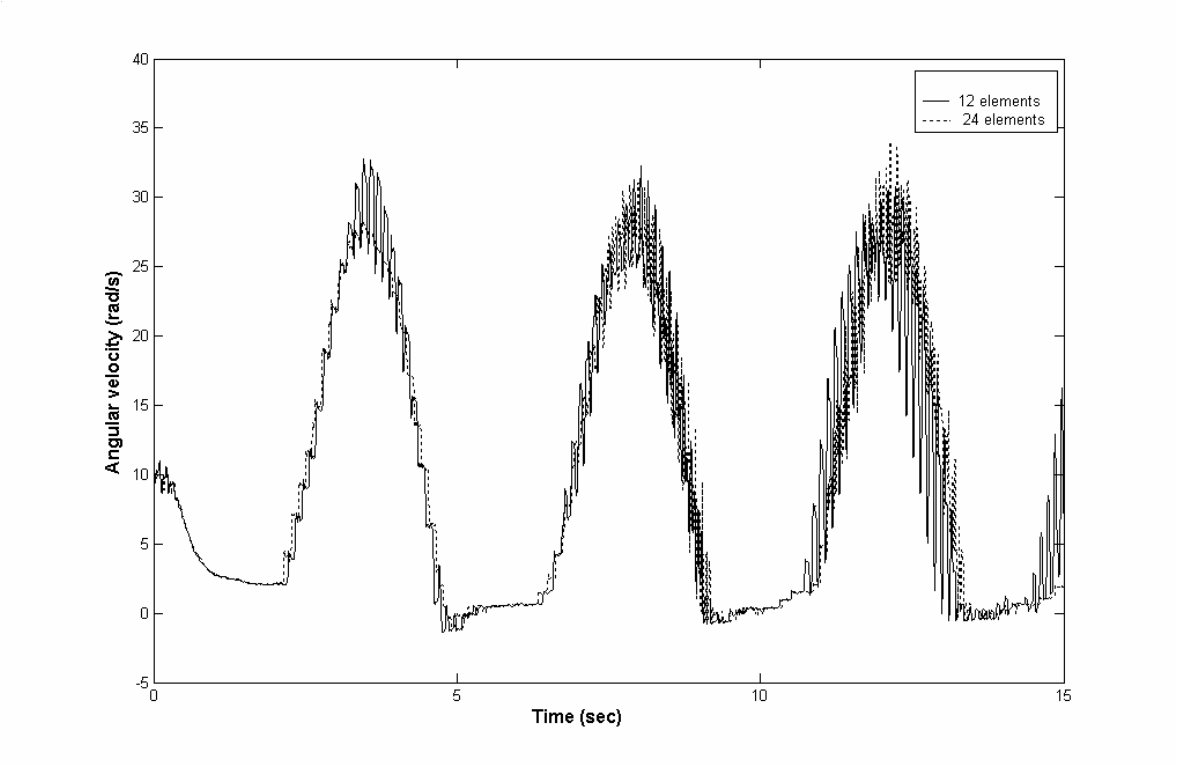

Figure 5.2 : Comparison of stick-slip response for 12 and 24 elements

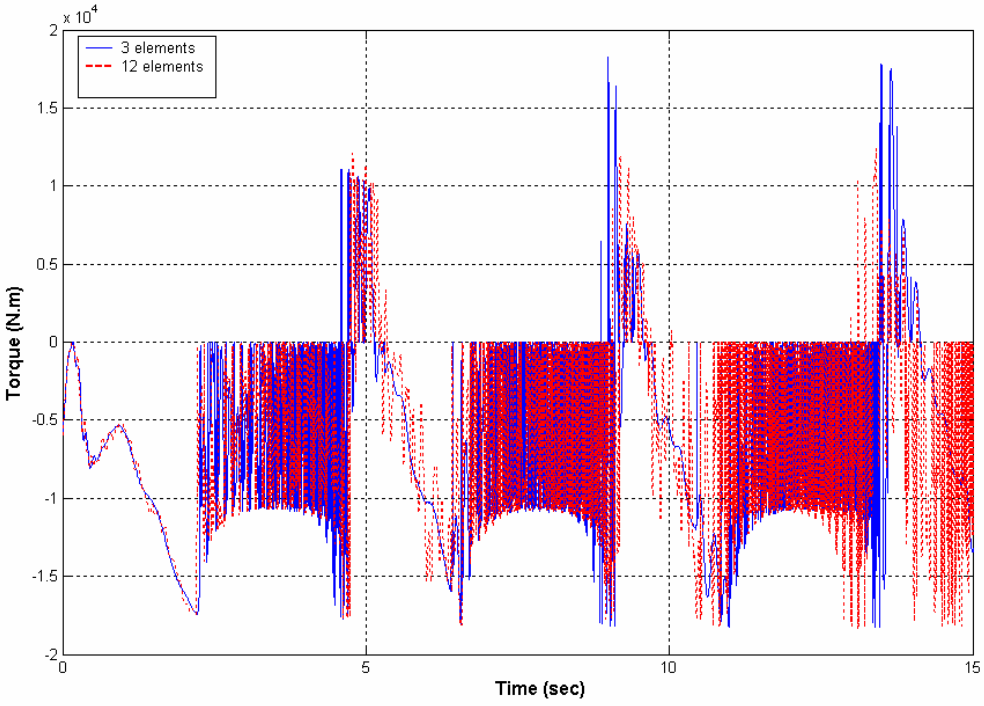

Figure 5.3 : Comparison of torque profiles for 3 and 12 elements.

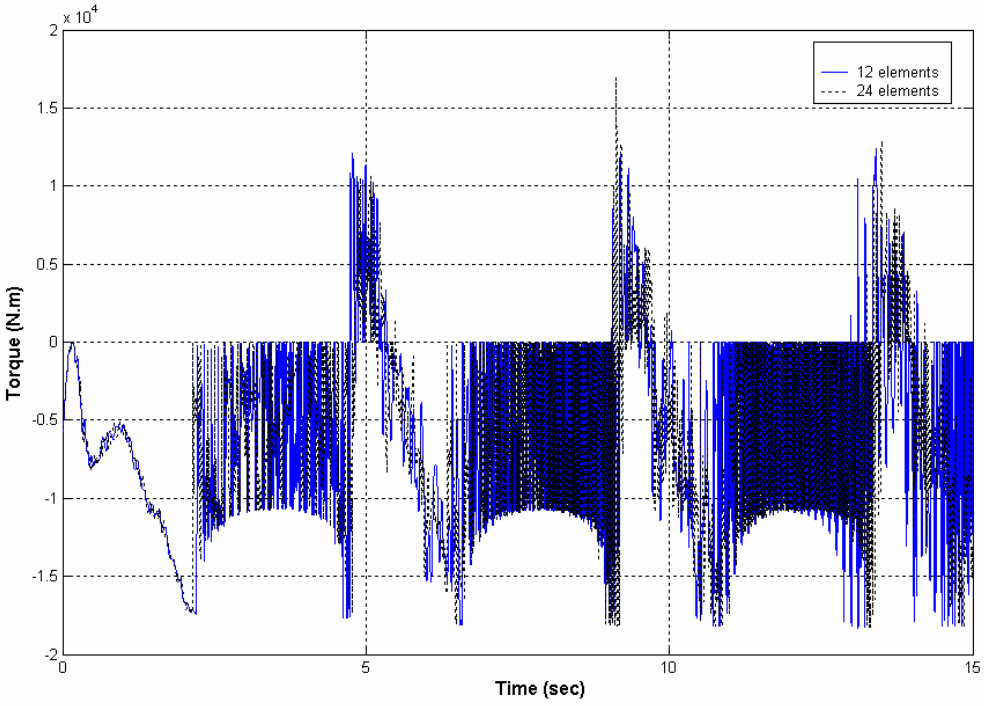

Figure 5.4 : Comparison of torque profiles for 3 and 12 elements.

5.2. Modal Analysis of the Drillstring

In this section, the modal characteristics of the drillstring system are examined. The free vibrational equations of the system are solved in the state-space form to extract the complex eigenvalues and eigenvectors of the system. The free vibrational conditions can be achieved by setting the forcing vector to zero in equation (4.7). In modal analysis, $[A]$ and $[B]$ will retrieve their symmetric properties since the nonlinear coupling will vanish. Hence, $[A]$ will be skew symmetric matrix and $[B]$ will be symmetric matrix. The developed program has the capability to obtain axial, bending and torsional frequencies for different drillpipe/drillcollar length ratios. Bending frequencies, both forward and backward, could be obtained for any prescribed rotary table speed. Such distinction between forward and backward frequencies vanishes for a non-rotating drillstring. The bending natural frequencies of the drillstring configuration shown in Table 5-1 have been studied earlier [57]. In that study, bending natural frequencies of the drillstring under various speeds of the rotary table were obtained and reproduced in Table 5-2. These results have not been compared with any experimental or field data due to lack of reported information in the available literature.

It is important to note that, unlike bending frequencies, the frequencies of torsional and axial vibrations are not directly affected by the rotational rate, neutral point location or WOB. Torsional and axial natural frequencies can be calculated using the nominal geometric and physical parameters of the drillstring. Axial and torsional frequencies of the system with parameters given in Table 5-1 are obtained and listed in Table 5-3. The fundamental natural frequencies of axial and torsional vibrations are calculated to be 0.27 Hz and 0.64 Hz respectively. In stick-slip analysis, the attention is mainly towards torsional and axial frequencies since they are the dominant frequencies. Unlike rotational speed and neutral point location, the change in the drillpipe length influenced the torsional and axial

natural frequencies. However, this influence is more significant for higher natural frequencies. Torsional and axial frequencies for different drillpipe lengths are listed in Table 5-4 to show the effect of drillpipe length on natural frequency. As expected, as the length of the drillpipe is increased the drillstring becomes less stiff. The influence of the drillpipe length is more significant for higher natural frequencies. Hence, torsional and axial frequencies were seen to be very sensitive to geometric parameters of drillpipe and drillcollar.

In this study, torsional and axial frequencies obtained using the developed finite element model are compared with the results available in the literature to validate the present finite element model. Two sets of measurements are reported to validate drillstring torsional natural frequencies. As a first comparison, the drillstring considered in reference [22] with the data summarized in Table 5-5 is utilized. Measured and calculated torsional natural frequencies are presented in Table 5-6, where the first column represents the actual natural frequency recorded from field measurements, while the second and third columns are for the calculated frequencies using the present finite element scheme and the finite element model developed in reference [22]. Table 5-6 shows that the present finite model predicted the natural frequency of the drillstring more precisely for the fundamental frequency. The difference is relatively greater for higher frequencies. This could be attributed to the overestimation resulting from consistent FEM formulation. In addition, measurements conditions are not known.

Table 5-1: Parameters used in the simulation of the drillstring system

		Drillpipe	Drillcollar
material properties	density (ρ)	7850 kg/m^3	
	Modulus of elasticity (E)	210 x 10^9 N/m^2	
	Shear modulus (G)	7.6923 x 10^{10} N/m^2	
Geometrical properties	Length (L)	1000 m	200 m
	Outside diameter (D_o)	0.127 m	0.2286 m
	Inside diameter (D_i)	0.095 m	0.0762 m

Another set of torsional natural frequencies was reported by Halsey et al. [9]. The data was recorded in a 1000m deep, nearly vertical well with approximately 120 m of 6 ½ inch drillcollar. The rest of the drillstring was 5 inch drillpipe. The measured and calculated frequencies were reported in reference [9] and reproduced in Table 5-7 alongside the calculated frequencies by the present finite element model. These results demonstrate clearly that the finite element model developed in this thesis manifests good accuracy.

A further check of the developed approach is by examining axial frequency of the system. A comparison with calculated axial natural frequencies is given in Table 5-8. The length of drillstring from surface to bit is about 145 m with average drillcollar outer diameter of 0.21 m and 0.14 m thickness and drillpipe outer diameter of 0.16 and 0.1 m thickness [76].

The comparison of the results tabulated for torsional and axial natural frequencies, shown in tables Table 5-6 through Table 5-8, displays a very good agreement with measured frequencies of the significant modes in frequency spectra. This agreement confirms the reliability of the developed approach in estimating the drillstring modal characteristics. The slight discrepancy between measured and calculated frequencies may be due to either non-linearity in the measured system, or variation in boundary conditions with frequency.

Another interesting behavior could be observed by plotting mode shapes of the lowest three torsional natural frequencies, which are depicted in Figure 5.5. In drillpipe segment, larger deflection can be observed due to its lower stiffness. The twist at the top of the drillcollar is almost the same as it is at the bottom. This may, to some extent justify the assumption made in single degree of freedom models of the drillstring which neglects the twisting of the drillcollar and models the drillstring as a torsional pendulum. The displacement of the drillpipe is the greatest at the drillpipe/drillcollar connection and gradually decreases to zero at the surface. In contrast, the internal torque is minimum at the

bottom of the drillcollar and increases to a maximum value at the drillcollar/drillpipe connection. Then, the toque is nearly constant along the drillpipe, if one neglects the drillpipe/borehole interaction. This means that drillpipe connections are exposed to an equal torque to the applied surface torque. Figure 5.5 demonstrates the importance of including drillpipe in this study because of its large deflections.

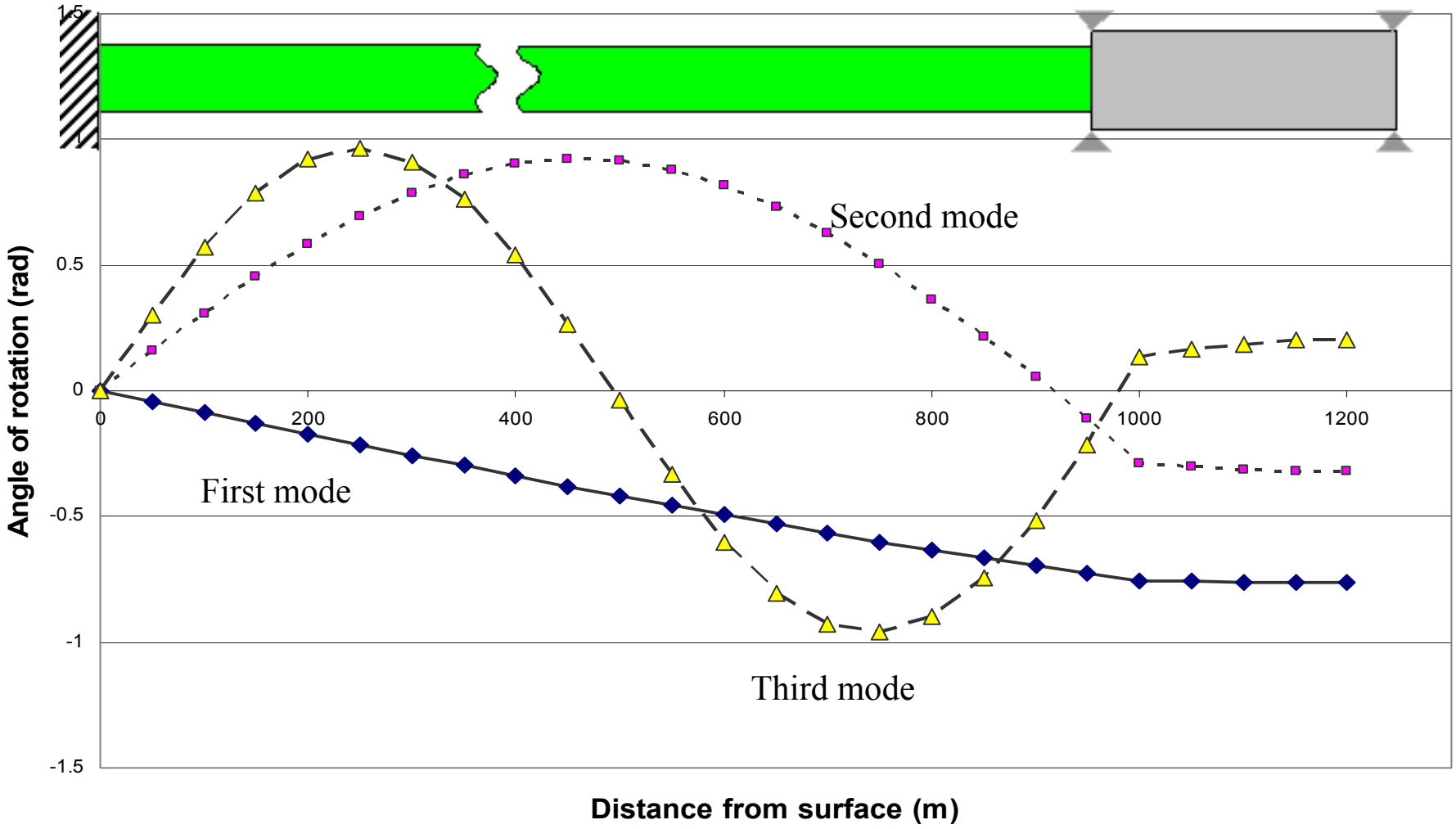

Figure 5.5 : Mode shapes of the lowest three torsional natural frequencies.

Table 5-2 : Bending natural frequencies for rotating drillstring in rad/sec.

Ω (RPM)		f_1	f_2	f_3	f_4	f_5	f_6	f_7	f_8	f_9	f_{10}
0		0.1694	0.3488	0.4272	0.5327	0.7134	0.8927	0.951	1.0879	1.2761	1.4663
30	B	0.1692	0.3487	0.4272	0.5325	0.7133	0.8926	0.951	1.0878	1.276	1.4662
	F	0.1695	0.3489	0.4273	0.5328	0.7135	0.8928	0.951	1.088	1.2762	1.4664
60	B	0.1691	0.3486	0.4272	0.5324	0.71132	0.8925	0.9509	1.0877	1.2756	1.4661
	F	0.1696	0.3491	0.4273	0.5329	0.7136	0.8929	0.951	1.0881	1.2763	1.4665
100	B	0.1689	0.3484	0.4272	0.5322	0.713	0.8924	0.9509	1.0876	1.2758	1.466
	F	0.1698	0.3493	0.4273	0.5331	0.7138	0.893	0.9511	1.0883	1.2764	1.4666
500	B	0.1671	0.3467	0.4269	0.5306	0.7115	0.8911	0.9505	1.0863	1.2746	1.4648
	F	0.1717	0.351	0.4276	0.5347	0.70153	0.8943	0.9515	1.0896	1.2776	1.4678
1000	B	0.1649	0.3446	0.4265	0.5286	0.7096	0.8895	0.9501	1.0847	1.273	1.4634
	F	0.174	0.3532	0.428	0.5386	0.7173	0.8959	0.9519	1.0912	1.2791	1.4692

Table 5-3 : Torsional and Axial natural frequencies for rotating drillstring in rad/sec.

rad/sec		f_1	f_2	f_3	f_4	f_5	f_6	f_7	f_8	f_9	f_{10}
Torsional		1.705	10.1197	19.8168	29.7083	39.699	48.6099	52.2853	61.5118	72.4139	83.8122
axial		4.0076	17.2617	32.8832	48.9437	65.028	79.0416	87.6804	102.2349	119.8074	138.3143

Table 5-4 : Torsional and axial frequencies for different drillpipe length.

Drillpipe length (m)	Torsional natural frequency (rad/sec)			Axial natural frequency (rad/sec)		
	f_1	f_4	f_8	f_1	f_4	f_8
300	3.2	69.0	176.2	7.8	114.8	291.2
600	2.2	48.0	105.5	5.4	77.6	172.2
1000	1.7	29.7	61.5	4.0	48.9	102.2

Table 5-5: Structural characteristics of the drillstring used in Table 5-6.

	GJ ($N.m^2$)	**I (Kg.m)**	**L (m)**
Drillpipe	1.66E+06	0.173	479
Drillcollar	4.32E+06	0.450	198

Table 5-6: Comparison between measured and calculated torsional natural frequencies.

MEASUREMENTS	**Calculated by FEM model (48 elements)**	**Calculated by Reference [22]**
0.87	0.86	0.85
3.15	3.29	3.33
5.57	5.97	6.04

Table 5-7: Comparison between measured and calculated torsional natural frequencies.

MEASUREMENTS	Calculated by Present FEM model	Calculated by Reference [9]
0.52	0.52	0.53
1.90	1.89	1.89
3.47	3.48	3.47
5.13	5.13	5.10

Table 5-8: Comparison between axial frequencies calculated by FEM model and frequencies calculated in references [76].

Calculated by Present FEM model	Calculated by Reference [76]
7.4	7.4
24.3	21.1
43.3	43.0

The following sections are devoted to study the dynamic response of the drillstring. Firstly, the capability of the finite model in simulating the dynamic coupling between bending and torsional motion and the kinematic coupling between bending and axial motion is tested. Secondly, the self-excited stick-slip motion is simulated by applying appropriate downhole conditions. These results are investigated to test the accuracy of the developed model. This is followed by our attempt to study the effect of WOB and rotary table speed on the severity of stick-slip once excited. The drillstring configuration used for the analysis is similar to the one adopted in references [30]. The geometric and material properties of the drillstring are shown in Table 5-1.

5.3. Nonlinear Coupling

The first stage in analyzing the dynamic response is to investigate the effect of coupling between axial-torsional-lateral structural vibrations of the drillstring. Coupling could be a potential source of unexpected vibrations of the drillstring. It is essential to consider coupling while simulating a real drilling process, otherwise the model is rendered inadequate to acquire a comprehensive insight of the dynamic behavior. The time responses of the drillstring system are evaluated under various lateral conditions to measure their effects on axial and torsional directions.

The drillstring is exposed to an initial displacement, initial velocity and constant force in lateral direction. To calculate the initial displacement field, a force is applied at approximately midway of drillpipe and the displacement field is calculated from the following static equilibrium equation:

$$\{y\} = [K]^{-1}\{F\} \tag{5.1}$$

where $\{y\}$ is the lateral displacement of all nodes, $[K]$ is the global stiffness matrix and $\{F\}$ is the applied force. The initial displacement field is represented in Table 5-9. It is

noted that the existing boundary conditions imply zero lateral displacement at the rotary table (first node), neutral point (twentieth node) and the bit (last node). Initial velocity is essentially equivalent to an impulsive force application. An impulsive force is applied to produce an initial velocity of 0.05 m/s at midway of the drillpipe. The third excitation is a step force function applied at the midway of drillpipe to excite the drillstring laterally. The transient responses at the bit in axial and torsional directions due to these excitations are shown in Figure 5.6 through Figure 5.11.

As mentioned earlier, axial-bending coupling was introduced as an intrinsic expression of stiffness matrix of the system. This coupling is associated with the geometric nonlinearity of the system. In other words, if lateral deflection is large, its effect can be significant. Figure 5.6, Figure 5.7 and Figure 5.8 show the axial response at the bit due to initial displacement, initial velocity and constant force in the lateral directions respectively. Although the axial displacement is excited, the amplitude is very small for the case study described in this thesis. This is the reason why such coupling is usually neglected. However, this coupling could be significant for inclined wells or in the case of impact between the drillstring and the borehole.

Torsional-lateral coupling is introduced in the inertia matrix of system. This coupling is essential if large lateral forces are encountered. To check the severity of transversally applied excitations on torsional direction, several excitations were applied in lateral direction to observe the consequent responses in torsional direction. Figure 5.9, Figure 5.10 and Figure 5.11 show the torsional responses, which are solely due to coupling with bending motion because no torsional load is applied to the drillstring. In the present case study, torsional response due to different bending excitations is very small compared to the responses due to external or self-induced torsional excitations.

Table 5-9 : Nodal lateral initial displacement of drillstring

Node No.	Initial Displacement (m)
1	0
2	0.0051
3	0.0109
4	0.0172
5	0.0238
6	0.0309
7	0.0385
8	0.0466
9	0.0554
10	0.0649
11	0.0754
12	0.0868
13	0.0987
14	0.0957
15	0.0912
16	0.0858
17	0.0791
18	0.0705
19	0.0583
20	0.0374
21	0
22	0
23	0
24	0
25	0

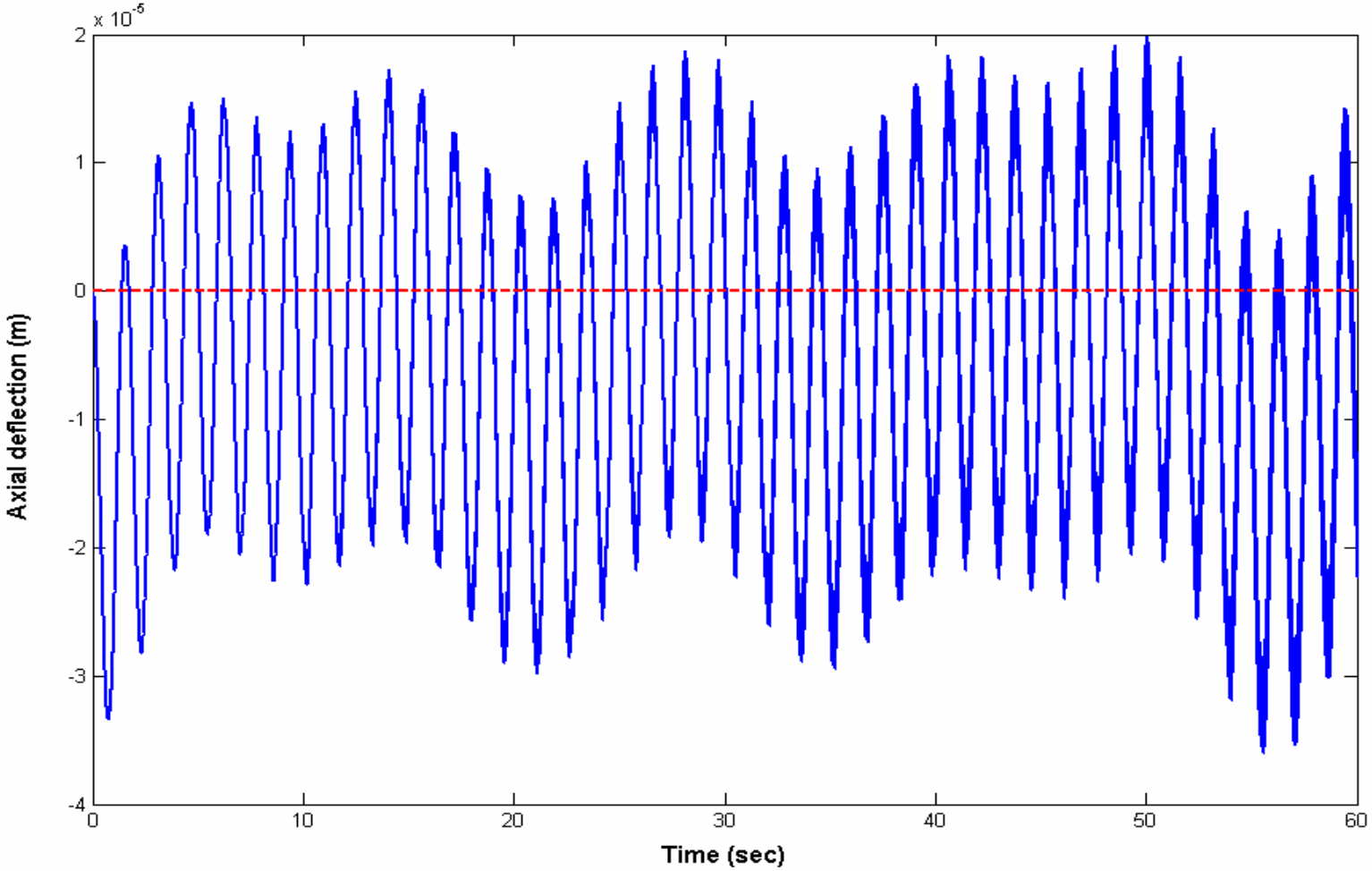

Figure 5.6 : Axial deflection due to lateral initial displacement.

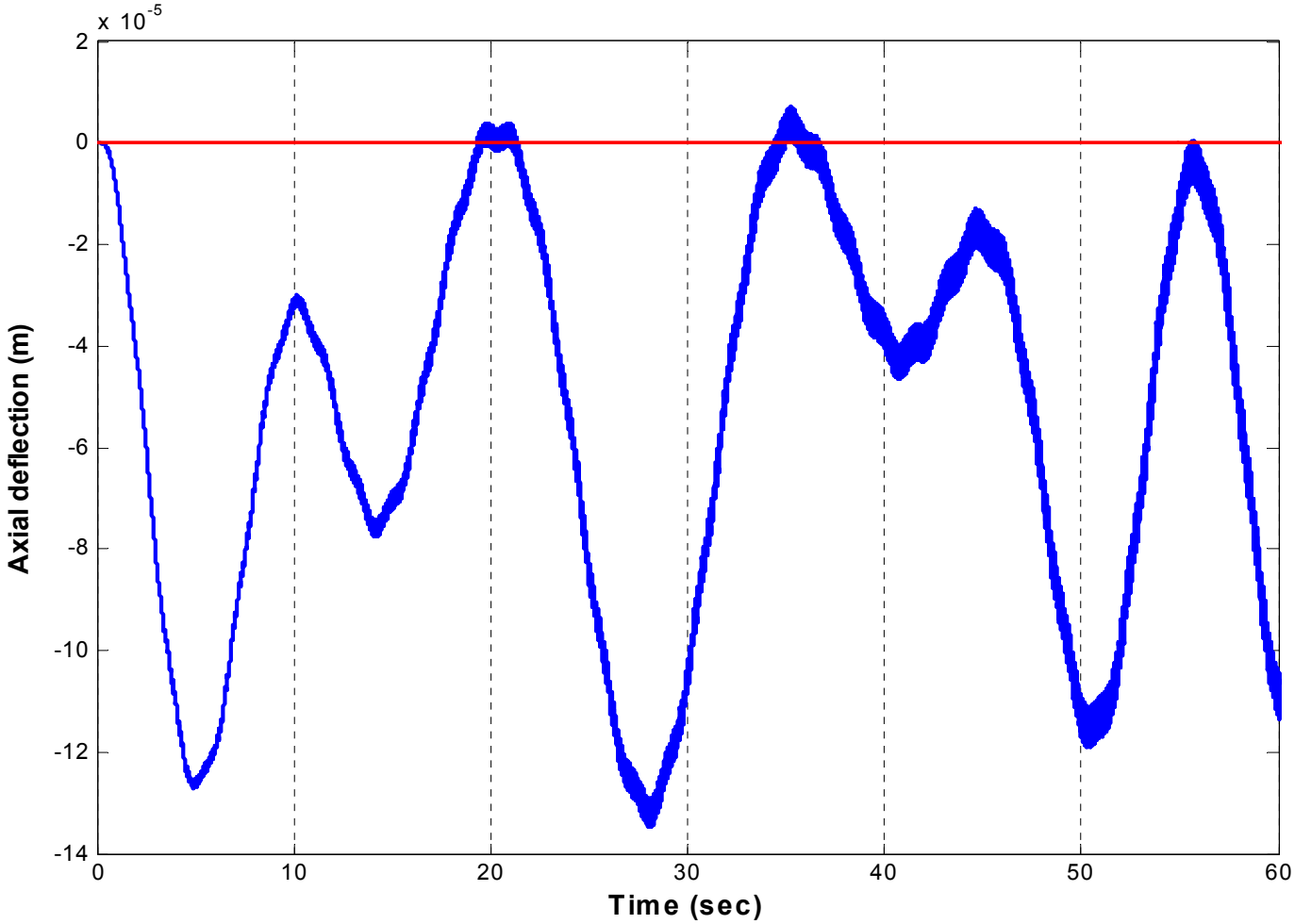

Figure 5.7 : Axial deflection due to lateral velocity.

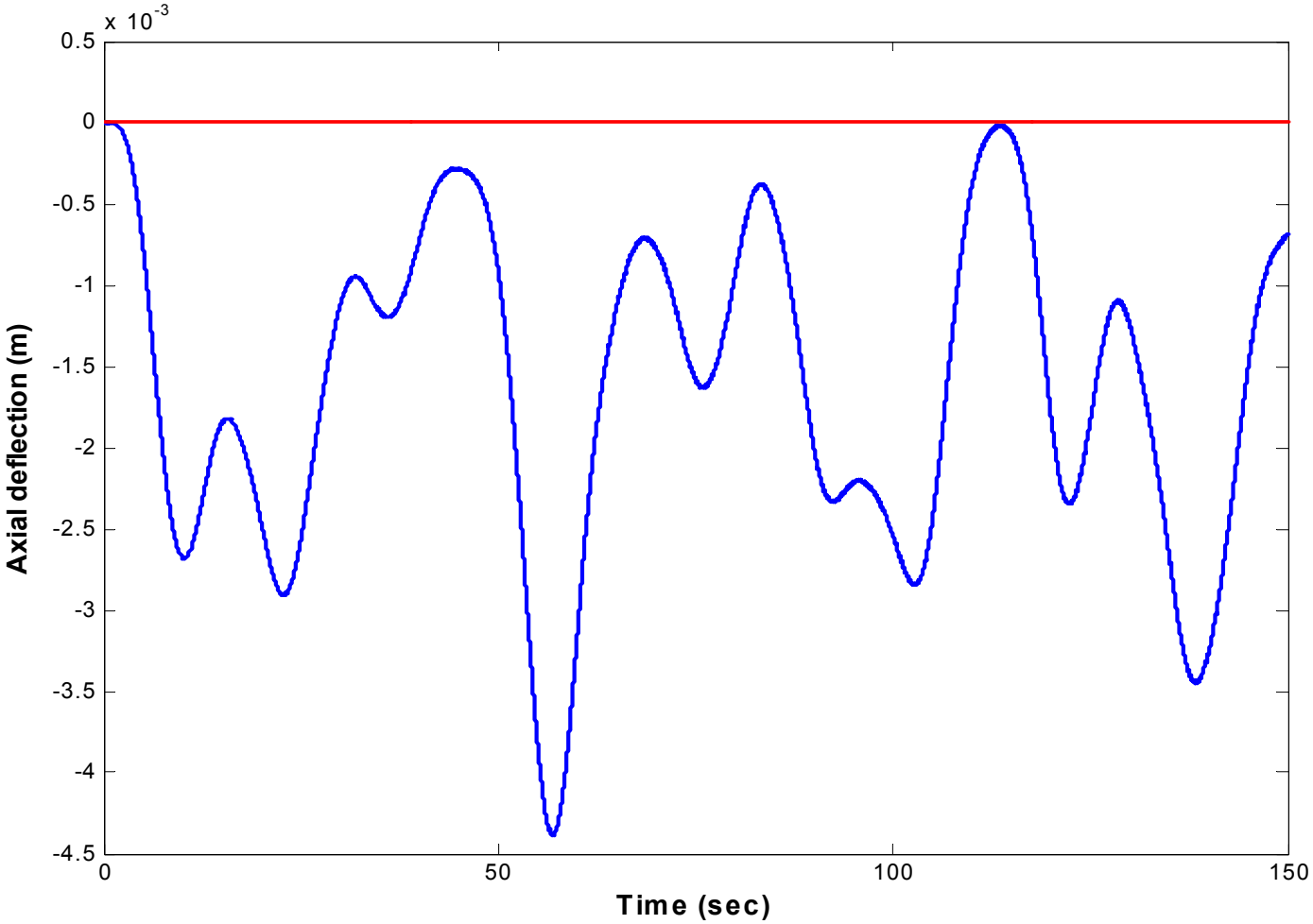

Figure 5.8 : Axial deflection due to lateral constant force.

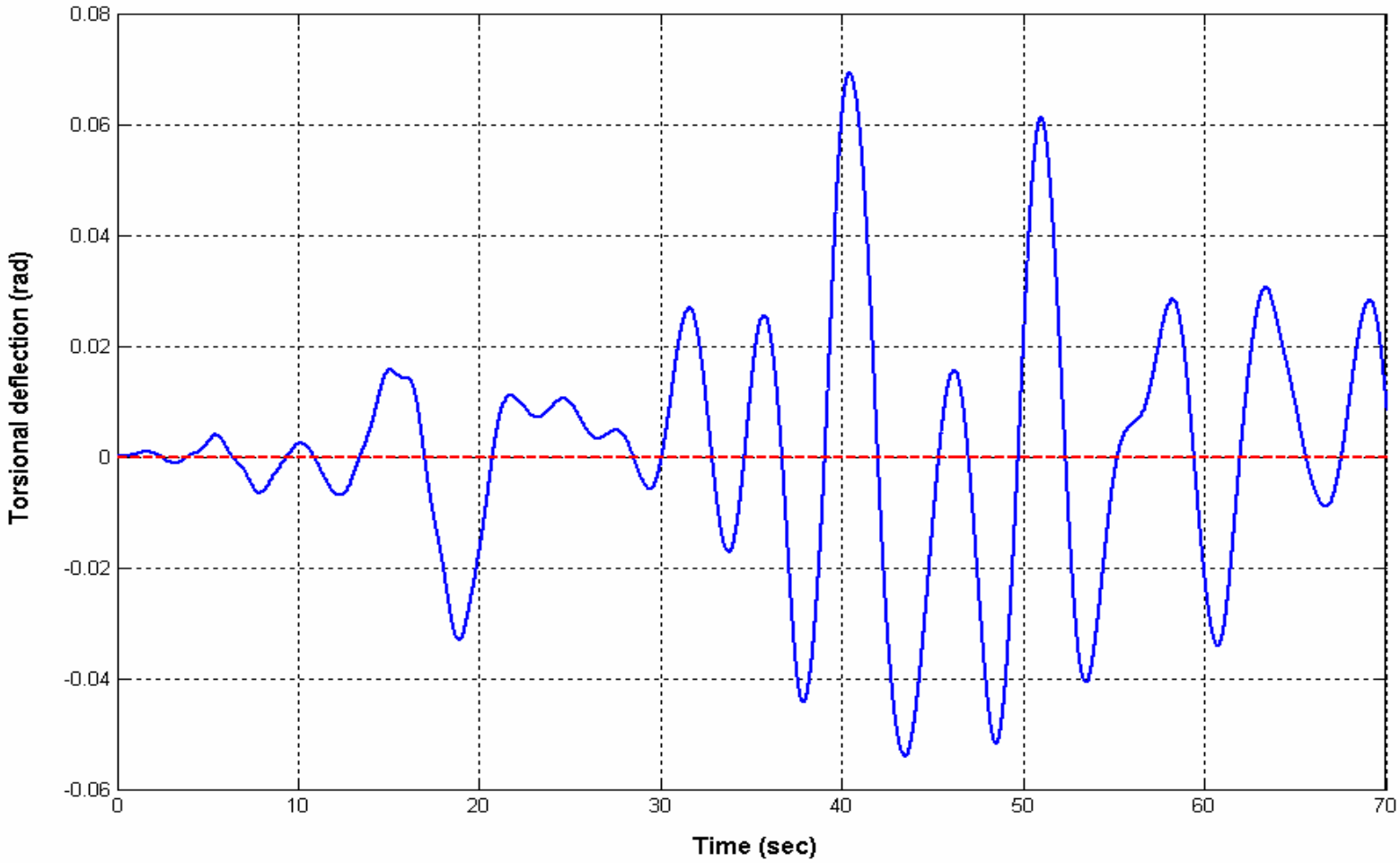

Figure 5.9 : Torsional response due to lateral initial displacement.

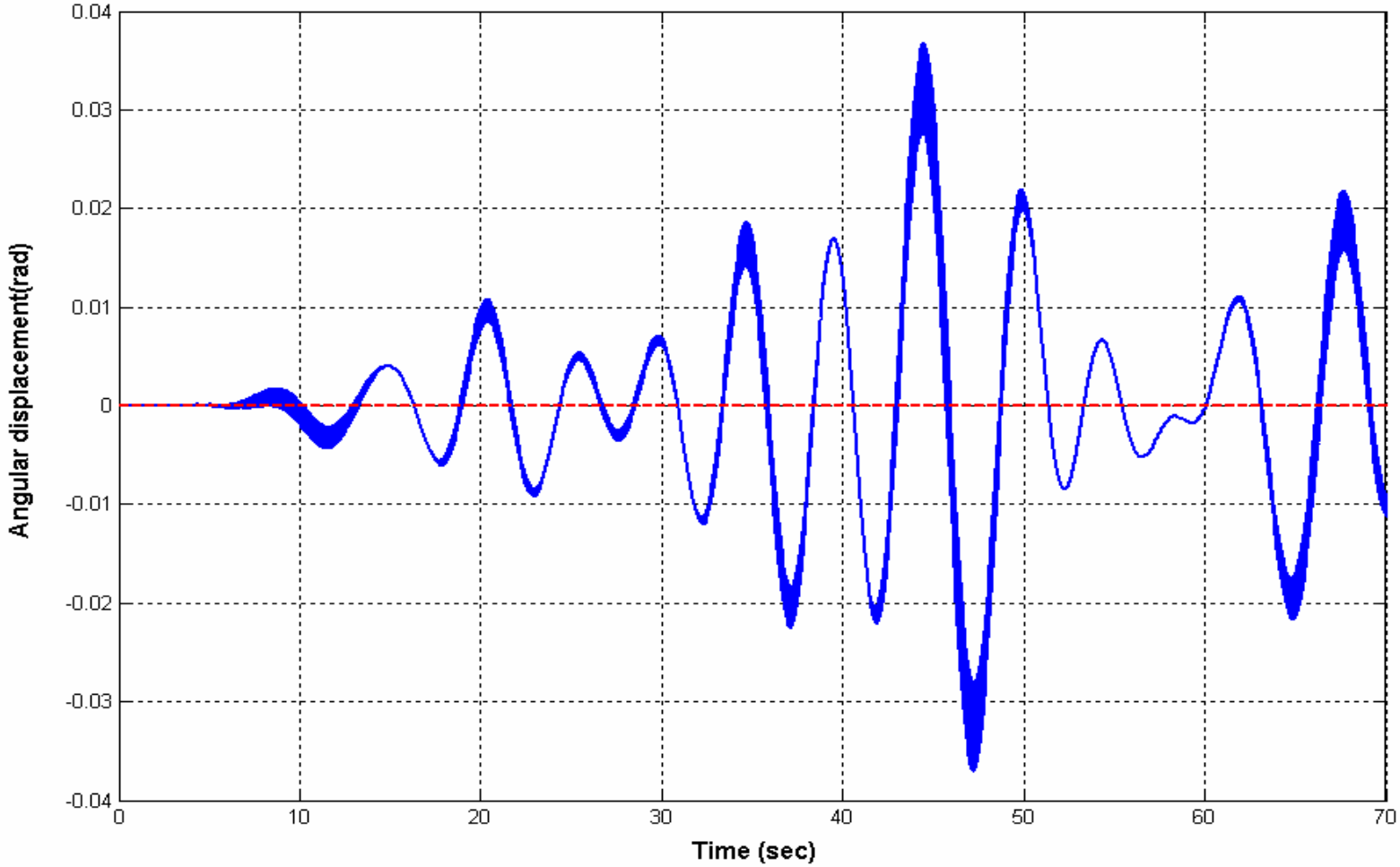

Figure 5.10 : Torsional response due to lateral initial velocity.

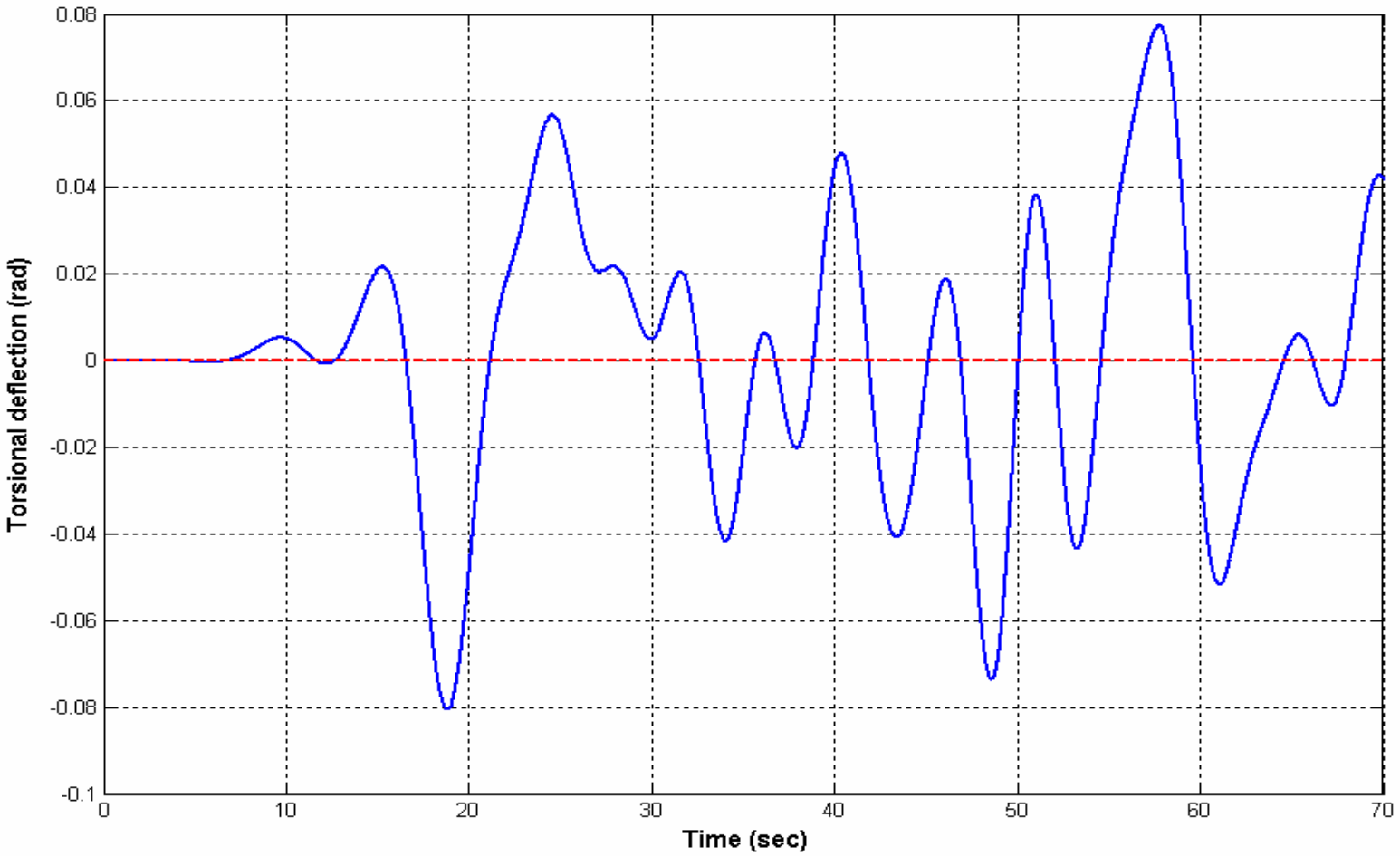

Figure 5.11 : Torsional response due to lateral constant force.

5.4. Stick-slip Responses

The friction torque is responsible for the severe stick-slip vibrations in drillstrings. To obtain the drillstring response due to friction excitation torque, appropriate torque term is included in the forcing vector of the governing equation. The parameters used in the following simulations are shown in Table 5-10 and represent a typical case in oil well drilling operations. Moreover, it is important to include the appropriate initial condition, which is set to represent the case where the whole drillstring is rotating at same speed as the rotary table. The governing equations can be solved numerically with the abovementioned forces and boundary conditions to produce the stick-slip oscillation. Since the main emphasis of the study is to investigate the effect of stick-slip oscillations on the drillstring characteristics, it is essential to focus on the various outputs of this study case. Figure 5.12 shows the instantaneous bit angular speed over a period of 20 seconds of fully developed stick-slip while drilling. The mean angular speed of the rotary table is 110 RPM (10.5rad/sec), which is constant over time while the bit is oscillating between a complete standstill, and a very high velocity reaches about 3 times the surface velocity. The average torque is about 5 kN.m. Initial rotation is chosen to be equal to zero while initial speed is same as rotary speeds for all the points, thus affecting the stationary solution. In fact, field measurements have shown that when there are significant torsional vibrations, the bit speed differs from the rotary table speed by as much as three times, which is also in agreement with the present results. Hence, this demonstrates clearly that the finite element model developed in this thesis manifests good accuracy.

It is worthwhile mentioning that the natural frequency of the first torsional mode has been calculated as 0.27 Hz. As shown in Figure 5.12, stick-slip oscillation frequency does agree with the statement in the literature that stick-slip oscillations occur at frequencies somewhat close to the first torsional natural frequency of the drillstring. While

the period of stick-slip is about four seconds, the bit is motionless in about 50% of this time.

It has been demonstrated in Figure 5.5 that the drillcollar is very stiff compared to the drillpipe. Similar conclusion can be drawn from Figure 5.13, which shows the time histories at different locations of the drillstrings. It is obvious that the response at the bit and top of the drillcollar -200m above the bit- are nearly identical. This means that the twist of the drillcollar is negligible. Close to the rotary table, the instantaneous speed is almost equivalent to the constant rotary table, which verifies that the rotary table speed remains unchangeable regardless of the downhole conditions.

Another important parameter to be investigated in stick-slip problems is the developed torque profile. The fluctuations of torque could be very detrimental to the drilling bit and downhole equipment. Typical torque evolution during stick-slip oscillation is shown in Figure 5.14 [31, 30]. During slip phase, there are periodic fluctuations in the torque profile around the mean value 5000 N.m. The amplitude of this fluctuation is relatively small but the fluctuation frequency is high. Suddenly, the toque mean value drops to minimum value, which indicates that the bit is about to stick. In stick regime, the bit momentarily stops causing the top Torque and TOB to build up in almost linear fashion to reach very large value. As shown in Figure 5.15, torque profile is more obvious when plotting the response of the reduced-order model, which neglects higher frequencies. The top end of the drillstring is fixed to the rotary table, which keeps rotating at constant speed regardless of downhole speed. The bottom end is in complete standstill during stick phase. Therefore, the drillstring winds up and absorbs energy. This energy causes the internal torque to builds up linearly until it reaches ultimate value which is same as the static value essential to break sticking condition.

Table 5-10: Data used in the numerical simulations.

W_0	100 kN
k_f	25000 kN/m
x_0	0.001 m
μ_k	0.04
α_1	2
α_2	1

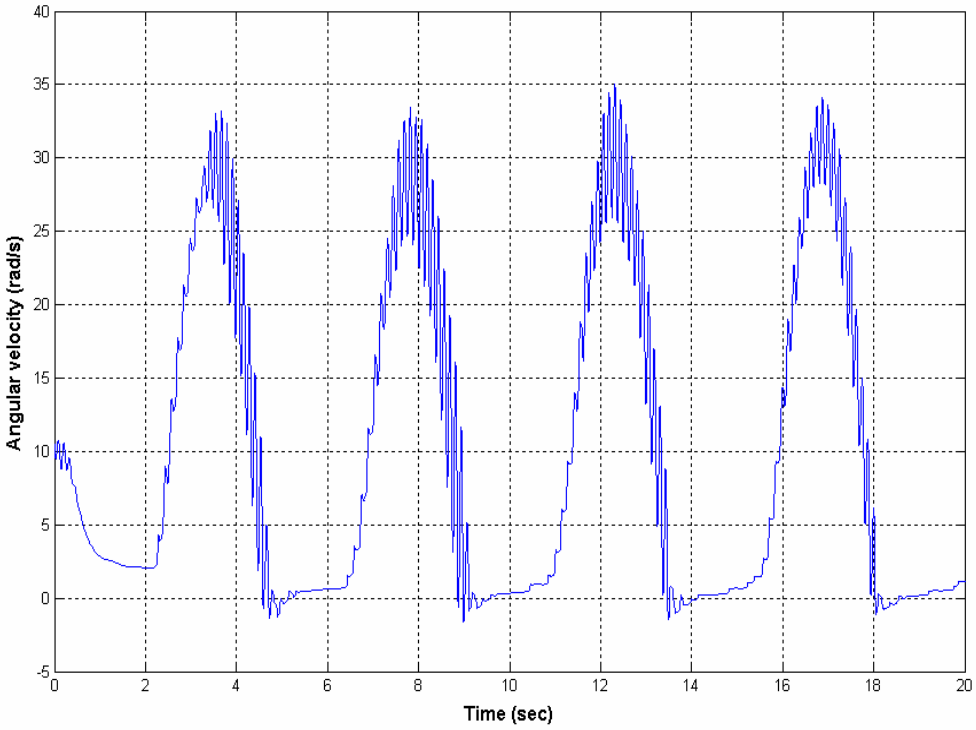

Figure 5.12: Torsional stick-slip oscillation at the drilling bit.

The stick regime can be seen clearly in Figure 5.14 which is represented as a sudden drop in the torque profile followed by a linear increase to a value greater than the nominal torque. This is very important observation because it can be measured from the surface. The main difficulty with velocity profile is that it can't be detected from the surface because the rotary table speed is forced to be constant which does not reflect the downhole situation. The measurement of torque from the top can be a clear evidence of the presence of stick-slip oscillations downhole. A series of sudden drops followed by a linear increase of torque to a value higher than the nominal one is an indication of stick-slip oscillation and immediate remedies should be followed to suppress this dysfunction.

In the previous chapter, we have discussed the profile that accommodates the expected variation of the friction torque as a function of angular velocity. It is noteworthy to investigate the relation between downhole angular velocity and TOB from the simulated results. In Figure 5.16, TOB is plotted versus drilling instantaneous angular velocity to confirm the assumed relation between TOB and downhole velocity. At low velocities, torque increased suddenly from zero at motionless state to an ultimate value. Then, it is steadily decreases to a constant value. In Figure 5.12, the velocity of the bit is not totally zero at stick regime. The reason of this can be observed in Figure 5.16 at low velocities. In stick phase, the standard discontinuous models assumed that the evolution of torque takes place at zero velocity only. By smoothing the standard models into continuous relation, torque evolution is assumed to take place over a very small region near zero velocity, i.e. it is assumed that small amount of slippage may occur during stick phase. Although the results depicted in Figure 5.16 involves some noise, the mean profile of the curve complies with the expected results. High fluctuations in the torque, which is due to the energy gained in the stick phase, can't be dissipated immediately due to the low stiffness of the drillpipe. The same torque profile is reproduced using the reduced-order model and depicted in

Figure 5.17. The bit may even spin backward for short intervals of time causing negative values of TOB as seen in Figure 5.14 and Figure 5.16 which are in close qualitative agreement with field measurements. The bit rotary speed periodically fluctuates between 35 rad/sec and -2 rad/sec. The above results confirm field measurements encountered in practice [27, 31, 30].

It is worthwhile to monitor the evolution of angular displacement during stick-slip oscillations. Figure 5.18 represents the angular displacement of the drilling bit during stick-slip event with respect to the fixed frame. The profile shown takes the shape of stairway. Comparison between Figure 5.12 and Figure 5.18 reveals that the effect of stick-slip oscillations on the angular displacement is easily identified. Stick phases are represented in Figure 5.18 by the lines parallel to the horizontal axes which imply that the bit is motionless for a short period of time. Sudden movement of the bit in the slip phase is represented by near vertical portions of the line. The major slope of this curve is the rotary table speed.

Figure 5.19 represents the trajectory of the bit displacement relative to the rotary table versus the bit instantaneous velocity. The initial bit speed is 100 RPM which is same as rotary speed. A straight line at zero speed represents the stick phase. The transition from stick to slip phase represents the maximum twist that drillstring can withstand. During slip phase, the velocity increases while the displacement returns back to its equilibrium position. In Figure 5.19, the zero value on the displacement axis represents the location of the rotary table. The region to the left side of this point (negative displacement) implies that bit is lagging behind the rotary table. Positive values of the displacement means that the bit is leading the rotary table at this regions i.e. the instantaneous speed of the bit is greater than the rotary speed.

It is difficult to notice backward motion of the drilling bit although it is represented by negative slope of the profile at slip-stick transitions. This backward motion is very observable at the slip stick transition region in Figure 5.19. Backward motion implies that some of the energy stored in the drillpipe during stick phase doesn't dissipate in slip phase. Hence, this extra energy forces the bit to rotate backward to dissipate all the remaining energy before a new stick-slip cycle starts. Moreover, smoother profile is achieved when solving the reduced-order model as illustrated in Figure 5.20. Displacement and velocity of plots versus time can be combined in a 3-D plot as depicted in Figure 5.21.

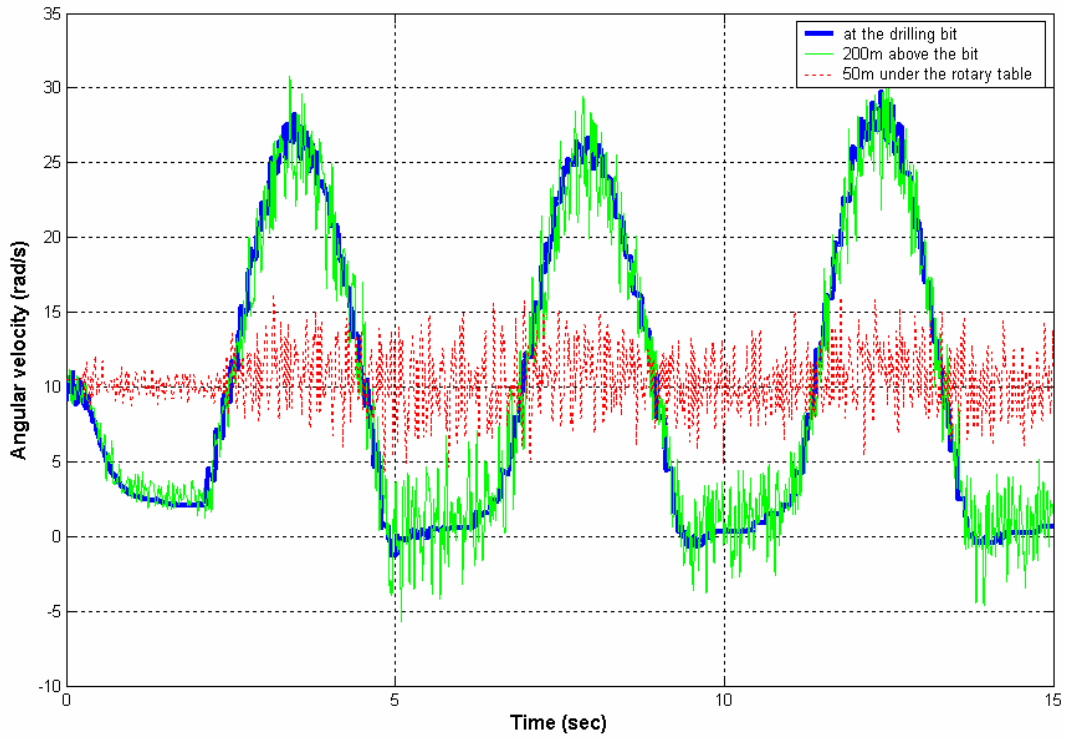

Figure 5.13: Comparison of stick-slip time histories at different locations.

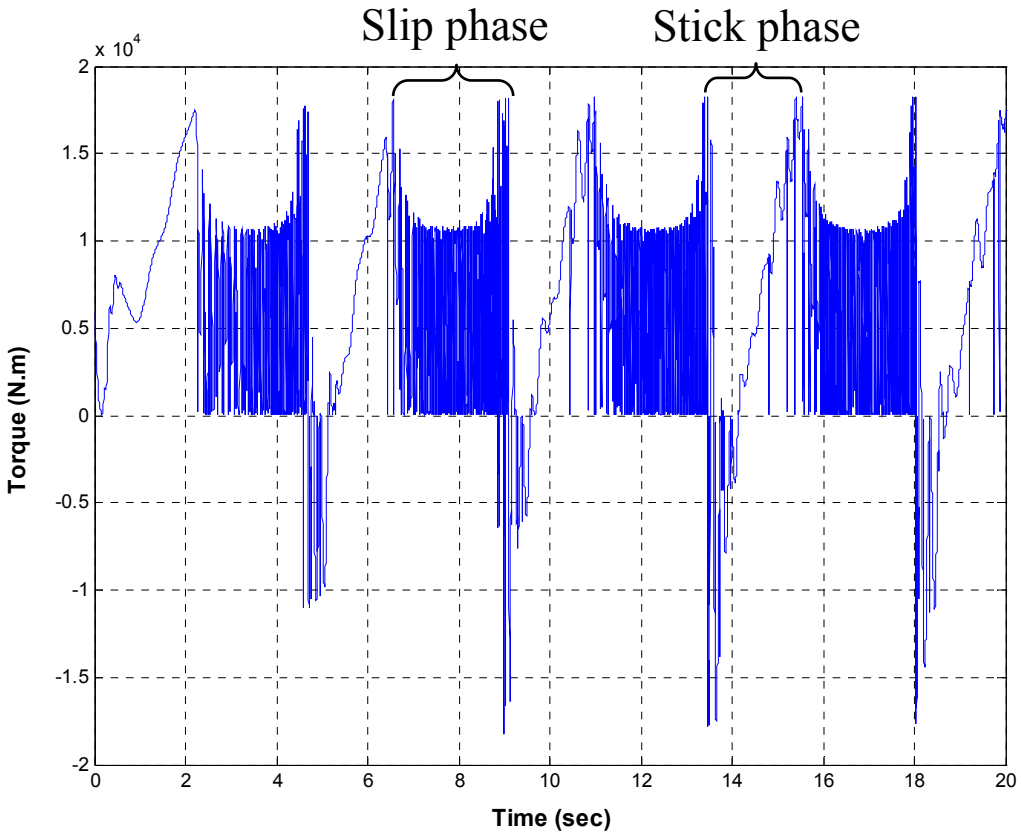

Figure 5.14 : Torque on bit profile for stick-slip oscillations (Full-order model).

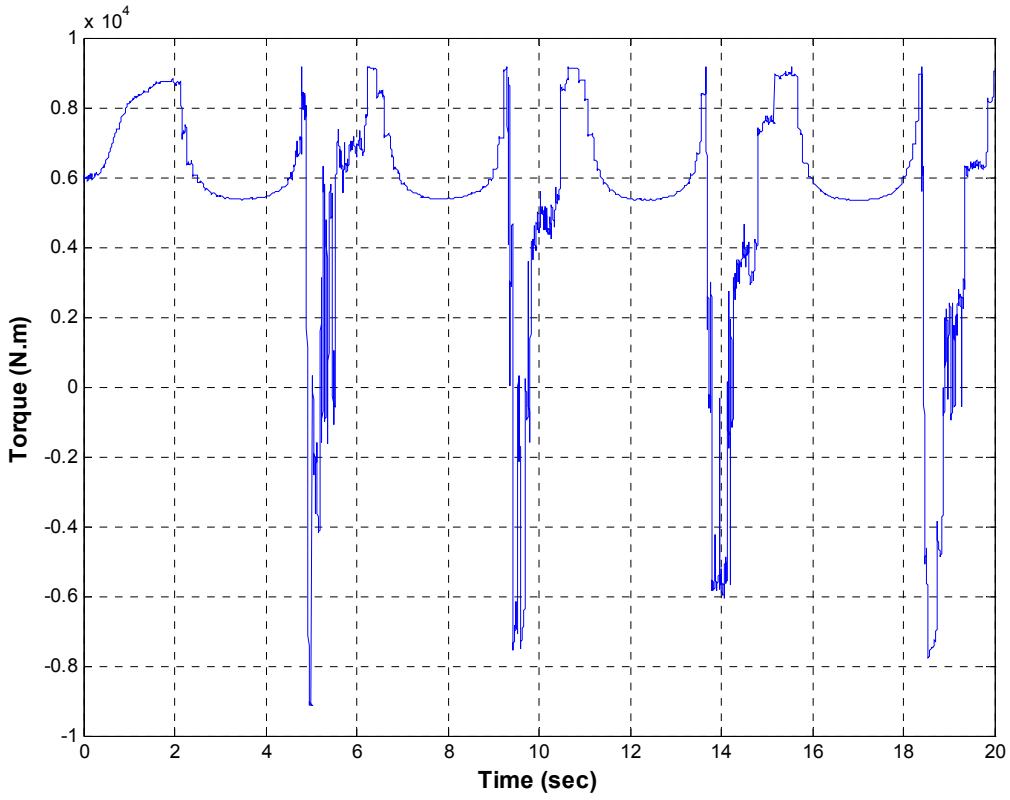

Figure 5.15: Torque on bit profile for stick-slip oscillations

(Reduced-order model).

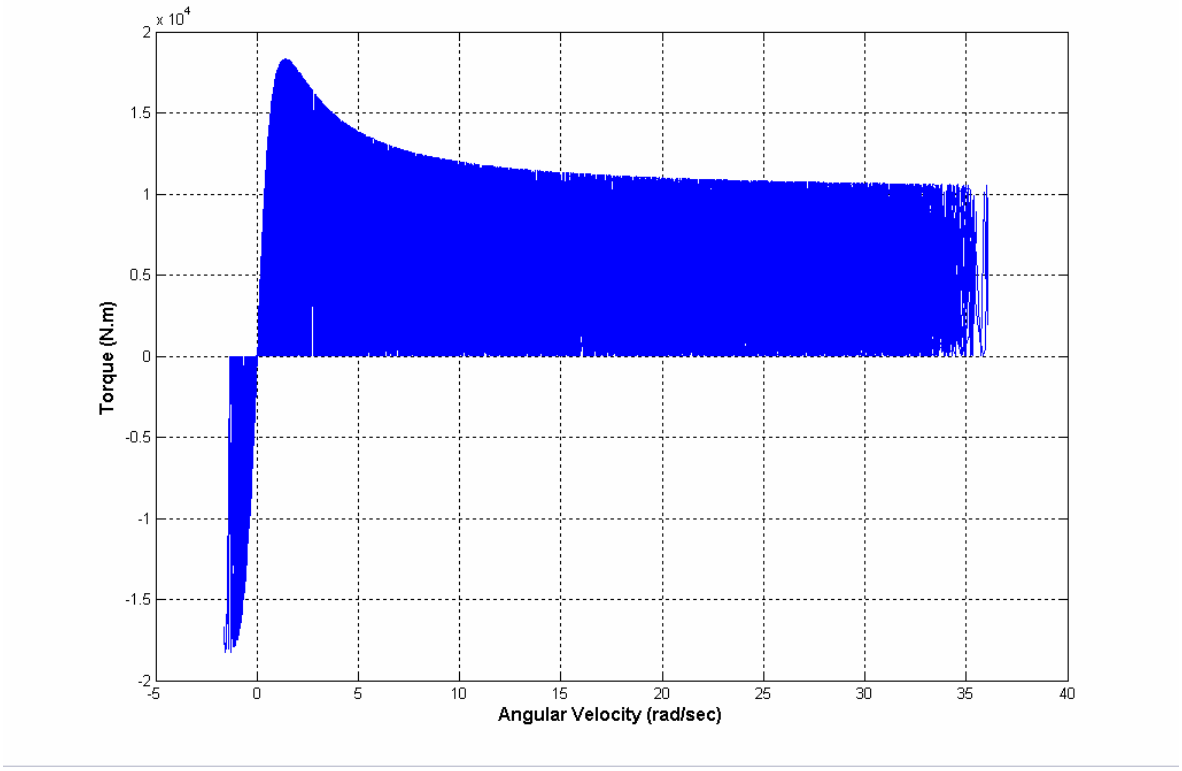

Figure 5.16: Torque vs. instantaneous angular velocity of the bit (Full-order model).

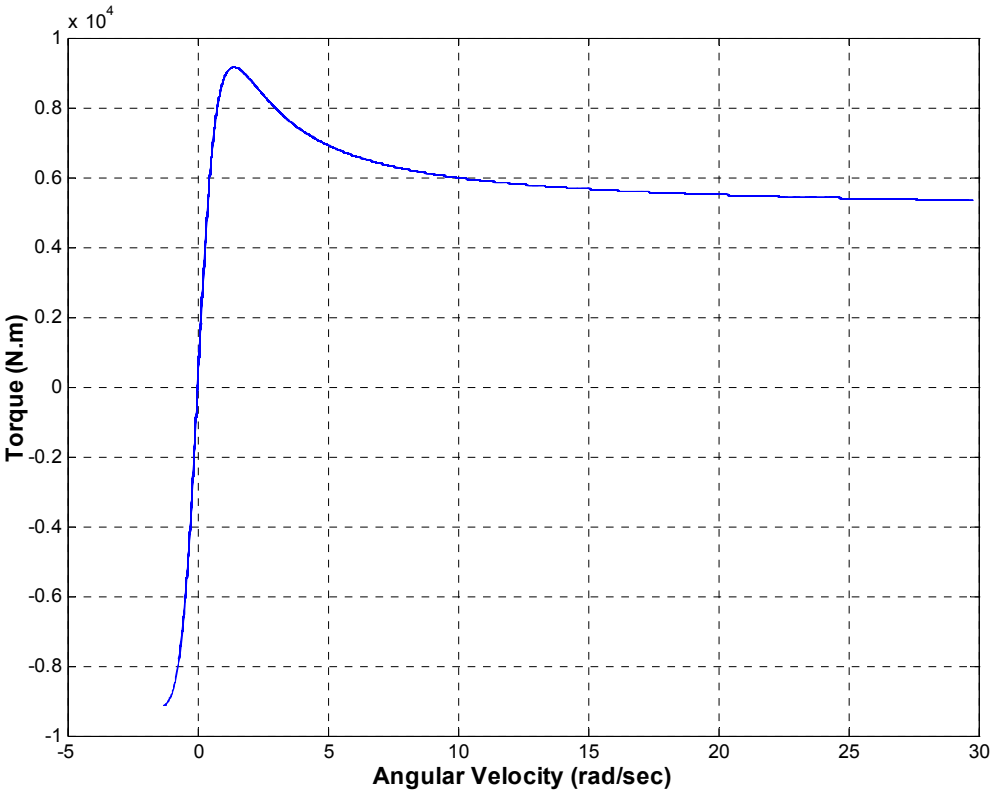

Figure 5.17: Torque vs. instantaneous angular velocity of the bit (Reduced-order model).

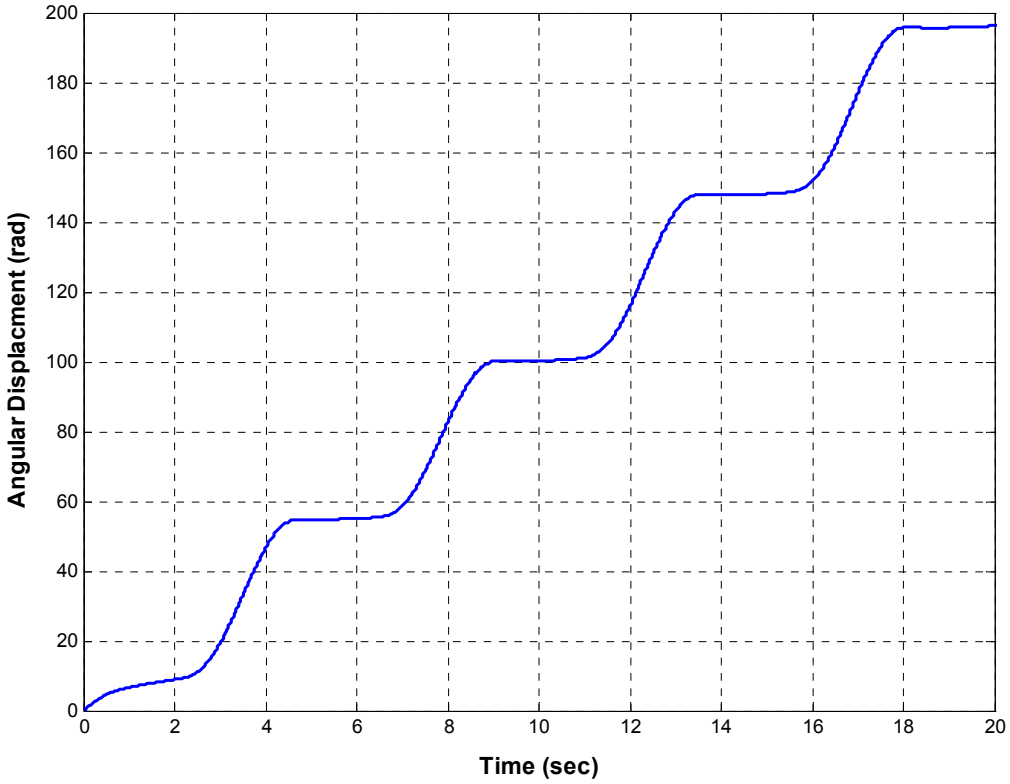

Figure 5.18 : Torsional displacement vs. time during stick-slip oscillations.

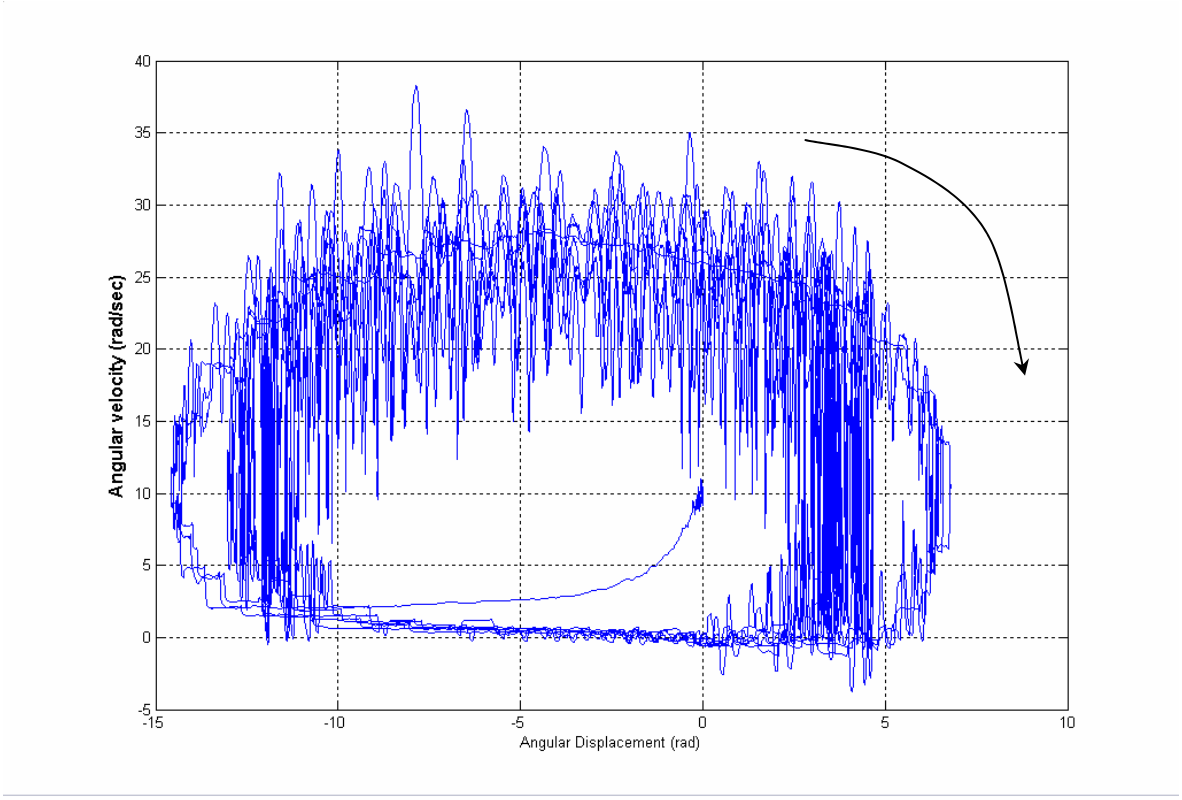

Figure 5.19 : Phase plane of the bit during stick-slip oscillations (Full-order model).

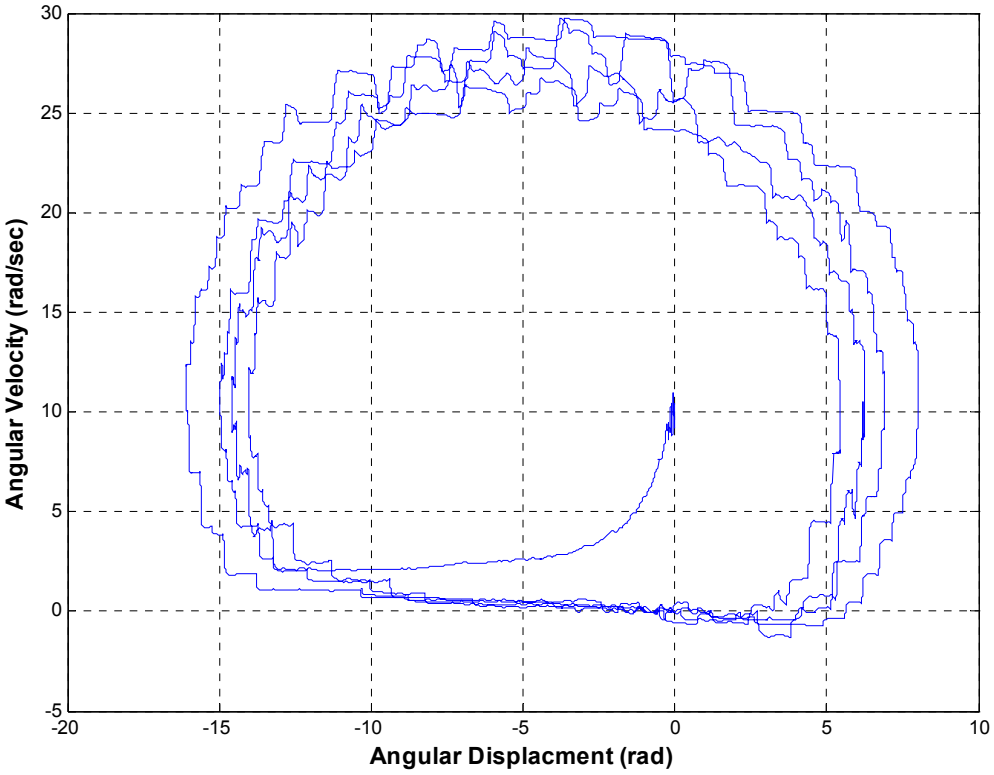

Figure 5.20: Phase plane of the bit during stick-slip oscillations (Reduced-order model).

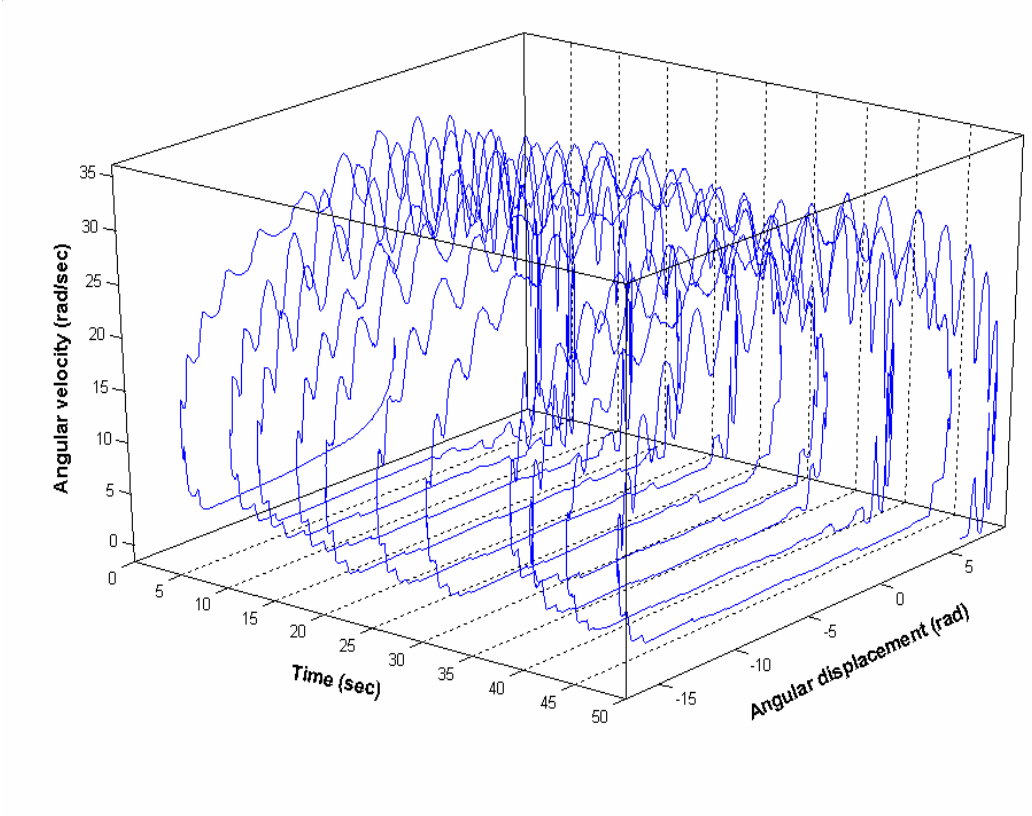

Figure 5.21: A 3-D plot of bit motion with time.

5.5. Effects of Rotary Table Speed

This section is devoted to study the stick-slip response under various rotary speeds. The downhole speed during stick-slip events depicted in Figure 5.12 is reproduced in Figure 5.22. In addition, Figure 5.22 compares this response with the results obtained with different rotary speeds. Stick-slip behavior disappears as rotary table speed increases. The purpose of Figure 5.23 is to show how torque changes with rotary speed. As rotary speed increases, the torsional oscillations become less severe. Figure 5.24 shows that as rotary speed increases, the curve becomes smoother which is evidence that stick-slip behavior disappears. An important remark can be drawn from Figure 5.25, which depicts the downhole phase plane. It is clear that the magnitude of the angular displacement (angle of twist) decreases as rotary speed increases. Furthermore, at 400 and 600 RPM the curve experience small fluctuations around the mean velocity value. Although the cycles of rotation for higher speeds did not suffer from stick-slip, the fluctuation of downhole speed is more significant.

It has been demonstrated that increasing the rotary speeds beyond a threshold value results in smoother drilling with respect to stick-slip oscillation. The critical speed for the system prescribed in Table 5-1 is found to be about 170 RPM (17.8 rad/sec). Unfortunately, the necessary speeds may not be attainable because of rig limitations or because the speeds are incompatible with other drilling parameters. For instance, high speeds may cause problems in the lateral motion such as whirling and parametric resonance. Therefore, it is of interest to find ways to increase the range of speeds at which smooth drilling is still possible.

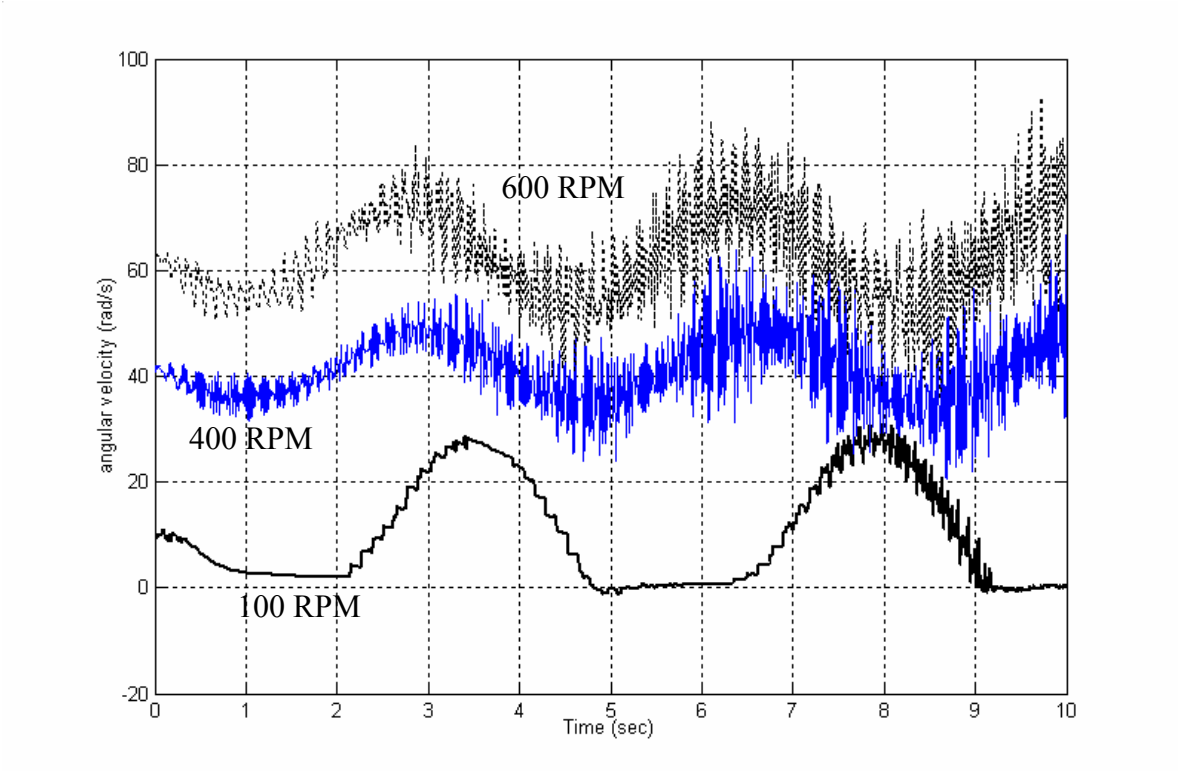

Figure 5.22 : Comparison of drilling bit velocities under stick-slip oscillations at different rotary table speeds.

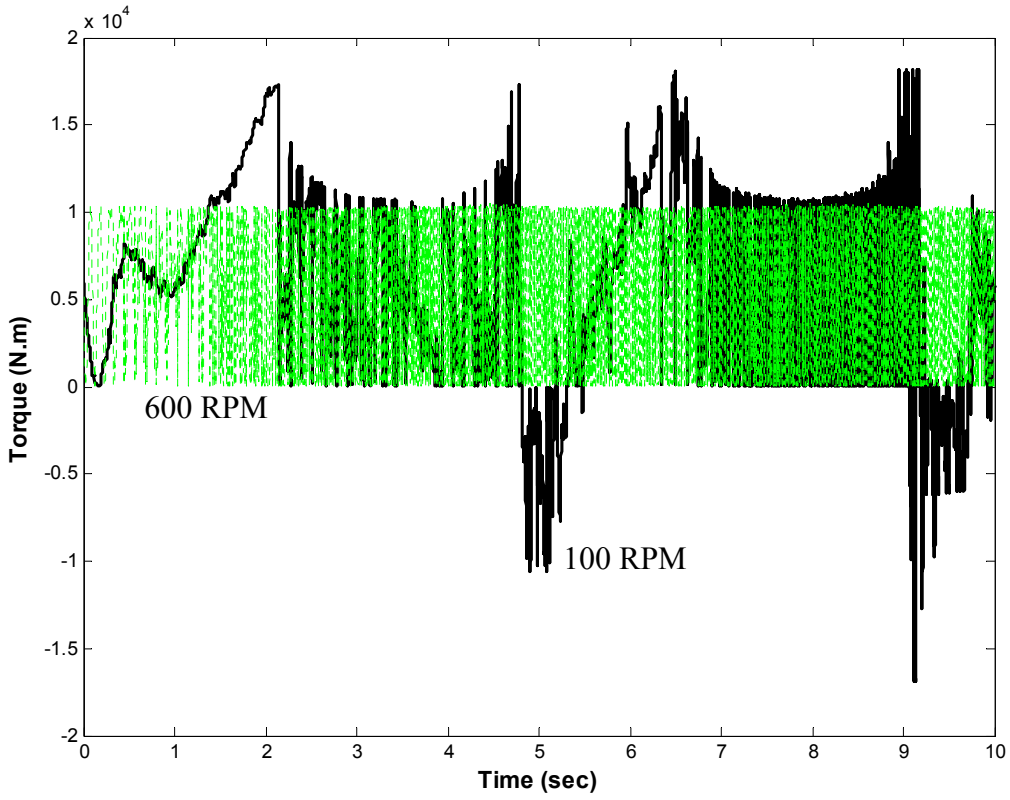

Figure 5.23 : Comparison of torque profiles for 100 RPM and 600 RPM.

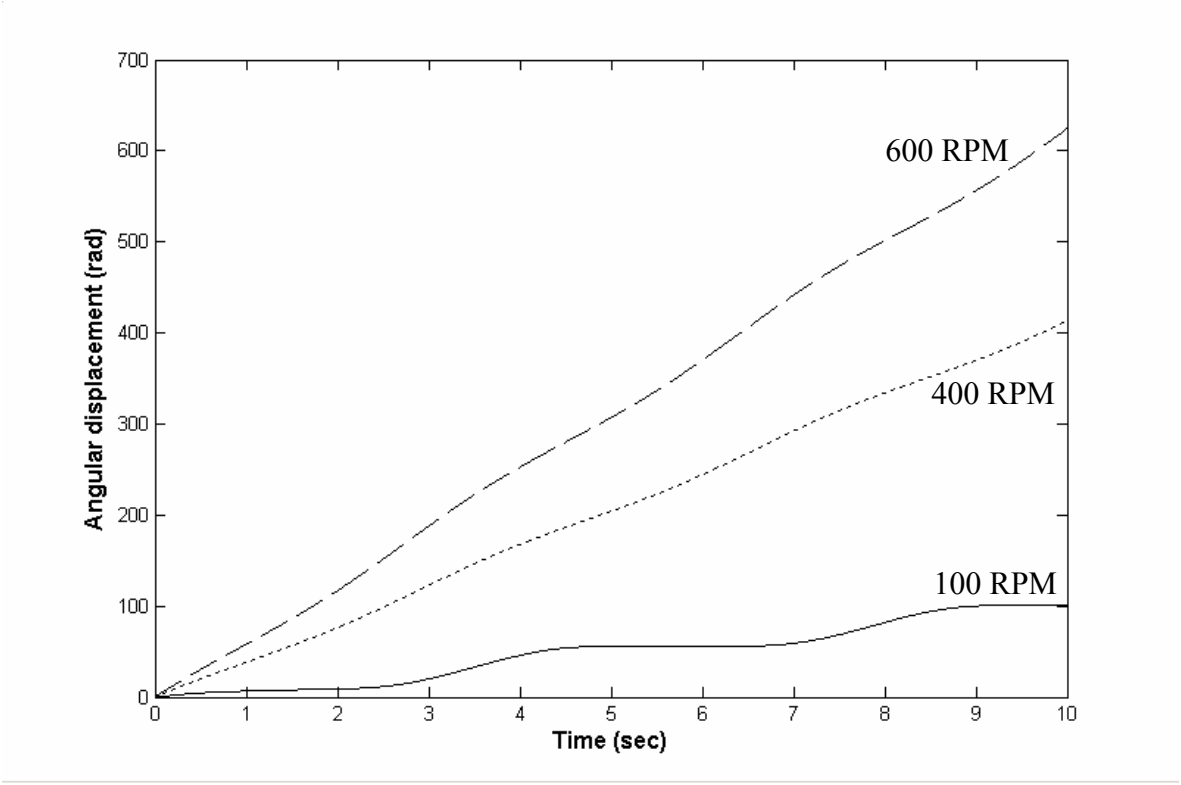

Figure 5.24 : Torsional displacement vs. time during stick-slip oscillations for 100 RPM, 400 RPM and 600 RPM.

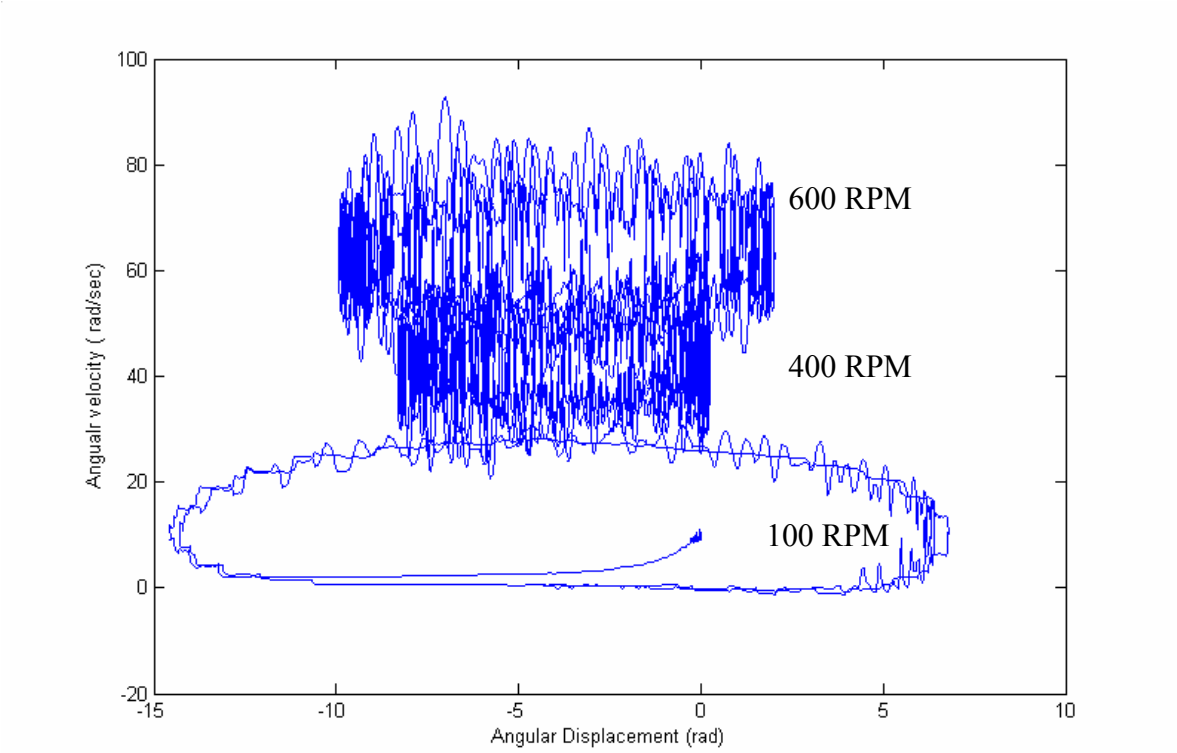

Figure 5.25 : Angular velocity versus angular displacement of the bit during stick-slip oscillations

5.6. Effect of Weight on Bit

During stick-slip event, it was intentionally attempted to test the stick-slip severity for different WOB. Figure 5.26 to Figure 5.29 show that stick-slip depends strongly on WOB. Stick-slip oscillations increased in severity as WOB increases. In all these figures, smoother drilling is achieved by reducing WOB. The threshold value of the system shown in Table 5-1 is about 2 kN. These results confirm the field observations reported [32]. Therefore, reducing WOB is considered as a remedy to reduce the severity of stick-slip oscillations.

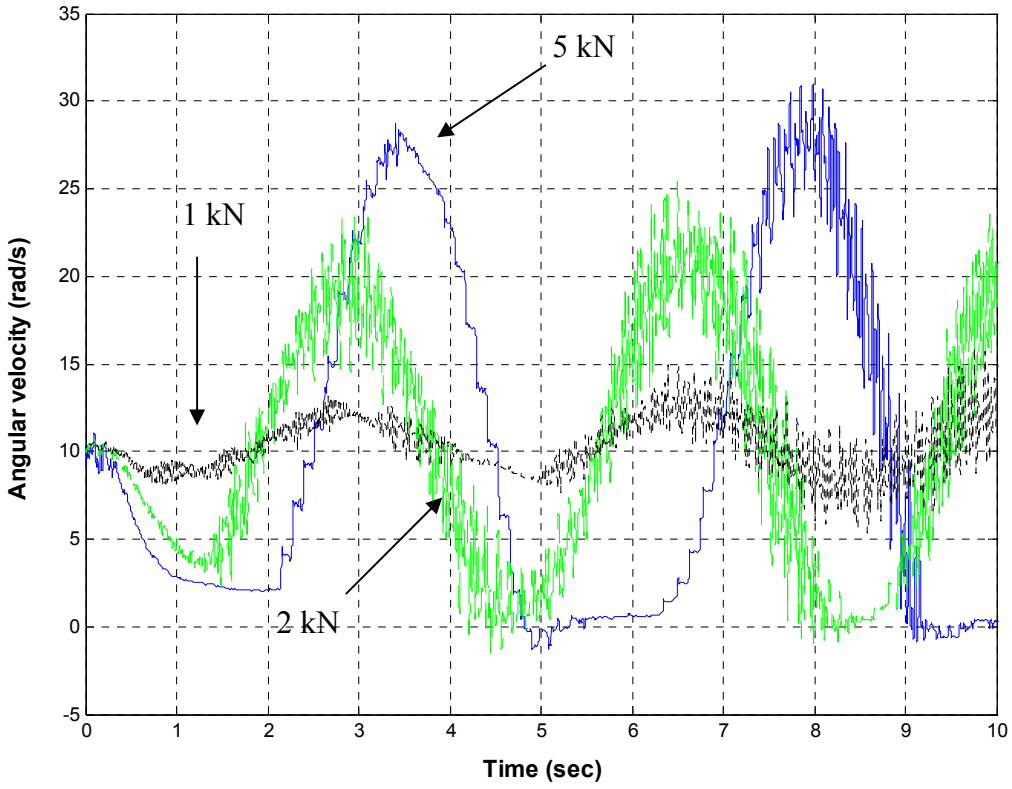

Figure 5.26: Comparison of drilling bit velocities under stick-slip oscillations at different WOB.

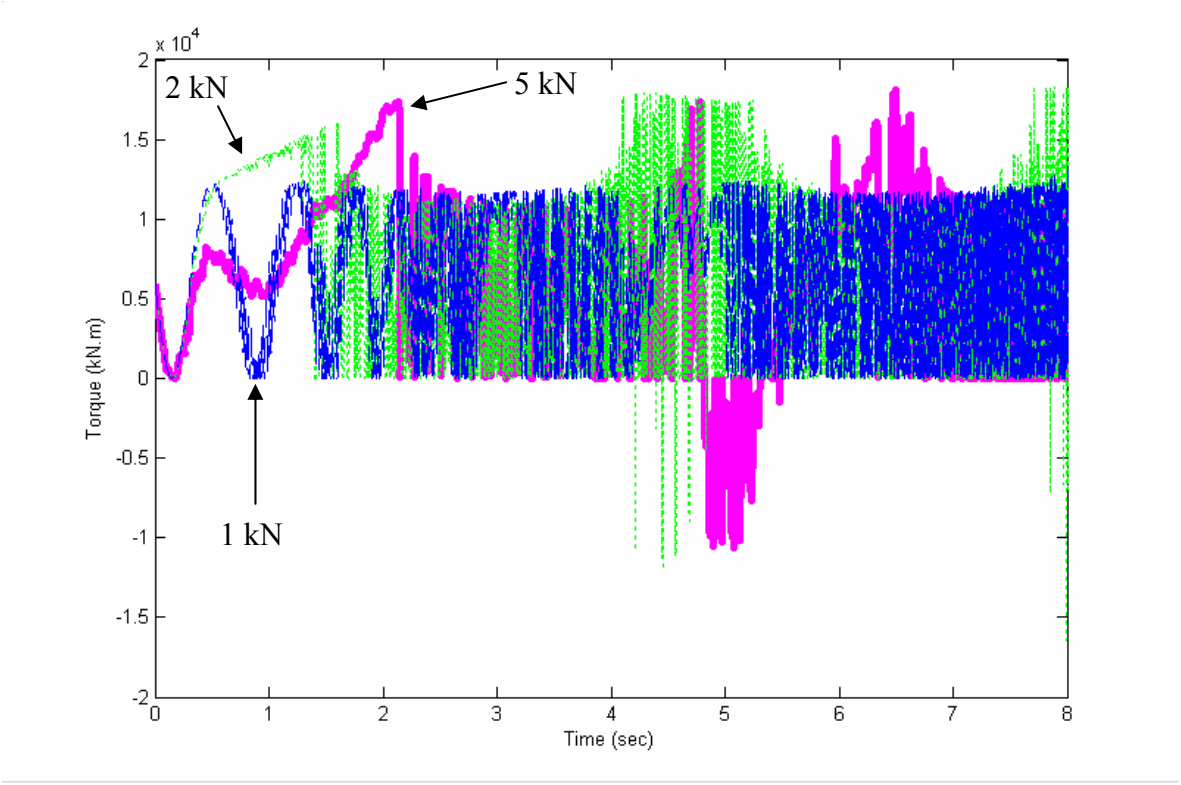

Figure 5.27: Comparison of torque profiles for 5 kN, 2kN and 1kN.

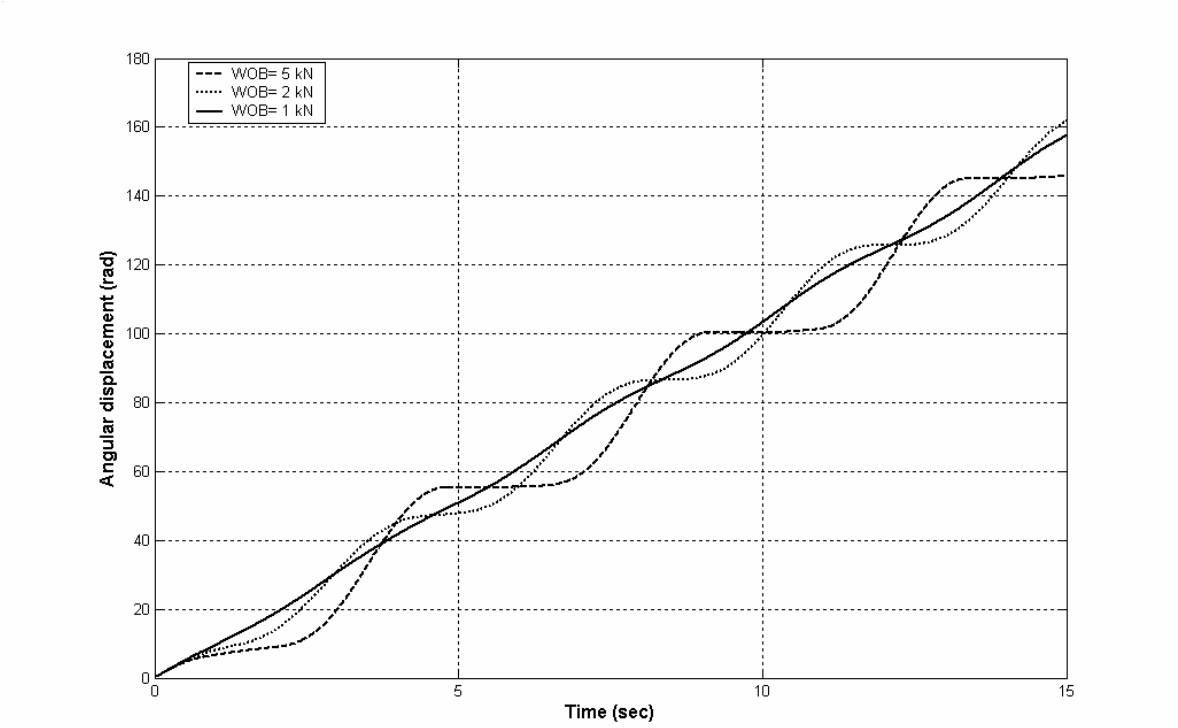

Figure 5.28 : Torsional displacement vs. time during stick-slip oscillations for 5 kN, 2kN and 1kN.

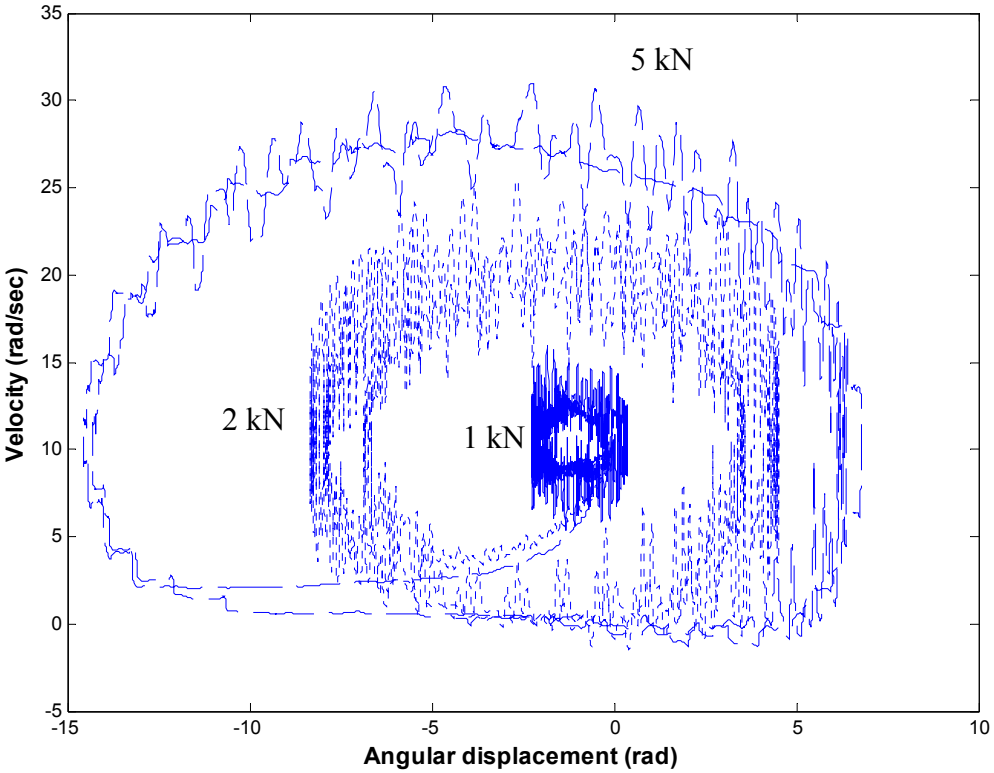

Figure 5.29: Angular velocity versus angular displacement of the bit during stick-slip oscillations

6. CONCLUSIONS

A coupled finite element formulation is presented to study the vibration characteristics of drillstrings at different operating conditions. The explicit mass, stiffness and gyroscopic matrices of the rotating finite element have been developed using Euler-Bernoulli beam theory. The model is three-dimensional to account for any inclination or spiral motion of the drillstring. The equations of motion of the drillstring are derived using Lagrangean formulation, and accounts for the rotation of the drillstring. In addition, the developed model accounts for the dynamic coupling between axial, bending and torsional vibrations as well as the effect of rotary inertia, gyroscopic moment and gravitational axial stiffening.

The developed computational scheme has the following capabilities:

a) Perform modal analysis of the drillstring,

b) Perform modal transformations to generate a reduced-order drillstring model,

c) Integrate the equations of motion to calculate the drillstring time-response due to various external excitations. Equations of motion can be in the full-order or reduced-order forms.

d) Perform dynamic response analysis of the stick-slip self-excited oscillations of the drillstring.

e) The developed scheme can handle large complex structural configurations. Furthermore, the model shows excellent adequacy in terms of accuracy, efficiency and versatility.

f) This scheme can accommodate various boundary conditions and external excitations that may exist in real life drilling.

Several conclusions can be drawn from the present study. Modal analysis of the drillstring shows that the change in the drillpipe length influenced torsional and axial natural frequencies. However, this influence is more significant for higher modes. Hence, torsional and axial frequencies are very sensitive to geometric parameters of drillpipes and drillcollars. In this study, torsional and axial frequencies obtained using the developed finite element model were compared with the results available in the literature to validate the present finite element model. The results demonstrate clearly that the finite element model developed in this study manifests good accuracy.

The coupled model was utilized to obtain the dynamic response of the drillstring due to stick-slip excitations, for a wide range of parameter variations; e.g. rotary table speed, WOB, TOB, etc. A continuous function is used to simulate the relationship between TOB and angular velocity of the drilling bit. This approximation is fairly accurate and can replace the discontinuous traditional models used to simulate stick-slip problems. As encountered in practice, the developed model showed evidence of backward spinning of the bit during stick-slip oscillations, which was unfeasible in torsional pendulum models.

Simulation results show that stick-slip vibrations disappear as the rotary table speed increases beyond a threshold value. A similar observation was noticed while examining the influence of WOB in stick-slip. Stick-slip oscillations disappear as the WOB decreases beyond a threshold value. The obtained results demonstrate the applicability and reliability of the developed computer scheme in simulating large drillstring systems, which are often found in real life. The analysis results agree with the published data, as well as field measurements reported by several investigations.

7. RECOMMENDATIONS FOR FUTURE WORK

The following recommendations are made for future research:

1) The drillstring is assumed to be vertical. However, inclined wells may also have severe stick-slip oscillations. Therefore, it is a direct extension to study the effects of stick-slip vibration in inclined or horizontal drillstrings.
2) Another extension is to take the effect of the drilling mud into consideration in order to understand the complex vibrations of the drillstring. The associated inertia and damping effects may also be included.
3) Dynamic responses due the impact between the drillstring and the borehole can be augmented to the developed scheme. Impact is known to give rise to impulsive excitations and is encountered in drilling process.
4) Torque feedback systems have been utilized in the drilling process to suppress stick-slip oscillations once they are initiated. Including such systems is essential to cure stick-slip vibrations, and can be easily accommodated by the developed dynamic model.

APPENDIX (A)

Glossary

Angle of Inclination	:	That angle, in degrees, taken at one or at several points of variation, from the vertical as revealed by a deviation survey; sometimes called the inclination or angle of deviation.
Annular Velocity	:	The velocity of a fluid moving in the annulus.
Annulus or Annular Space	:	The space between the drillstring and the wall of the hole or casing.
Anti-whirl bit	:	A drill bit, usually a polycrystalline diamond bit that is designed to prevent backward whirling, wobbling and downhole vibrations.
Barite, Barytes, Or Heavy Spar	:	Weighting material (barium sulfate) used to increase the density of drilling fluids.
Bentonite	:	A clay material, composed primarily of montmorillonite, that swells when wet. Because of its gel-forming properties, bentonite is a major component of water-base drilling mud.
Bit	:	The tool used to crush of cut rock while drilling oil and gas wells.
Bit bounce	:	When the bit loses the contact with the hole bottom, it bounces up and down on the bottom of the hole.
Bit whirl	:	The motion a bit makes when it does not rotate around its center but instead drills with a spiral motion.
Blowout	:	An uncontrolled escape of: drilling fluid, gas, oil, or water from the well caused by the formation pressure being greater than the hydrostatic head of the fluid in the hole.
Borehole	:	The wellbore; the hole made by drilling or boring a well.
Bottom-hole Assembly (BHA)	:	Assembly composed of the bit, stabilizers, reamers, drillcollars, subs, etc. used at the bottom of the drillstring.

Casing	**:**	Steel pipe placed in an oil or gas well to prevent the wall of the hole from caving in, to prevent movement of fluids from one formation to another and to improve the efficiency of extracting oil if the well is productive.
Circulation	**:**	The movement of drilling fluid from the suction pit through pump, drillpipe, bit, annular space in the hole, and back again to the suction pit. The time involved is usually referred to as circulation time.
Circulation Rate	**:**	The volume flow rate of the circulating fluid usually expressed in gallons or barrels per minute.
Clay	**:**	A plastic, soft, variously colored earth, commonly hydrous silicates of alumina, formed by the decomposition of feldspar and other aluminum silicates. Clay minerals are essentially insoluble in water but disperse under hydration, shearing forces such as grinding, velocity effects, etc., into the extremely small particles varying from submicron to 100-micron sizes.
Control/Directional Drilling	**:**	The art and science involving the intentional deflection of a wellbore in a specific direction in order to reach a predetermined objective below the surface of the earth.
Cuttings	**:**	Small pieces of rock that are the result of the chipping and/or crushing action of the bit.
Differential pressure	**:**	The difference in pressure between the hydrostatic head of the drilling-fluid column and the formation pressure at any given depth in the hole. It can be positive, zero, or negate with respect to the hydrostatic head.
Differential sticking	**:**	The action of a differential pressure holding the drillstring against the wall of the borehole.
Downhole Motor	**:**	A power source located just above the bit to rotate the bit.
Drillcollars	**:**	Round, square, and triangular drillstring elements utilized to provide a load on the bit for the purpose of drilling.
Drilling Mud or Fluid	**:**	A circulating fluid used during rotary drilling to perform any or all of various functions required in the drilling operation.

Drillpipe	**:**	The tubular member of the drillstring to which tool joints are attached.
Drillstring	**:**	The column or string that includes drillpipe, drillcollar and bit.
Fatigue	**:**	The tendency of material to break under repeated cyclic loading at a stress considerably less than the tensile strength shown in a static test.
Fishing	**:**	Operations on the rig for the purpose of retrieving from the well bore sections of pipe, collars, junk, or other obstructive item which are in the hole.
Forced vibrations	**:**	Forced vibration responses are produced by an external force which is independent from the motion it produces.
Horizontal drilling	**:**	Deviation of the borehole at least 80^0 from vertical so that the borehole penetrates a productive formation in a manner parallel to the formation. A single horizontal hole can eliminate the need for several vertical boreholes.
Kick	**:**	An entry of water, gas, oil or other formation fluid into the wellbore during drilling. It occurs because the pressure exerted by the column of drilling fluid is not great enough to overcome the pressure exerted by the fluids in the formation drilled. If prompt action is not taken to control the kick, a blowout may occur.
Measurement While Drilling (MWD)	**:**	Any system of measuring downhole conditions during routine drilling operations.
Mud logging	**:**	A method of determining the presence or absence of oil or gas in the various formations penetrated by the drill bit. The drilling fluid and the cuttings are continuously tested on their return to the surface, and the results of these tests are correlated with the depth or origin.
Rate of Penetration (ROP)	**:**	The speed with which the bit drills the formation.
Rotary Drilling	**:**	The method of drilling wells that depends on the rotation of drillpipe to the bottom of which is attached a bit. A mud is circulated to remove the cuttings.
Rotary speed	**:**	The speed at which the rotary table is operated.

Self-excited vibrations	**:**	Case of vibrations when the exciting force is coupled with the motion it produces.
Shock sub	**:**	A tool used to absorb the axial movement which results in changing the resonant frequency of the BHA.
Stabilizer	**:**	Stabilizer is a coarsely grooved cylindrical element of a larger diameter than the drillcollar that loosely fit in the borehole.
Tool joint	**:**	A drillpipe coupler consisting of a pin and a box of various designs and sizes. The internal design of tool joints has an important effect on mud hydraulics.
Torque	**:**	The measure of the force or effort applied to a shaft and causing it to rotate. On a rotary rig this applies especially to the rotation of the drillstring in its action against the bore of the hole. Torque reduction can usually be accomplished by the addition of various drilling-fluid additives.
Torque on Bit (TOB)	**:**	Required torque to rotate the bit.
Tripping	**:**	The operation of hoisting the drillstring out of and returning it to the wellbore.
Twist-off	**:**	A complete break in pipe caused by metal fatigue.
Weight on Bit (WOB)	**:**	The compressive force on the bit.
Wellbore	**:**	The hole drilled by the bit.

APPENDIX (B)

Table B-1

Explicit expression of the shape functions

$N_{v1} = 1 - 3\left(\frac{x}{l}\right)^2 + 2\left(\frac{x}{l}\right)^3$	$N_{\theta 3} = \frac{6}{l}\left(\frac{x}{l} - \left(\frac{x}{l}\right)^2\right)$
$N_{v2} = l\left(\frac{x}{l} - 2\left(\frac{x}{l}\right)^2 + \left(\frac{x}{l}\right)^3\right)$	$N_{\theta 4} = 3\left(\frac{x}{l}\right)^2 - 2\frac{x}{l}$
$N_{v3} = 3\left(\frac{x}{l}\right)^2 - 2\left(\frac{x}{l}\right)^3$	$N_{\varphi 1} = 1 - \frac{x}{l}$
$N_{v4} = l\left(-\left(\frac{x}{l}\right)^2 + \left(\frac{x}{l}\right)^3\right)$	$N_{\varphi 2} = \frac{x}{l}$
$N_{\theta 1} = \frac{6}{l}\left(\left(\frac{x}{l}\right)^2 - \frac{x}{l}\right)$	$N_{u1} = 1 - \frac{x}{l}$
$N_{\theta 2} = 1 - 4\left(\frac{x}{l}\right) + 3\left(\frac{x}{l}\right)^2$	$N_{u2} = \frac{x}{l}$

Table B-2

Elastic stiffness matrix of rotating drillstring element $\left[K_e\right] = EI\left[K_{ab}^e\right]$

The non-zero entries of the upper triangular part of $[K_{ab}]$ *a, b*= 1, 2, ……,12

$$K_{22}^e = -K_{28}^e = K_{33}^e = -K_{29}^e = K_{88}^e = K_{99}^e = \frac{12}{l^3}$$

$$K_{25}^e = K_{211}^e = -K_{34}^e = -K_{310}^e = K_{49}^e = -K_{58}^e = -K_{811}^e = K_{910}^e = \frac{6}{l^2}$$

$$K_{44}^e = K_{55}^e = K_{1010}^e = K_{1111}^e = \frac{4}{l}$$

$$K_{410}^e = K_{511}^e = \frac{2}{l}$$

Table B-3

State independent axial stiffness matrix of rotating drillstring element $\left[K_a\right] = EA\left[K_{ab}^a\right]$

The non-zero entries of the upper triangular part of [K_{ab}], a, b= 1, 2, ……,12

$$K_{11}^a = K_{77}^a = \frac{2}{l}$$

$$K_{17}^a = \frac{1}{l}$$

Table B-4

State-dependent axial stiffness matrix of rotating drillstring element $[K_a] = EA[K_{ab}^a]$

The non-zero entries of the upper triangular part of $[K_{ab}]$, a, b= 1, 2, ……,12

$$K_{11}^a = K_{77}^a = -K_{71}^a = -K_{17}^a = -\frac{3(u_1 - u_2)}{2l^2}$$

$$K_{12}^a = K_{78}^a = -K_{18}^a = -K_{72}^a = -\frac{12(v_1 - v_2) + l\theta_{z1} + l\theta_{z2}}{20l^2}$$

$$K_{13}^a = K_{79}^a = -K_{73}^a = -K_{19}^a = -\frac{12(w_1 - w_2) - l\theta_{y1} - l\theta_{y2}}{20l^2}$$

$$K_{15}^a = -K_{75}^a = -\frac{3(v_1 - v_2) + 4l\theta_{z1} - l\theta_{z2}}{60l}$$

$$K_{711}^a = -K_{1,11}^a = \frac{3(v_1 - v_2) - l\theta_{z1} + 4l\theta_{z2}}{60l}$$

$$K_{14}^a = -K_{74}^a = \frac{3(w_1 - w_2) - 4l\theta_{y1} + l\theta_{y2}}{60l}$$

$$K_{110}^a = -K_{710}^a = \frac{3(w_1 - w_2) + l\theta_{y1} - 4l\theta_{y2}}{60l}$$

$$K_{22}^a = K_{88}^a = -K_{82}^a = -K_{28}^a = K_{33}^a = K_{99}^a = -K_{93}^a = -K_{39}^a = -\frac{6(u_1 - u_2)}{5l^2}$$

$$K_{52}^a = K_{11,2}^a = K_{25}^a = -K_{85}^a = -K_{58}^a = -K_{118}^a = K_{211}^a = -K_{811}^a = -\frac{(u_1 - u_2)}{10l^2}$$

$$K_{43}^a = K_{103}^a = K_{34}^a = -K_{94}^a = -K_{49}^a = -K_{109}^a = K_{310}^a = -K_{910}^a = \frac{(u_1 - u_2)}{10l^2}$$

$$K_{55}^a = K_{1111}^a = K_{444}^a = K_{1010}^a = -\frac{2(u_1 - u_2)}{15}$$

$$K_{115}^a = K_{511}^a = K_{104}^a = K_{410}^a = \frac{(u_1 - u_2)}{30}$$

Table B-5

Torsional stiffness matrix of rotating drillstring element $\left[K_{\varphi}\right]= GI_{p}\left[K_{ab}^{\varphi}\right]$

The non-zero entries of the upper triangular part of $[K_{ab}]$, a, b= 1, 2, ……,12

$$K_{66}^{\varphi} = -K_{612}^{\varphi} = K_{1212}^{\varphi} = \frac{1}{l}$$

Table B-6

Axial stiffening matrix of rotating drillstring element $\left[K_{as}\right]= \rho gA\left[K_{ab}^{as}\right]$

The non-zero entries of the upper triangular part of $[K_{ab}]$, *a, b*= 1, 2, ……,12

for drillpipe (under tension)

$$K_{22}^{as} = K_{33}^{as} = -K_{28}^{as} = -K_{39}^{as} = K_{88}^{as} = K_{99}^{as} = \frac{3}{5} + \frac{6}{5}\frac{L_t}{l_i}$$

$$K_{25}^{as} = -K_{34}^{as} = K_{49}^{as} = -K_{58}^{as} = \frac{1}{10}L_t$$

$$K_{211}^{as} = -K_{310}^{as} = K_{910}^{as} = -K_{811}^{as} = \frac{1}{10}l_i + \frac{1}{10}L_t$$

$$K_{44}^{as} = K_{55}^{as} = \frac{1}{10}l_i^2 + \frac{2}{15}L_t l_i$$

$$K_{410}^{as} = K_{511}^{as} = -\frac{1}{60}l_i^2 - \frac{1}{30}L_t l_i$$

$$K_{1010}^{as} = K_{1111}^{as} = \frac{1}{30}l_i^2 + \frac{2}{15}L_t l_i$$

Table B-7

Axial stiffening matrix of rotating drillstring element $[K_{as}] = \rho g A [K_{ab}^{as}]$

The non-zero entries of the upper triangular part of $[K_{ab}]$, $a, b = 1, 2, \ldots\ldots, 12$

for drillcollar (under compression)

$$K_{22}^{as} = K_{33}^{as} = -K_{28}^{as} = -K_{39}^{as} = K_{88}^{as} = K_{99}^{as} = \frac{3}{5} + \frac{6}{5}\frac{L_c}{l_i}$$

$$K_{25}^{as} = -K_{34}^{as} = K_{49}^{as} = -K_{58}^{as} = \frac{1}{10} l_i + \frac{1}{10} L_c$$

$$K_{211}^{as} = -K_{310}^{as} = K_{910}^{as} = -K_{811}^{as} = \frac{1}{10} L_c$$

$$K_{44}^{as} = K_{55}^{as} = \frac{1}{30} l_i^{\,2} + \frac{2}{15} L_c l_i$$

$$K_{410}^{as} = K_{511}^{as} = -\frac{1}{60} l_i^{\,2} - \frac{1}{30} L_c l_i$$

$$K_{1010}^{as} = K_{1111}^{as} = \frac{1}{10} l_i^{\,2} + \frac{2}{15} L_c l_i$$

Table B-8

Translational mass matrix of rotating drillstring element $[M_t] = \mu A[M^e_{ab}]$

The non-zero entries of the upper triangular part of $[M_{ab}]$, a, b= 1, 2, ……,12

$$M^e_{11} = M^e_{77} = \frac{1}{3}l$$

$$M^e_{17} = \frac{1}{6}l$$

$$M^e_{22} = M^e_{33} = M^e_{88} = M^e_{99} = \frac{13}{35}l$$

$$M^e_{25} = -M^e_{34} = -M^e_{811} = M^e_{910} = \frac{11}{210}l^2$$

$$M^e_{28} = M^e_{310} = \frac{9}{70}l$$

$$M^e_{44} = M^e_{55} = M^e_{1111} = M^e_{1010} = \frac{l^3}{105}$$

$$-M^e_{211} = M^e_{310} = -M^e_{49} = M^e_{58} = \frac{13}{420}l^2$$

$$M^e_{410} = M^e_{511} = -\frac{l^3}{140}$$

Table B-9

Rotary inertia mass matrix of rotating drillstring element $\left[M_r\right] = I_D\left[M^r_{ab}\right]$

The non-zero entries of the upper triangular part of $[M_{ab}]$, *a, b*= 1, 2, ……,12

$$M^r_{22} = M^r_{33} = -M^r_{28} = -M^r_{39} = M^r_{88} = M^r_{99} = \frac{6}{5l}$$

$$M^r_{25} = M^r_{211} = -M^r_{310} = -M^r_{811} = M^r_{910} = -M^r_{34} = M^r_{410} = -M^r_{59} = \frac{1}{10}$$

$$M^r_{44} = M^r_{55} = M^r_{1010} = M^r_{1111} = \frac{2}{15}l$$

$$M^r_{410} = M^r_{511} = -\frac{1}{30}l$$

Table B-10

Torsional mass matrix of rotating drillstring element $\left[M_\varphi\right] = I_p\left[M^\varphi_{ab}\right]$

The non-zero entries of the upper triangular part of $[M_{ab}]$, *a, b*= 1, 2, ……,12

$$M^\varphi_{66} = 2M^\varphi_{612} = M^\varphi_{1212} = \frac{1}{3}l$$

Table B-11

Torsional and lateral coupling mass matrix of rotating drillstring element $\left[M_e\right] = I_p \left[M_{ab}^c\right]$

The non-zero entries of $\left[M_{ab}\right]$, $a, b = 1, 2, \ldots\ldots, 12$

$$M_{62}^c = -M_{68}^c = \frac{-6w_1 + 6w_2 + l\theta_{y2}}{10l}$$

$$M_{63}^c = -M_{69}^c = \frac{6v_1 - 6v_2 + l\theta_{z2}}{10l}$$

$$M_{64}^c = -\frac{l\left(6\theta_{z1} - \theta_{z2}\right)}{60}$$

$$M_{65}^c = \frac{l\left(6\theta_{y1} - \theta_{y2}\right)}{60}$$

$$M_{610}^c = -\frac{6v_1 - 6v_2 - l\theta_{z1} + 2l\theta_{z2}}{60}$$

$$M_{611}^c = -\frac{6w_1 - 6w_2 + l\theta_{y1} - 2l\theta_{y2}}{60}$$

$$M_{122}^c = -M_{128}^c = \frac{-6w_1 + 6w_2 + l\theta_{y1}}{10l}$$

$$M_{123}^c = -M_{129}^c = \frac{6v_1 - 6v_2 + l\theta_{z1}}{10l}$$

$$M_{124}^c = -\frac{6v_1 - 6v_2 + 2l\theta_{z1} - l\theta_{z2}}{60}$$

$$M_{125}^c = -\frac{6w_1 - 6w_2 - 2l\theta_{y1} + l\theta_{y2}}{60}$$

$$M_{1210}^c = \frac{l\left(\theta_{z1} - 6\theta_{z2}\right)}{60}$$

$$M_{1211}^c = -\frac{l\left(\theta_{y1} - 6\theta_{y2}\right)}{60}$$

Table B-12

Gyroscopic matrix of rotating drillstring element $[G] = I_p [G_{ab}]$

The non-zero entries of the upper triangular part of $[G_{ab}]$, $a, b = 1, 2, \ldots\ldots, 12$

$$G_{23} = G_{29} = G_{38} = G_{89} = -\frac{6}{5l}$$

$$G_{24} = G_{210} = G_{35} = G_{311} = G_{48} = G_{59} = -G_{810} = -G_{911} = \frac{1}{10}$$

$$G_{45} = G_{1011} = -\frac{2}{15} l$$

$$G_{411} = -G_{510} = -\frac{1}{30} l$$

REFERENCES

1. Jackson, W.E. *Making Hole*, (PETEX, 2000).
2. Leine, R. I., Van Campen, D. H. and Keultjes, W. J. “Stick-slip Whirl Interaction in Drillstring Dynamics,” *Journal of Sound and Acoustics* vol. 124, pp. 209-220, 2002.
3. Serrarens, A. F., Van de Molengraft, M. J., van den Steen, L. and Kok, J. “H∞ Control for Suppression Stick-Slip in Oil well Drillstrings,” *IEEE Control Systems*, vol. 18, no. 2, 19-30, 1998.
4. Leseultre, A., Lamine, E., and Jonsson, A., "An Instrumented Bit: A necessary step to the intelligent BHA," SPE 39341, IADC/SPE Drilling Conference, Dallas, Texas, 1998.
5. Jansen, J. D., "Non-Linear Rotor Dynamics as Applied to Oilwell Drillstring Vibrations," *Journal of Sound and Vibration*, vol. 147, pp. 115-135, 1991.
6. Heisig, G., Sancho, J. and Macpherson, J., "Downhole Diagnosis of Drilling Dynamics Data Provides New Level Drilling Process," SPE 49206, SPE Annual Technical Conference and Exhibition, New Orland, 1998.
7. Defeyte, M., and Henneuse, H.," Detection and Monitoring of the Slip-Stick Motion: Field Experiments," SPE 21945, IADC/SPE Drilling Conference in Amsterdam, March, 1991.
8. Jardine, S., Malone, L., and Sheppard, M., "Putting a Damper on Drilling's Bad Vibration," *Oil Field Review*, pp. 15-20, 1994.
9. Halsey, G. w., Kyllingstad, A., Aarrestad, T. V. and Lysne, D., " Drillstring Torsional Vibrations: Comparison between Theory and Experiment on a Full-Scale Research Drilling Rig,” SPE 15564, SPE Annual Technical Conference and Exhibition, New Orleans, Oct, 5-8. 1986.

10. Halsay, G. W., Kyllingstad, A. and Kylling A., "Torque Feedback Used to Cure Slip-Stick Motion," SPE 18049, 63rd Annual Technical Conference of the SPE, Houston, Texas, Oct., 1988.
11. Shuttleworth, N. E., Kerkoerle, E., and Foekema, N., "Revised Drilling Practices, VSS-MWD Tool Successfully Addresses Catastrophic Bit/Drillstring Vibration," SPE 39314, IADC/SPE Drilling Conference, Dallas Texas, 1998.
12. Ashley, D. K. and Tomlinson, J. C., "Extending BHA Life with Multi Vibration Measurements," SPE 67696, SPE/IADC drilling conference, Amsterdam, 2001.
13. Fear, M. J., and Abbassian, F., "Experience in the Detection and Suppression of Torsional Vibration from Mud Logging Data," SPE 28908, SPE Europe Conference held in London, Oct., 1994.
14. Sananlkone, P., Kamoshima, O., and White, D. B., "A Field Method for Controlling Drillstring Torsional Vibrations," SPE 23891, SPE Drilling Conference, New Orleans, 1992.
15. Chen, S. L., Blackwood, K., and Lamine, E., "Field Investigation of the Effects of Stick-Slip, Lateral, and Whirl Vibrations on Roller Cone Bit Performance," SPE 56439, SPE Annual Technical Conference and Exhibition, Houston, 1999.
16. Richard, T., Detournay, E., Fear, M., Miller, B., Clayton, R., and Matthews, O., "Influence of Bit-Rock Interaction on Stick-Slip Vibrations of PDC bits," SPE 77616, SPE Annular Technical Conference and Exhibition, San Antonio, Texas, 2002.
17. Zannoni, S. A., Cheatham, C. A., Chen, C., and Golla, C. A., "Development and Field Testing of a New Downhole MWD Drillstring Dynamics Sensor," SPE 26341, 68th Annular Technical Conference and Exhibition, Houston, Texas, 1993.

18. Jansen, J. D., Van den Steen, L., and Zachariasen, E., "Active Damping of Torsional Drillstring Vibrations with a Hydraulic Top Drive," SPE 28911, European Petroleum Conference, London, 1994.
19. Jansen, J. D. and van den Steen, L., "Active Damping of Self-Excited Torsional Vibration in Oil Well Drillstrings," *Journal of Sound and Vibration*, vol. 179**,** pp. 647-668, 1995.
20. Lin, Y. Q., and Wang, Y. H., "Stick –Slip Vibration of the Drill strings," *journal of Engineering for Industry, Trans. ASME, Series B*, vol. 113, pp. 38-43, 1991.
21. Kriesels, P. C., Keultjes, W. G., Dumont, P., and Huneidi, I., "Cost Savings through an Integrated Approach to Drillstring Vibration Control," SPE 57555, SPE/IADC Middle East Drilling Technology, Abu Dhabi, 1999.
22. Challamel, N., and Sellami, E., Chenevez, E., and Gossuin, L., "A Stick-slip Analysis Based on Rock/Bit interaction: Theoretical and Experimental Contribution," SPE 59230, IADC/SPE Drilling Conference, Orleans, Louisiana, 2000.
23. Brett, J. F. "The Genesis of Bit-Induced Torsional Drill String Vibrations," SPE 21943, SPE/IADC Drilling Conference, Amsterdam, march 1991.
24. Schmalhorst, B., Brommundt, E., Baumgart, A., and Richter, U., "Drilling Dynamics in the Presence of Mud Flow," SPE 59236, SPE/IADC Drilling Conference, New Orleans, 2000.
25. Yigit, S. A. and Christoforou, A. P., "Dynamic Modeling of Rotating Drillstrings with Borehole Interaction," *Journal of Sound and Vibration*, vol. 206**,** pp. 243-260, 1997.
26. Kyllingstad, A., and Halsey, G. W., "A study of slip/stick Motion of the Bit," SPE 16659, 62nd Annual Technical Conference of the SPE, Dallas, Texas, Sept. 1987.

27. Robnett, E. W., Hood, J. A., Heisig, G., and Macpherson, J., "Analysis of the Stick-Slip Phenomenon Using Downhole Drillstring Rotation Data," SPE 52821, SPE/IADC Drilling Conference, Holland, 1999.
28. Warren, T. M. and Oster J, H., "Torsional Resonance of Drill Collars with PDC Bits in Hard Rock," SPE 49204, SPE Annual Technical Conference, New Orland, 1998.
29. Baumgart, A., "Stick-Slip and Bit-Bounce of Deep-Hole Drillstrings," *Journal of Energy Resources and Technology*, vol. 122, pp. 78-82, 2000.
30. Yigit, A. S. and Christoforou, A. P., "Coupled torsional and Bending Vibrations of Actively Controlled Drillstrings," *Journal of Sound and vibration*, vol. 234, 2000.
31. Yigit, A. S. and Christoforou, A. P., "Active Control of Stick-Slip Vibrations: The role of Fully Coupled Dynamics," SPE 68093, SPE Middle East Oil Show, Bahrain, 2001.
32. Rappold, K., "Drilling Dynamics Conclusion, Drillstring Vibration Measurements Detect Bit Stick-Slip," *Oil & Gas Journal*, pp. 66-70, 1993.
33. Tucker, R. W. and Wang, C., "On The Effective Control of Torsional Vibrations in Drilling Systems," *Journal of Sound and Vibration*, vol. 224, pp. 101-122, 1999.
34. Fear, M. J., Abbasian, F., Parfitt, S. H., and McClean, A., "The Destruction of PDC Bits by Severe Slip-Stick Vibration," SPE 37639, SPE/IADC Drilling Conference, Amsterdam, March 1997.
35. Pavone, D. R. and Desplans, J.P., "Application of High Sampling Rate Downhole Measurements for Analysis and Cure of Stick-Slip in Drilling," SPE 28324, SPE Annual Technical Conference and Exhibition, New Orleans Sept. 1994.
36. Al-Harthi, M. and Yaz, E. E., "Reduced Order Proportional Integral compensator for Disturbance Suppression in Oil Well Drillstring," IEEE International Conference on Control Applications, Scotland, 2002.

37. Javanmardi, K., and Gaspard, D. T., "Application of Soft –Torque Rotary Table in Mobile Bay," SPE 23913, IADC/SPE Drilling Conference held in New Orleans, Louisiana, 1992.

38. Tucker, R. W. and Wang, C., "The Excitation and Control of Torsional Slip-Stick in the Presence of Axial Vibrations," (1997) www.lancs.ac.uk/uses/SPC/Physics.htm

39. Dubinsky, V. S., Hughes, B., and Beacker, D. R., "An Interactive Drilling Dynamics Simulator for Drilling Optimization and Training," SPE 49205, Annual Technical Conference and Exhibition, Orleans, Louisiana, 1998.

40. Leine, R. I., Van Campen, D. H., de Kraker, A., and van den Steen, L., "Stick-Slip Vibrations Induced by Alternate Friction Models," *Nonlinear Dynamics*, vol. 16, pp. 41-54, 1998.

41. Tucker, R. W. and Wang, C., "An Integrated Model for Drillstring Dynamics," *Journal of Sound and Vibration*, vol. 224, pp. 123-165, 1999

42. Dawson, R., Lin, Y. Q., and Spanos, P. D., "Drillstring Stick-Slip Oscillations," Spring Conference of the Society for Experimental Mechanics, Houston, Texas, 1987.

43. Fritz, R. J., "The Effect of an Annular Fluid on the Vibrations of a Long Rotor, Part 1-Theory," *Journal of Basic Eng.*, vol. 92, pp. 923-929, 1970.

44. Clayer, F., Vandlver, J. K., and Y., L. H., "The Effect of Surface and Downhole Boundary Conditions on the Vibration of Drillstring," SPE 20447, SPE Annual Technical Conference and Exhibition, New Orleans, 1990.

45. Richard, T., and Detournay, E., "Stick-slip Vibrations of PDC bits," *Pacific Rocks*, pp. 33-40, 2000.

46. Wolf, S. F., Zacksenhouse, M., and Arian, A., "Field measurements of Down hole Drillstring Vibrations," SPE 14330, SPE Annual Conference, Las Vegas, Nevada, Sept. 1985.

47. Close, D., Owens, S., and Macpherson, J., "Measurement of BHA Vibration Using MWD," SPE 17273, IADC/SPE Drilling Conference, Dallas, Texas, 1988.
48. Dubinsky, V., Henneuse H., and Kirkman, M., " Surface Monitoring of Downhole Vibrations: Russian, European and American Approaches," SPE 24969, European Petroleum Conference in Cannes, France, 1992.
49. Henneuse, "Surface Detection of Vibrations and Drilling Optimization: Field Experience," SPE 23888, IADC/SPE Drilling Conference in New Orleans, Louisiana, Feb. 1992.
50. Macpherson, J., Mason, J. S., and Kingman, J. E., "Surface Measurement and Analysis of Drillstring vibrations While Drilling," SPE 25777, SPE/IADC Drilling Conference, Amsterdam, 1993.
51. Warren, T., Oster J, Sinor, L., and Chen, D., "Shock Sub Performance Tests," SPE 39323, IADC/SPE Drilling Conference, Dallas, Texas, 1996.
52. Dykstra, M. W., Warren, T. K., and Chen, D. C., "Experimental Evaluation of Drill Bit and Drillstring Dynamics," SPE 28323, SPE Annual Technical Conference and Exhibition, New Orleans, Louisiana, 1999.
53. Galvanetto, U. and Bishop, S., "Dynamics of a Simple Damped Oscillator Undergoing Stick-Slip Vibrations," *Meccanica,* vol. 34, pp. 337-347, 1999.
54. Oden, J. T. and Martins, J. A., "Models and Computational Methods for Dynamic Friction Phenomena," *Computer Methods in Applied Mechanics and engineering*, vol. 52, pp. 527-634, 1985.
55. Martins, J. A. and Oden, J. T., "A Study of Static and Kinetic Friction," *International Journal of Engineering Science*, vol. 28, (1), pp. 29-92, 1990.
56. Schmalhorst, B., and Baumgart, A., “Combined Simulation of Whirl and Stick-Slip Phenomena using a Nonlinear Finite Element Model,” Drilling and production engineering Conference. pp. 53-60, 1997.

57. Al-Naser, H. A., "Finite Element Dynamic Analysis of Drillstring," Master Thesis, KFUPM, Department of Mechanical Engineering, Dhahran 2002.
58. Mohiuddin, M. A. and Khulief, Y. A., "Coupled Bending and Torsional Vibration of Rotors Using Finite Element," *Journal of Sound and Vibration,* vol. 223 pp. 297-316, 1999.
59. Hibbeler, R. C., *Engineering Mechanics Statics*, 7th edition, Prentice Hall International, 1995.
60. Persson, B. N., *Sliding Friction: Physical Principles and Applications,* New York, Springer, 1998.
61. Logan, D., *A First Course in the Finite Element Method,* 3rd edition, Brooks/Cole, 2002.
62. Kwon, Y. and Bang, H., *The Finite Element Method Using MATLAB,* CRC Press, 1997.
63. Fung, Y. C., *A First Course in Continuum Mechanics,* 3ed, Prentice Hall International, 1994.
64. Cheung, Y. and Leung, A. *Finite Element Methods in Dynamics,* CRC Press, 1997.
65. Millheim, K., Jordan, S., and Ritter, C., "Bottom-Hole Assembly Analysis Using the Finite-element Method," SPE 6057, 1978.
66. Dunayevsky, V. A., Abbassian, F., and Judzls, A., "Dynamic Stability of Drillstrings under Fluctuating Weight on Bit," SPE 14329, SPE Annual Technical Conference and Exhibition, Las Vegas, 1993.
67. Zamudio, C. A., Tlusty, J. L., and Dareing, D. W., "Self-Excited Vibrations in Drillstrings," SPE 16661, 62nd Annual Technical Conference and Exhibition, Texas, 1987.
68. Mitchell, R. F. and Allea, M. B., "Case Studies of BHA Vibration Failure," SPE 16675, 62nd Annual Technical Conference and Exhibition, Texas, 1987.

69. Mao, C. and Qin, Q., "Coupled Torsional-Flexural Vibration of Shaft Systems in Mechanical Engineering-I. Finite Element Model," *Computers & Structures,* vol. 58, pp. 835-843, 1996.

70. Mao, C. and Qin, Q., "Coupled Torsional-Flexural Vibration of Shaft Systems in Mechanical Engineering-II. FE-TM Impedance Coupling Method," *Computers & Structures,* vol. 58, pp. 845-849, 1996.

71. Przemieniecki, J., *Theory of Matrix Structural Analysis,* New York, McGraw-Hill. 1968.

72. Trindade, M., Wolter, C., and Sampaio, R., "Karhunen-Loève Decomposition of Coupled Axial/Bending Vibrations of Beams Subject to Impact," Journal of Sound and Vibration (In Press).

73. Walker, B. H. and Friedman, M. B., "Three-Dimensional Force and Deflection Analysis of a Variable Cross Section Drillstring," *Journal of Pressure Vessel Technology,* pp. 367-373, 1977.

74. Mohiuddin, M. A. "Coupled Bending Torsional Vibration of Rotating Shafts Using Finite Element," Master Thesis, KFUPM, Department of Mechanical Engineering, Dhahran 1992.

75. Mohiuddin, M. A. "Finite Element Dynamic Analysis of Multibody Rotor-Bearing System With Cracked Shaft," PhD Dissertation, KFUPM, Department of Mechanical Engineering, Dhahran 1997.

76. Macpherson, J. and Jogi, P., "Application and Analysis of Simultaneous Near Bit and Surface Dynamics Measurements," SPE 39397, IADC/SPE Drilling Conference, Texas, 1998.

Vita

- Salem Mohammed Bashmal
- Born on June 01, 1978, at Doan, Yemen.
- Received Bachelor of Science degree in Mechanical Engineering from King Fahd University of Petroleum and Minerals, Dhahran, KSA in 2001.
- Received Master of Science degree in Mechanical Engineering from King Fahd University of Petroleum and Minerals, Dhahran, KSA in 2005.
- Worked as Research Assistant in Mechanical Engineering Department, KFUPM, November 2001-May 2005.